

# **Studies on Suppressing Electromagnetic Wave Propagation at Specific Frequency Bands Using Resonators-Loaded Built-in Dielectric Substrates**

Satoshi Yoneda

A dissertation submitted in partial fulfillment of the requirements  
for the degree of Doctor of Philosophy in Engineering

The University of Electro-Communications  
Department of Communication Engineering and Informatics

December 2021

# Document description

## Title:

Studies on Suppressing Electromagnetic Wave Propagation at Specific Frequency Bands Using Resonators-Loaded Built-in Dielectric Substrates

## Title (in Japanese):

共振器装荷誘電体基板による特定周波数帯の電磁波伝搬の抑制に関する研究

## Author:

Satoshi Yoneda

## Approved by the Dissertation Committee:

Chairperson: Prof. Koji Wada

Member: Prof. Fengchao Xiao

Member: Assoc. Prof. Yoshiaki Ando

Member: Assoc. Prof. Yoshiki Kayano

Member: Assoc. Prof. Satoshi Ono

## **Copyright Notice:**

© 2021 Satoshi Yoneda

All Rights Reserved

# Acknowledgement

I, the author, would like to express my sincerest appreciation and respect to Professor Koji Wada for his kind guidance and advice regarding the application for the examination of this dissertation. I would also like to express my appreciation to Professor Fengchao Xiao, Associate Professor Yoshiaki Ando, Associate Professor Yoshiki Kayano, and Associate Professor Satoshi Ono for being members of the judging committee for this dissertation.

Since all researches described in this dissertation are indebted to the sponsorship of Mitsubishi Electric Corporation, I wish to express my thanks to all members in this company who have kindly contributed to the progress of the researches. I would like to express my deep gratitude to Dr. Naofumi Yoneda, Mr. Yuichi Sasaki, and Dr. Chiharu Miyazaki for giving me an opportunity to apply for the examination of this dissertation in my company career. I also would like to express my appreciation to Professor Yoshihiko Konishi, Mr. Hideyuki Oh-hashii, Dr. Yasuhiro Shiraki, Dr. Hiromitsu Uchida, Ms. Miyuki Tanaka, Mr. Takuro Sasaki, and Dr. Koichiro Misu for giving me the opportunities to participate in such fascinating researches in this dissertation. I also wish to thank Mr. Takeshi Ohshima, Dr. Yosuke Watanabe, Mr. Kenji Hirose, Mr. Akihito Kobayashi, and Mr. Tetsu Ohwada for their technical supports and helps in my company career.

I would also like to thank Mr. Shinji Suzuki of the Ministry of Education, Culture, Sports, Science and Technology (MEXT) for his kind and accurate checks and corrections for my English manuscript related to this dissertation while my secondment to the MEXT.

Finally, I would like to express my special thanks to my family, my wife and my naughty twin daughters for always helping, supporting, and entertaining my life, and my parents who warmly encourage and support me all the time.

# 概要

本稿は、共振器装荷誘電体基板を用いた電磁波伝搬の抑制方法に関し、従来よりも簡易な構成で薄型な導波管 BRF (Band Rejection Filter: 帯域阻止フィルタ) と、周波数選択性を有する非接触型の電磁波シールド構造について、それぞれの設計手法、設計結果、及び試作評価結果についてまとめたものである。

2 章では、共振器装荷誘電体基板を用いる導波管 BRF として、異なる共振器を用いる 2 種類の構成について説明する。どちらの構成も、高精度な機械加工が不要なため従来よりも構成が簡易であり、また、導波管の外側に構成要素がないため従来の導波管 BRF よりも薄型化が可能である。

2 章第 1 節では、両端開放  $\lambda/2$  マイクロストリップ共振器を装荷した誘電体基板を用いる導波管 BRF について説明する。誘電体基板に両端開放  $\lambda/2$  マイクロストリップ共振器を等間隔で配置し、その誘電体基板を導波管の左右内壁に配置して構成している。この構成により、導波管を伝搬する電磁波は両端開放  $\lambda/2$  マイクロストリップ共振器の共振周波数において両端開放  $\lambda/2$  マイクロストリップ共振器と磁界結合する。その結果、両端開放  $\lambda/2$  マイクロストリップ共振器の共振周波数において電磁波の伝搬を抑制することができる。フィルタ理論と電磁界計算に基づく設計手法に従い、Q 帯 (47 GHz 帯) 向けの導波管 BRF を設計、及び試作評価した結果、Q 帯において 50 dB 以上の急峻な減衰特性が得られ、その有効性が確認できた。

2 章第 2 節では、SIW (Substrate Integrated Waveguide: 基板集積導波路) 共振器を装荷した誘電体基板を用いる導波管 BRF について説明する。誘電体基板に SIW 共振器を等間隔で配置し、その誘電体基板を導波管の上下内壁に配置して構成している。この構成により、導波管を伝搬する電磁波は SIW 共振器の共振周波数において SIW 共振器と電界結合し、その結果、SIW 共振器の共振周波数において電磁波の伝搬を抑制することができる。前述の構成と同様に、フィルタ理論と電磁界計算に基づく設計手法に従い、Q 帯向けの導波管 BRF を設計、及び試作評価した結果、Q 帯において同じく 50 dB 以上の急峻な減衰特性が得られ、その有効性が確認できた。

このように、第 2 章で説明した導波管 BRF により、従来よりも簡易な構成で薄型の導波管 BRF を実現できる。この構成は、波長が比較的小さいために機械加工精度による影響が大きくなるミリ波帯等の高周波帯において、特に有効であると考えられる。また、導波管の外側に構成要素がないので、導波管系システム全体の小型化や高密度化への貢献も期待できる。これらの特長から、例として、ミリ波帯通信システムの送受信機や車載ミリ波レーダー機器、或いは電波天文学の測定器等への適用が期待できる。

両者を比較すると、主導波管の分割箇所の違いにより、マイクロストリップ共振器を用い

る構成の方が低損失性を期待できると考えられる。一方、システム全体の組み立てや、或いはパッチアレーアンテナや同軸導波管変換器等の他の機器との組み合わせ等を考慮すると、主導波管を側壁面で分割して構成せざるを得ない場合もあり、その場合は SIW 共振器を用いる構成の適用が適切となると考えられる。

3 章では、周波数選択性を有する非接触型の電磁波シールド構造として、多段化した SIW 共振器を用いる 3 種類の構成について説明する。多段化した SIW 共振器を装荷した誘電体基板をシールド扉と扉枠の間に配置することで、接触型の導電性ガスケットとは異なり、周波数選択性を有し、且つ、経年劣化に強いシールド扉の実現が可能となる。この構成は、無線 LAN の帯域において周波数選択性を有する構成とすることで、無線 LAN の帯域では室外との不要干渉や室外への情報漏洩等のリスク低減が要求される一方で、携帯電話等の他の通信機器の帯域では室外と通常通りの通信が可能となることが要求されるシールドオフィスのような環境に対して有効であると考えられる。また、無線マイクの帯域において周波数選択性を有する構成とすることで、放送スタジオや劇場等、無線マイク間の混信の低減が求められる環境においても有効であると考えられる。なお、一般的には、これらのような用途に対しては、当該帯域において 40 dB 以上の SE (Shielding Effectiveness: シールド特性) が求められる。

3 章第 1 節では、12 - 15.5 GHz 向けとして、一般的な構造の SIW 共振器を用いる構成について説明する。シールド帯域内に共振周波数を有する複数の SIW 共振器を多段化して誘電体基板に装荷し、その誘電体基板を間隙の内壁に配置して構成している。この構成により、間隙内を伝搬する電磁波は多段化した SIW 共振器の共振周波数において SIW 共振器と電界結合し、その結果、それらの共振周波数近傍におけるシールド特性を実現できる。電磁界計算と多項式近似に基づく設計手法に従って設計、及び試作評価した結果、多段 SIW 共振器装荷誘電体基板の配置により、当該帯域において間隙単体の場合よりも約 25 dB 大きい 40 dB 以上の SE が得られ、その有効性が確認できた。

3 章第 2 節では、2.4 GHz 帯向けとして、FQ (Folded Quarter-wavelength) -SIW 共振器を用いる構成について説明する。FQ-SIW 共振器は、多層基板を用いることで電磁波伝搬方向の寸法を小型化した SIW 共振器であり、それにより、比較的低い周波数帯においても多段化した構成を現実的な寸法で実現可能となる。前節と同様に、電磁界計算と多項式近似に基づく設計手法に従って設計、及び試作評価した結果、多段 FQ-SIW 共振器装荷誘電体基板の配置により、2.4 GHz 帯において間隙単体の場合よりも約 30 dB 大きい 60 dB 以上のシールド特性が得られ、その有効性が確認できた。

3 章第 3 節では、2.4 GHz 帯と 5 GHz 帯の複数帯域向けとして、DB (Dual Behavior) -SIW 共振器を用いる構成について説明する。DB-SIW 共振器は、結合スロットを共有化した 2 つの FQ-SIW 共振器で構成されており、ほぼ独立した 2 つの共振周波数を設定することが可能である。前節と同様に、電磁界計算と多項式近似に基づく設計手法に従って設計、及び試作評価した結果、高周波側への全体的な周波数シフトが見られたものの、多段 DB-SIW 共

振器装荷誘電体基板の配置により、2.4 GHz 帯及び 5 GHz 帯近傍において間隙単体の場合よりも約 20 dB 大きい 50 dB 以上のシールド特性が得られ、その有効性が確認できた。また、電磁界計算により誤差要因を分析した結果、前記周波数シフトが発生した主要因は via 直径の製造誤差と考えられることがわかった。

今後、ますますの高周波化と複雑化が予想される無線通信技術分野において、本研究に関する構造が何かしら貢献できることを期待する。

# Abstract

A conventional waveguide band rejection filter (BRF) has been well known as a configuration to suppress a propagation of electromagnetic waves in a waveguide at a specific frequency band. The conventional waveguide BRF is usually configured by arranging cavity resonators outside the main waveguide at regular intervals along the waveguide axis. The electromagnetic waves propagating in the waveguide couple to the cavity resonators via coupling slots on the upper or lower wall of the waveguide, and as a result, the propagation of the electromagnetic waves in the waveguide is suppressed at the resonant frequency of the cavity resonators. However, the configuration is difficult to be made low-profile since the cavity resonators are arranged outside the main waveguide, and is also difficult to be made with high precision at relatively high frequency bands, millimeter wave bands for example, since wavelength at the bands becomes relatively small against accuracy of machining process which is necessary for manufacturing the configuration.

As one of the solutions for these problems, a waveguide BRF using resonators-loaded dielectric substrates is proposed. The waveguide BRF is configured with dielectric substrates those are loaded with resonators at regular intervals and are located on the inner walls of the waveguide. In this configuration, the electromagnetic waves propagating in the waveguide couple to the resonators at their resonant frequency, and the propagation is suppressed at that frequency. This configuration has lower-profile than the conventional waveguide BRF since nothing is located outside the waveguide. Moreover, high-precision waveguide BRF can be expected at relatively high frequency bands, since patterning process is available for the resonators loaded on the dielectric substrates instead of machining process.



In this dissertation, the design procedures for the waveguide BRFs using open-ended  $\lambda/2$  microstrip resonators and substrate integrated waveguide (SIW) resonators are shown, followed by evaluated results of the waveguide BRFs designed according to the design procedures based on filter theory and EM-analysis. Although the types of the resonators used in two configurations are different, a steep and relatively high attenuation characteristic more than 50 dB at 47-GHz band were obtained in measured results of both configurations. Because of the difference in assembly of the main waveguide, lower insertion loss can be expected for the first configuration than the second one. However, though its disadvantage in the insertion loss, the second configuration is preferable when the main waveguide is required to be separated at the side walls in the assembly process. The configurations are suitable for use in systems where miniaturization and high attenuation at relatively high frequency band are required, for example, the millimeter-wave frequency band wireless communication system, automotive millimeter-wave radar systems, measuring systems for radio astronomy, and so on.

As another application for applying resonators-loaded dielectric substrates, a gasket-free electromagnetic shielding structure is proposed in this dissertation. The shielding structure is configured by arranging cascaded SIW resonators having slightly different resonant frequencies on dielectric substrates those located on the inner walls of a gap between a shielded door and a door frame. In this configuration, the electromagnetic waves propagating through the gap couple to the SIW resonators at their resonant frequencies, and the propagation is suppressed at those frequencies. As a result, frequency selectivity can be realized at the gap. In addition, a high contact pressure is not required when the door is closed since the structure is a non-contact type, which is contrary to the conventional contact-type conductive shielding gaskets. Therefore, the structure is almost free from deterioration caused by opening and closing operations of the door, and moreover, opening and closing structure can be simplified compared with an ordinary shielded door. These characteristics are suitable

for use in shielded environments with frequency selectivity, for example, an office in an urban area where electromagnetic interference with outside and unauthorized access from outside should be suppressed in wireless LAN bands, while communication with outside in cell phone bands is required at the same time. Other possible examples are laboratories using local wireless LAN communication systems inside, and broadcast studios and theaters where interferences of wireless microphones should be prevented. For such shielded environments, shielding effectiveness (SE) of more than 40 dB is generally required in the shield band.

In this dissertation, the design procedures for the gasket-free shielding structures for 12 - 15.5 GHz using conventional SIW resonators, for 2.4 GHz band using Folded Quarter-wavelength (FQ)-SIW resonators, and for 2.4 GHz and 5 GHz bands using Dual Behavior (DB)-SIW resonators are shown, followed by evaluated results of the structures designed according to the design procedures based on EM-analysis and a polynomial approximation. The measured results showed 40 - 60 dB of SE at specific frequency bands, those are improved by 20 - 30 dB from the gap alone by placing the resonators-loaded dielectric substrates on the inner walls of the gap.

The author would like to expect that the configurations and structures described in this dissertation contribute in some way to the radio communication technology field where higher frequency and more complex environment are anticipated.

# Contents

<b>Chapter 1. Introduction</b>	<b>1</b>
1.1 Background of the study	1
1.2 Outline of the dissertation	5
<b>Chapter 2. Configurations for a Low-profile Waveguide Band Rejection Filter (BRF)</b>	<b>9</b>
2.1 Introductory Remarks	9
2.2 A Q-band Waveguide BRF Using Open-ended $\lambda/2$ Microstrip Resonators	12
2.2.1 Design	12
2.2.2 Experiment	21
2.3 A Q-band Waveguide BRF Using Substrate Integrated Waveguide (SIW) Resonators	23
2.3.1 Design	23
2.3.2 Experiment	31
2.4 Summary	33
References	35
<b>Chapter 3. Configurations for a Gasket-free Electromagnetic Shielding Structure</b>	<b>37</b>
3.1 Introductory Remarks	37
3.2 A Gasket-free Electromagnetic Shielding Structure for 12 – 15.5 GHz Using Cascaded SIW Resonators	41
3.2.1 Configuration	41
3.2.2 Design	42
3.2.3 Experiment	49

3.3	A Gasket-free Electromagnetic Shielding Structure for 2.4 GHz band Using Folded $\lambda/4$ SIW Resonators .....	53
3.3.1	Configuration .....	53
3.3.2	Design .....	56
3.3.3	Experiment .....	62
3.4	A Gasket-free Electromagnetic Shielding Structure for 2.4 GHz and 5 GHz Bands Using Dual-Behavior SIW Resonators.....	66
3.4.1	Configuration .....	66
3.4.2	Design .....	69
3.4.3	Experiment .....	80
3.5	Summary .....	85
	References .....	87

**Chapter 4. Conclusions** **90**

Publication list .....	94
------------------------	----

Appendix A Representations of Equivalent circuits for a BRFB .....	98
--	----

# List of Figures

## Chapter 1

- 1.1.1 The millimeter-wave frequency band wireless communication system mounted on an airplane where waveguide BRFs of the proposed configuration are used.
- 1.1.2 A simplified concept of the shielded room having frequency selectivity.
- 1.2.1 A flowchart of this dissertation.

## Chapter 2

- 2.1.1 A configuration of a conventional waveguide BRF.
- 2.2.1 A configuration of the waveguide BRF using open-ended  $\lambda/2$  microstrip resonators.
- 2.2.2 The dielectric substrates shown in Fig. 2.2.1.
- 2.2.3 The dominant resonant mode of the microstrip resonators at the resonant frequency.
- 2.2.4 The equivalent circuit (i) of the waveguide BRF using open-ended  $\lambda/2$  microstrip resonators.
- 2.2.5 The equivalent circuits (ii) of the waveguide BRF using open-ended  $\lambda/2$  microstrip resonators (basic 4th order BRF).
- 2.2.6 The EM-analysis model for estimating  $Q_e$  of the microstrip resonators.
- 2.2.7 The relations between ( $w_{res}$ ,  $w_{wg}$ ) and  $Q_e$ .
- 2.2.8 Calculated results of the prototype filters.
- 2.2.9 The EM-analysis results of the waveguide BRF using open-ended  $\lambda/2$  microstrip resonators.
- 2.2.10 The fabricated waveguide BRF using open-ended  $\lambda/2$  microstrip resonators.
- 2.2.11 The measured results of the fabricated waveguide BRF using open-ended  $\lambda/2$  microstrip resonators.
- 2.3.1 A configuration of the waveguide BRF using SIW resonators.

- 2.3.2 The dielectric substrates shown in Fig. 2.3.1.
- 2.3.3 The dominant resonant mode of the SIW resonator at the resonant frequency.
- 2.3.4 The EM-analysis model of the SIW resonator.
- 2.3.5 The EM-analysis model for estimating  $Q_e$  of the SIW resonators.
- 2.3.6 The relations between  $(w_{\text{slot}}, L_{\text{slot}})$  and  $Q_e$ .
- 2.3.7 Calculated results of the prototype filters.
- 2.3.8 The EM-analysis results of the waveguide BRF using SIW resonators.
- 2.3.9 The fabricated waveguide BRF using SIW resonators.
- 2.3.10 The measured results of the fabricated waveguide BRF using SIW resonators.

## Chapter 3

- 3.1.1 A simplified configuration of the gasket-free shielding structure.
- 3.1.2 A simplified shielding effectiveness of the gasket-free shielding structure.
- 3.2.1 Cascaded SIW resonators embedded in a double-layered dielectric substrate.
- 3.2.2 The dominant resonant mode of the SIW resonator at the resonant frequency.
- 3.2.3 The EM-analysis model to obtain more accurate  $d(f_r)$  of SIW resonators.
- 3.2.4 An example of the EM-analysis result of a SIW resonator ( $d=10$  mm).
- 3.2.5 Relations between  $d$  and  $f_r$  of SIW resonators obtained from the EM-analysis results, the rough estimation of  $d(f_r)$  shown as (3.2.1), and the approximated equation shown as (3.2.2).
- 3.2.6 The EM-analysis model of the 8th order cascaded SIW resonators.
- 3.2.7 The EM-analysis result of the 8th order cascaded SIW resonators.
- 3.2.8 A flowchart of the design process for cascaded SIW resonators.
- 3.2.9 The measurement system for evaluating SE.
- 3.2.10 A simplified cross-sectional view of the gap in the measurement system.

- 3.2.11 The gap seen from both antenna sides.
- 3.2.12 The fabricated substrate of the cascaded SIW resonators.
- 3.2.13 The measured results of  $S_{21}$  of the cascaded SIW resonators.
- 3.2.14 The measured results of SE of the cascaded SIW resonators.
- 3.3.1 A cross-sectional view of an FQ-SIW resonator.
- 3.3.2 The dominant resonant mode of the FQ-SIW resonator at the resonant frequency.
- 3.3.3 The EM-analysis model to obtain more accurate  $d(f_r)$  of FQ-SIW resonators.
- 3.3.4 An example of the EM-analysis result of an FQ-SIW resonator ( $d=4.75$  mm).
- 3.3.5 Relations between  $d$  and  $f_r$  of FQ-SIW resonators obtained from the EM-analysis results, the rough estimation of  $d(f_r)$  shown as (3.3.1), and the approximated equation shown as (3.3.2).
- 3.3.6 The EM-analysis model of the 6th order cascaded FQ-SIW resonators.
- 3.3.7 The EM-analysis result of the 6th order cascaded FQ-SIW resonators.
- 3.3.8 A flowchart of the design process for cascaded FQ-SIW resonators.
- 3.3.9 The measurement system for evaluating SE.
- 3.3.10 A simplified cross-sectional view of the gap in the measurement system.
- 3.3.11 The gap seen from both antenna sides.
- 3.3.12 The fabricated substrate of the cascaded FQ-SIW resonators.
- 3.3.13 The measured results of  $S_{21}$  of the cascaded FQ-SIW resonators.
- 3.3.14 The measured results of SE of the cascaded FQ-SIW resonators.
- 3.4.1 A cross-sectional view of a DB-SIW resonator.
- 3.4.2 The dominant resonant mode of the DB-SIW resonator at the resonant frequencies.
- 3.4.3 The EM-analysis model to obtain more accurate  $d_1(f_1)$  and  $d_2(f_2)$  of DB-SIW resonators.
- 3.4.4 The EM-analysis result of  $S_{21}$  of a DB-SIW resonator with  $d_1=2.2$  mm and  $d_2=1.0$  mm.
- 3.4.5 The EM-analysis result of  $S_{21}$  of a DB-SIW resonator with  $d_1=2.6$  mm and  $d_2=1.0$  mm.

- 3.4.6 The EM-analysis result of  $S_{21}$  of a DB-SIW resonator with  $d_1=2.6$  mm and  $d_2=1.4$  mm.
- 3.4.7 Extracted  $f_1$  from the EM-analysis results of DB-SIW resonators.
- 3.4.8 Extracted  $f_2$  from the EM-analysis results of DB-SIW resonators.
- 3.4.9 Relations between  $d_1$  and  $f_1$  of DB-SIW resonators obtained from the EM-analysis results and the approximate equation shown as (3.4.2).
- 3.4.10 Relations between  $d_2$  and  $f_2$  of DB-SIW resonators obtained from the EM-analysis results and the approximate equation shown as (3.4.2).
- 3.4.11 The EM-analysis model of the 12th order cascaded DB-SIW resonators.
- 3.4.12 The EM-analysis result of  $S_{21}$  of designed configurations of 12th order cascaded DB-SIW resonators and 24th order cascaded FQ-SIW resonators having the same resonant frequencies.
- 3.4.13 A flowchart of the design process for cascaded DB-SIW resonators.
- 3.4.14 The measurement system for evaluating SE.
- 3.4.15 A simplified cross-sectional view of the gap of the measurement system.
- 3.4.16 The gap seen from both antenna sides.
- 3.4.17 The fabricated substrate of the cascaded DB-SIW resonators.
- 3.4.18 The measured results of  $S_{21}$  of the cascaded DB-SIW resonators.
- 3.4.19 The measured results of SE of the cascaded DB-SIW resonators.
- 3.4.20 The EM-analysis results of the 1st-order DB-SIW resonators considering manufacturing errors.

## Appendix A

- A.1 The equivalent circuit for a 4th order BRF using alternately connected ideal  $K$ -inverters and shunt-connected series resonators.



- A.2 The equivalent circuit for a 4th order BRF using alternately connected ideal  $K$ -inverters and series-connected parallel resonators.
- A.3 The equivalent circuit for a 4th order BRF using alternately connected ideal  $J$ -inverters and shunt-connected series resonators.
- A.4 The equivalent circuit for a 4th order BRF using alternately connected ideal  $J$ -inverters and series-connected parallel resonators.
- A.5 Calculated results of the prototype filter applying the four equivalent circuits.

# List of Tables

## Chapter 2

- 2.1.1 The comparison of the referred waveguide filters.
- 2.2.1 The design specification for the Q-band waveguide BRF using open-ended  $\lambda/2$  microstrip resonators.
- 2.2.2 The parameters of the prototype filter used in the design.
- 2.2.3 Required values of  $Q_{e,j}$  and  $w_{\text{res}} \times w_{\text{wg}}$  for the microstrip resonators.
- 2.2.4 Designed values of the Q-band waveguide BRF using open-ended  $\lambda/2$  microstrip resonators.
- 2.3.1 The design specification for the Q-band waveguide BRF using SIW resonators.
- 2.3.2 The parameters of the prototype filter used in the design.
- 2.3.3 Required values of  $Q_{e,j}$  and  $w_{\text{slot}} \times L_{\text{slot}}$  for the SIW resonators.
- 2.3.4 Designed values of the Q-band waveguide BRF using SIW resonators.

## Chapter 3

- 3.1.1 The comparison of the referred shielding structures.
- 3.2.1 Designed values of  $f_i$  and  $d$  of the cascaded SIW resonators.
- 3.3.1 Designed values of  $f_i$  and  $d$  of the cascaded FQ-SIW resonators.
- 3.4.1 Designed values of  $f_i$  and  $d_i$  ( $i=1, 2$ ) of the cascaded DB-SIW resonators.
- 3.4.2 The frequency shift obtained from the EM-analysis results.

## Appendix A

- A.1 The summary of  $K_{j,j+1}$  and  $J_{j,j+1}$  of the four equivalent circuits for an  $n$ -th order BRF.

# Chapter 1

## Introduction

### 1.1 Background of the study

Since Guglielmo Marconi invented the world's first wireless communication system more than 100 years ago, wireless communication has become an inseparable part in people's lives for its convenience. With the developments of the wireless communication equipment and technology, higher speed and larger capacity have been always required, and now the GHz band and millimeter wave band are in use. On the other hand, since radio resources are finite, an applicable bandwidth for each application is strictly defined. Therefore, a structure for attenuating electromagnetic waves in a specific frequency band is frequently required to suppress interference with other bands and unnecessary spurious responses.

In the case of a waveguide system, a configuration of conventional waveguide band rejection filter (BRF) is well known which employs cavity resonators located outside the main waveguide with periodic distance along the waveguide axis. However, the configuration is principally difficult to be made low-profile since cavity resonators are located outside the main waveguide. In addition, accuracy of the machining process necessary for manufacturing the cavity resonators is likely to be deteriorated at relatively high frequency bands, such as millimeter wave bands, because the wavelength at the bands becomes comparatively small against the accuracy of the machining process.

As one of the solutions for the problem, a configuration of waveguide BRF using resonators-

loaded dielectric substrates is proposed in this dissertation. In the configuration, resonators those resonate at a stop band are loaded at regular intervals on dielectric substrates those are placed on the inner walls of the waveguide. Since nothing is located outside the main waveguide, low-profile can be expected for the configuration. Moreover, higher precision can be expected since high-precision patterning process of the dielectric substrate is available for the resonators instead of machining process. The works on the proposed configurations are part of the results of "Research and Development on the Millimeter-wavelength High Speed Mobile Communication System" supported by the Ministry of Internal Affairs and Communications (MIC) of Japan from 2005 to 2009. One of the aims of the project was to establish a wireless communication system in the millimeter-wave frequency band (40 GHz bands) using Tx- and Rx- active phased array antennas (APAAs). Fig. 1.1.1 shows the system developed in the project. The system was mounted on an airplane, and high-speed wireless communication link in the millimeter-wave frequency band between the airplane in flight and the system on the ground was demonstrated. Waveguide BRFs of the proposed configuration were used in the system to ensure isolation between RF circuits in the Tx- and the Rx-systems. The

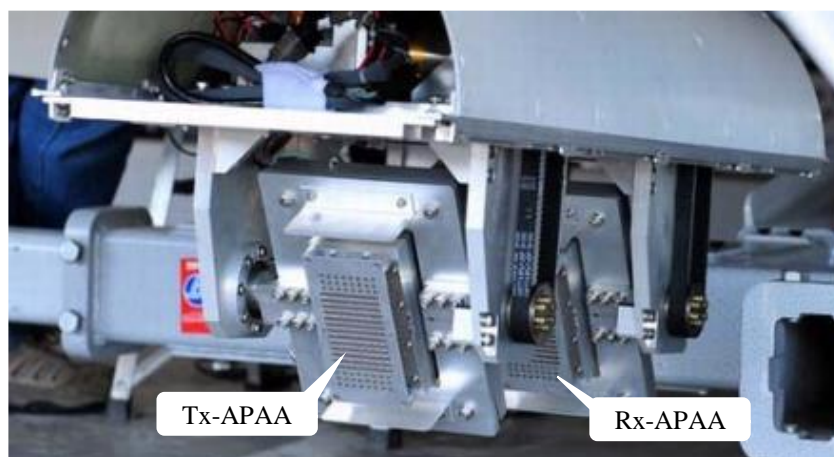


Fig. 1.1.1 The millimeter-wave frequency band wireless communication system where waveguide BRFs of the proposed configuration are used. The system is mounted on an airplane.

configurations are also applicable for other systems where miniaturization and high attenuation at relatively high frequency band are required, such as measuring systems for radio astronomy and automotive millimeter-wave radar systems, for example.

As another configuration for using resonators-loaded dielectric substrate, a gasket-free electromagnetic shielding structure for a shielded door is proposed in this dissertation. Currently, wireless local area network (LAN) access points are densely populated, especially in urban areas, and there is a problem that communication quality may deteriorates due to interferences and crosstalk from other access points or devices. Moreover, threat of unauthorized access may become higher in such a congested wireless communication environment. Therefore, it is sometimes required to suppress unintentional electromagnetic waves from the outside in the wireless LAN band. Even in such a situation, however, it is often required that communication devices using other frequency bands, cell phones for example, are available as usual.

Although a general shielded room would be the solution for the former requirement, the latter requirement cannot be met because the attenuation characteristics of the ordinal shielded room are continuous with respect to the frequencies. Instead, a shielded room with frequency selectivity would be a solution to satisfy the two requirements simultaneously. Fig. 1.1.2 shows a simplified concept of the shielded room having frequency selectivity, where unintentional electromagnetic waves from the outside in wireless LAN band, such as unauthorized access, interference, and crosstalk, are shielded to realize safe and comfort wireless LAN network inside, while at the same time, cell phones those use other frequency band are available inside as usual. Such frequency-selective shielded environments may also be beneficial for broadcast studios and theaters, for example, where interferences of wireless microphones should be prevented. For the frequency-selective shielded environments above, SE of more than 40 dB is generally required in the shield band for a practical use.

The main propagation paths of electromagnetic waves from the outside to the inside of a

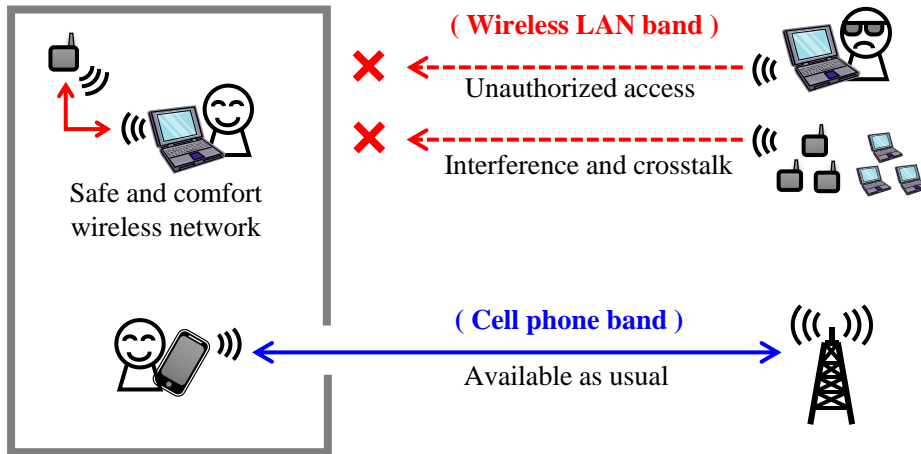


Fig. 1.1.2 A simplified concept of the shielded room having frequency selectivity.

shielded room are walls, windows, and the gaps between a shielded door and a door frame. For the walls and windows, some shielding structures with frequency selectivity, frequency selective surface (FSS) for example, are reported. For the gaps, on the other hand, contact-type conductive gaskets are usually used those physically connects the shielded door and the door frame when the door is closed to completely shut out the propagation of electromagnetic waves through the gap. However, the attenuation characteristics do not have frequency selectivity, and moreover, deterioration comes from opening and closing operations of the door is inevitable since high contact pressure is required when the door is closed. Applying resonators-loaded dielectric substrates would be a solution to realize frequency selectivity at the gap, because propagation of electromagnetic waves through the gap is suppressed only at resonant frequencies of the resonators. Furthermore, the structure is almost free from deterioration because its non-contact type structure excludes the need for high contact pressure when the door is closed.

The target of this dissertation is to establish a design process and confirm validity of the waveguide BRF and the gasket-free electromagnetic shielding structure mentioned above, both using the resonators-loaded dielectric substrates.

## 1.2 Outline of the dissertation

Fig. 1.2.1 shows a flowchart of this dissertation. The dissertation mainly consists of 4 chapters, starting with introduction in section 1 of Chapter 1. Then, as an application of this study, waveguide band BRFs and gasket-free electromagnetic shielding structures are proposed and evaluated in Chapter 2 and Chapter 3, respectively. And finally, conclusions are summarized in Chapter 4.

In Chapter 2, two configurations of the waveguide BRF using different type of resonators-loaded dielectric substrates are proposed and evaluated after introductory remarks in section 1.

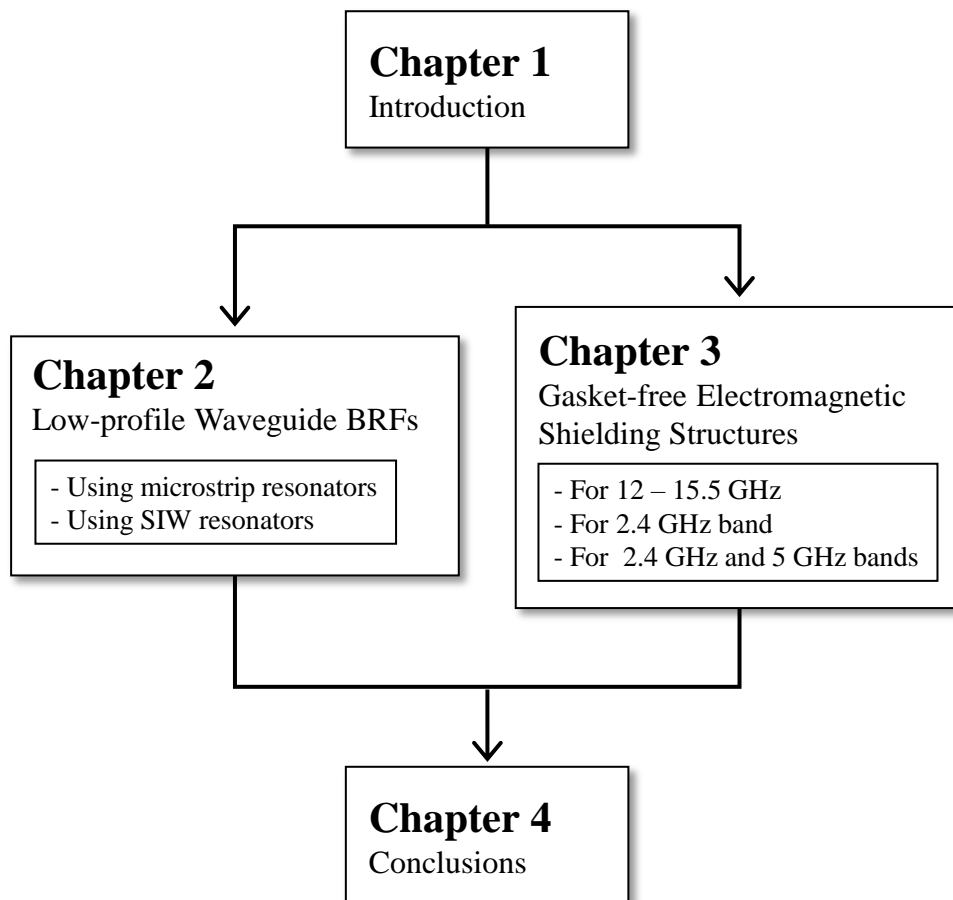


Fig. 1.2.1 A flowchart indicating outline of this dissertation.

Resonators-loaded dielectric substrates are placed on the inner walls of the waveguide in both configurations. By this configuration, lower-profile than conventional waveguide BRF can be expected which employs resonant cavities outside the waveguide.

In section 2 of Chapter 2, the configuration of the waveguide BRF using open-ended  $\lambda/2$  microstrip resonators is described. In the configuration, open-ended  $\lambda/2$  microstrip resonators those resonate at the stop band are mounted at regular intervals on two dielectric substrates placed on the both inner side walls of the waveguide. The electromagnetic waves propagating in the waveguide couple to the resonators at their resonant frequency, and as a result, propagation of the electromagnetic waves is suppressed at the stop band. After the design procedure based on filter theory and electromagnetic (EM)-analysis is described, evaluated results of the fabricated waveguide BRF for Q-band (47 GHz band) designed according to the procedure are shown.

In section 3 of Chapter 2, the configuration of the waveguide BRF using substrate integrated waveguide (SIW) resonators is described. SIW resonator is kind of a cavity resonator embedded in a dielectric substrate by conductive patterns and via holes. In the configuration, SIW resonators those resonate at the stop band are embedded at regular intervals in two dielectric substrates placed on the both upper and lower inner walls of the waveguide. As same with the previous configuration, the electromagnetic waves propagating in the waveguide couple to the resonators at their resonant frequency, and as a result, propagation of the electromagnetic waves is suppressed at the stop band. After the design procedure based on filter theory and EM-analysis is described, evaluated results of the fabricated waveguide BRF for Q-band (47 GHz band) designed according to the procedure are shown.

In Chapter 3, gasket-free electromagnetic shielding structures having frequency selectivity is proposed as another application using resonators-loaded dielectric substrates, and three configurations of the shielding structures for different shield bands are proposed and evaluated after



introductory remarks in section 1. In the structures, SIW resonators having slightly different resonant frequencies are arranged in a cascaded configuration along the direction of propagation of electromagnetic waves and are embedded in dielectric substrates placed on inner walls of a gap between a shielded door and a door frame. The electromagnetic waves propagating through the gap couple to the resonators at their resonant frequencies and the propagation is suppressed at those frequencies. As a result, the gap can be expected to have frequency selectivity with a non-contact type structure at their resonant frequencies.

In section 2 of Chapter 3, a gasket-free electromagnetic shielding structure for 12 - 15.5 GHz using conventional SIW resonators is described. A conventional SIW resonator has a coupling slot at the center and the size of the SIW resonator along the direction of propagation is  $\lambda/2$  at its resonant frequency in the substrate. After the design procedure based on EM-analysis and a polynomial approximation is described, evaluated results of the fabricated shielding structure using cascaded SIW resonators designed according to the procedure are shown.

In section 3 of Chapter 3, a gasket-free electromagnetic shielding structure for 2.4 GHz band using folded quarter-wavelength (FQ)-SIW resonators is described. Conventional SIW resonator is difficult to be applied for 2.4 GHz band, because  $\lambda/2$  inside the substrate becomes relatively large at 2.4 GHz band and the cascaded configuration is hard to be realized in a practical size. FQ-SIW resonators are used in the structure instead, whose size along the direction of propagation is miniaturized by applying a multilayered dielectric substrate. After the design procedure based on EM-analysis and a polynomial approximation is described, evaluated results of the fabricated shielding structure using cascaded FQ-SIW resonators designed according to the procedure are shown.

In section 4 of Chapter 3, a gasket-free electromagnetic shielding structure for 2.4 GHz and 5 GHz bands using dual behavior (DB)-SIW resonators is described. A DB-SIW resonator mainly consists of two FQ-SIW resonators sharing one coupling slot, and contrary to a conventional SIW

resonator and an FQ-SIW resonator those have one independent resonant frequency, a DB-SIW resonator has almost-independent two resonant frequencies. After the design procedure based on EM-analysis and a polynomial approximation is described, evaluated results of the fabricated shielding structure using cascaded DB-SIW resonators designed according to the procedure are shown.

Finally, in Chapter 4, conclusions of this dissertation are summarized and described.

# Chapter 2

## Configurations for a Low-profile Waveguide BRF

### 2.1 Introductory Remarks

Since people's demands for faster and larger capacities in communication systems never ends, frequency band in use has become higher and higher. Recently, millimeter-wave frequency bands are in practical use, and then, high performance BRF is sometimes required to obtain high spurious suppression at the bands. Fig. 2.1.1 shows a configuration of a conventional waveguide BRF which still can meet the requirement [2.1]. In the configuration, cavity resonators are located outside the main waveguide with periodic distance along the waveguide axis. However, low-profile configuration is difficult to be achieved by this configuration since the cavity resonators are located outside the main waveguide. Moreover, the configuration is not preferable for use in relatively high frequency bands, since the accuracy of the machining process necessary for manufacturing the cavity resonators is more likely to be deteriorated at such high frequency bands. Applying dielectric resonators instead of the cavity resonators may be another solution [2.2] - [2.5]. However, machining process is still necessary for manufacturing the dielectric resonators and their supporting structures, and therefore, they are not preferable for precise use in relatively high frequency bands as well.

To provide low-profile and high-precision waveguide filters at relatively high frequency bands, configurations applying resonant elements fixed inside the waveguide at the central E-plane

are proposed as E-plane waveguide filters [2.6] – [2.9]. In [2.6], three pairs of resonators on a double-sided dielectric substrate are applied for a dual-band waveguide BPF, and the measured result shows dual band-pass characteristic in two adjacent frequency bands at 30-GHz with high-selectivity. In [2.7], several lightning-shaped one-wavelength resonators of a metal plate are applied, and the measured result shows high attenuation characteristics more than 50 dB at 48 GHz. In [2.8], split ring resonators (SRRs), a kind of C-shaped microstrip resonator, on a double-sided dielectric substrate are applied, and measured result shows relatively wide-band band-stop characteristics at X-band. In [2.9], folded split ring resonators (FSRRs) on a dielectric substrate are applied, and simulated results demonstrated dual band-stop characteristics at both Ka- and W-bands. The configuration of these E-plane waveguide filters is rather simple; however, the resonant elements need to be fixed in the correct position on the central E-plane of the waveguide. This condition requires fixing and alignment processes when assembling like the conventional waveguide BRFs mentioned above.

In this chapter, two configurations employing resonators-loaded built-in dielectric substrates are proposed. In the two configurations, resonators-loaded dielectric substrates are placed on inner walls of the main waveguide, and the types of resonators are different; one is a microstrip resonator, and the other is an SIW resonator. An SIW is kind of a dielectric waveguide configured in a dielectric substrate by via-holes and metalized surfaces and has been gaining attentions recently for its affinity for use in high frequencies [2.10] - [2.12]. Though the types of the resonators are different, both configurations are low-profile compared with the conventional waveguide BRF since nothing is located outside the waveguide. Moreover, relatively high-precision can be expected since high-precision metal-patterning process of the dielectric substrates is available for the resonators in both configurations instead of the machining process. In addition, fixing and alignment process for the resonators are not needed when assembling since the resonator-loaded substrates are already positioned on inner walls of the waveguide. Waveguide filters referred above are compared in Table

2.1.1, showing the type of resonators, the location of the resonators, necessity of machining process for the resonators, possibility of low-profile configuration, and necessity of fixing and alignment processes in the assembly.

In each section of this chapter, the configuration of the proposed waveguide BRF is shown first. Design process based on filter theory and electromagnetic (EM) analysis is shown next, and finally, designed and measured results of fabricated waveguide BRFs for Q-band are shown.

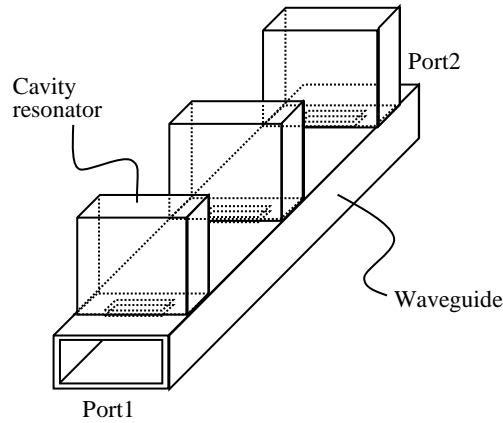


Fig. 2.1.1 A configuration of a conventional waveguide BRF.

Table 2.1.1 The comparison of the referred waveguide filters.

Type of resonators [ref]	Cavity resonator [2.1]	Dielectric resonator [2.2] - [2.5]	Microstrip or metal resonator [2.6] - [2.9]	SIW or microstrip resonator (This chapter)
Location of the resonators	Outside the waveguide	Outside the waveguide	Inside the waveguide (Fixed at the center E-plane)	Inside the waveguide (Placed on Inner walls)
Machining process for the resonators	Needed	Needed	Needed for metal resonators	Not needed
Low-profile configuration	Principally difficult	Difficult	Applicable	Applicable
Fixing and alignment process in assembly	Needed	Needed	Needed	Not needed

## 2.2 A Q-band Waveguide BRF Using Open-ended $\lambda/2$ Microstrip Resonators

### 2.2.1 Design

Fig. 2.2.1 shows a configuration of the proposed waveguide BRF, which simply consists of two dielectric substrates and a waveguide. The substrates are inserted inside the waveguide and placed on the both inner side walls by a conductive adhesive. At the substrates-located part of the waveguide, horizontal dimension is reduced from that of the I/O ports. Fig. 2.2.2 shows the dielectric substrates apart. On each substrate, four open-ended  $\lambda/2$  microstrip resonators of  $\lambda_{\text{MSL}}/2$ -length at  $f_0$  (center frequency of the stop band) are mounted  $\lambda_g/4$  at  $f_0$  apart from each other along the waveguide axis, where  $\lambda_{\text{MSL}}$  is the wavelength of the microstrip line on the substrate and  $\lambda_g$  is the guide wavelength in the waveguide. Fig. 2.2.3 shows dominant resonant mode of the microstrip resonators at  $f_0$ , where E-fields are directed perpendicular to the surface of the substrates and are the highest at their open ends. The comparison of this mode with the main propagation mode of the waveguide suggests that two modes are magnetically coupled, since their magnetic fields are in parallel with each other.

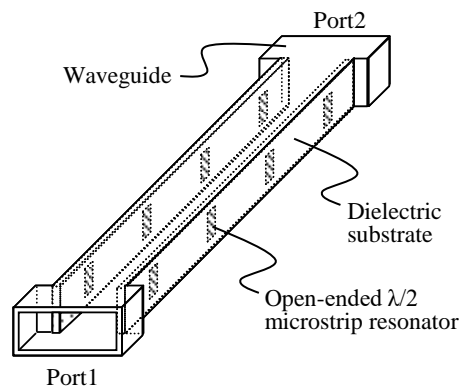


Fig. 2.2.1 A configuration of the waveguide BRF using open-ended  $\lambda/2$  microstrip resonators.

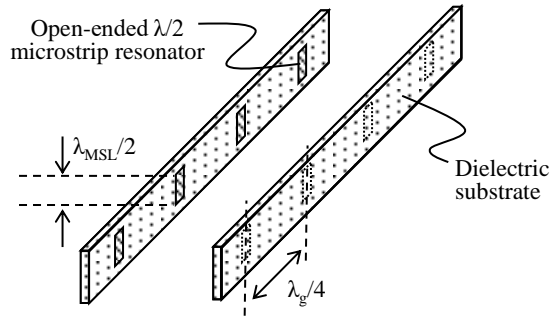


Fig. 2.2.2 The dielectric substrates shown in Fig. 2.2.1.

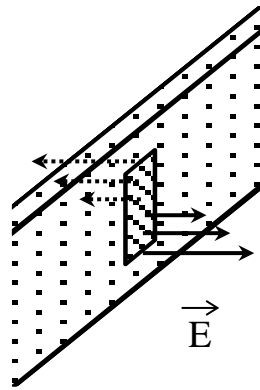


Fig. 2.2.3 The dominant resonant mode of the microstrip resonators at the resonant frequency.

Fig. 2.2.4 shows an equivalent circuit (i) of the waveguide BRF, where each series-connected parallel resonator represents opposing two open-ended  $\lambda/2$  microstrip resonators, and  $90^\circ$  transmission lines connecting them in series represent  $\lambda_g/4$ -length waveguides. The equivalent circuit (i) can be simplified to equivalent circuit (ii) shown by Fig. 2.2.5, by converting  $90^\circ$  transmission lines to ideal  $J$ -inverters. The equivalent circuit (ii) is the basic 4th order BRF, where,  $G_A$  and  $G_B$  are terminating conductance,  $B_j(\omega)$  is susceptance of the resonators,  $b_j$  is susceptance slope parameter of the resonators, and  $J_{j,j+1}$  are admittances of ideal  $J$ -inverters (note that  $J_{01}$  and  $J_{45}$  are included in the I/O ports). From filter theory,  $J_{j,j+1}$  and  $b_j$  can be obtained from well-known equations,

$$J_{01} = \sqrt{\frac{wG_A b_1 g_0 g_1}{\omega_1'}} , \quad (2.2.1)$$

$$J_{45} = \sqrt{\frac{w b_4 G_B g_4 g_5}{\omega_1'}} , \quad (2.2.2)$$

$$J_{j,j+1} \Big|_{j=1 \text{ to } 3} = \frac{w}{\omega_1'} \sqrt{b_j b_{j+1} g_j g_{j+1}} , \quad (2.2.3)$$

and

$$b_j = \frac{\omega_0}{2} \frac{dB_j(\omega)}{d\omega} \Big|_{\omega=\omega_0} , \quad (2.2.4)$$

where  $w$  is the fractional bandwidth,  $\omega_0$  is the center angular frequency of the stop band,  $g_j$  is  $g$ -values for the prototype filter, and  $\omega_1'$  is the cut-off angular frequency of the prototype filter [2.1]. In general, a BRF can be also represented by other equivalent circuits different from that shown in Fig. 2.2.5, and the other representations are described and summarized in Appendix A.

According to [2.13], when characteristic impedance of the  $90^\circ$  transmission lines in Fig. 2.2.4 are constant, coupling coefficients between the terminating conductance and each resonator can be represented as external  $Q$ -factors for individual resonators ( $Q_{e,j}$ ) as

$$Q_{e,j} = \frac{2}{\omega_1' w g_j} , \quad (2.2.5)$$

which is applicable in this case.



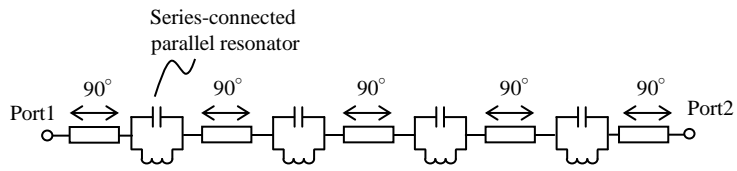


Fig. 2.2.4 The equivalent circuit (i) of the waveguide BRF.

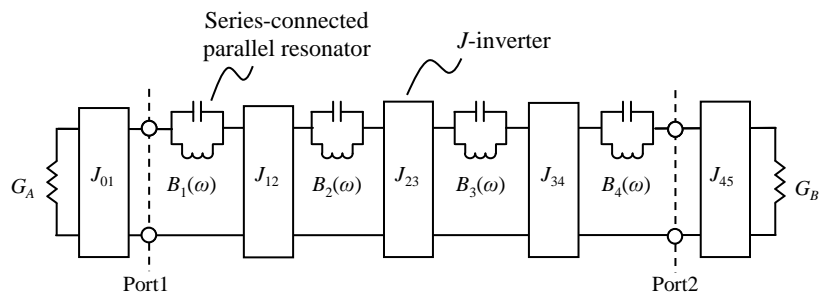


Fig. 2.2.5 The equivalent circuit (ii) of the waveguide BRF (basic 4th order BRF).

Table 2.2.1 shows the design specification for the waveguide BRF. High attenuation characteristic of 50 dB is required at the stopband (46.7 - 47.0 GHz), where  $f_0$  is 46.85 GHz and the fractional bandwidth is 0.6 %. Steepness is also required since the passband (44.2 – 44.5 GHz) is near the low frequency side of the stopband. An alumina substrate (relative dielectric constant ( $\epsilon_r$ ): 10.0,  $\tan\delta$ : 0.0001, thickness: 0.25 mm) is applied for its high-precision metal-patterning process. Dimension of cross-sectional areas of the I/O ports are  $2.4 \times 4.8 \text{ mm}^2$ , and the cut-off frequency is 31 GHz.

As shown in Fig. 2.2.2, length of the open-ended microstrip resonators is  $\lambda_{\text{MSL}}/2$ , and the distance between them along the waveguide axis is  $\lambda_g/4$ . Remained parameters to be determined in the design are  $w_{\text{res}}$  and  $w_{\text{wg}}$ , where  $w_{\text{res}}$  is the width of the open-ended  $\lambda/2$  microstrip resonators, and  $w_{\text{wg}}$  is the horizontal dimension of the waveguide. They can be obtained from the following procedure by EM-analysis, performed by a commercial Finite-Element-Method (FEM) software. Fig. 2.2.6 shows an EM-analysis model for estimating external  $Q$ -factor ( $Q_e$ ) of the microstrip resonators. The model consists of a waveguide and two dielectric substrates placed on both inner side walls of the waveguide, and one open-ended  $\lambda/2$  microstrip resonator is mounted on each substrate. Width of the open-ended  $\lambda/2$  resonators is  $w_{\text{res}}$ , and horizontal dimension of the waveguide is  $w_{\text{wg}}$ . At the resonant frequency, the electromagnetic wave would be more likely to resonate at the microstrip resonator than to propagate through the waveguide. As a result, the transmission coefficient  $S_{21}$  forms an attenuation pole at the resonant frequency. From the EM-analysis result,  $Q_e$  can be obtained from

Table 2.2.1 The design specification for the waveguide BRF using open-ended  $\lambda/2$  microstrip resonators.

	Passband 44.2 - 44.5 GHz	Stopband 46.7 - 47.0 GHz
$S_{21}$ [dB]	> -2	< -50

$$Q_e = \frac{f_0}{\Delta f} \left( 1 + \frac{1}{\beta_e} \right) \quad (2.2.6)$$

and

$$\beta_e = 10^{\frac{IL}{20}} - 1, \quad (2.2.7)$$

where  $\Delta f$  is the half bandwidth of  $S_{21}$  and  $IL$  is the insertion loss in dB at the resonant frequency.

Relations between  $(w_{res}, w_{wg})$  and  $Q_e$ , can be obtained from the EM-analysis results with several values

of  $w_{res}$  and  $w_{wg}$ , as shown in Fig. 2.2.7. From the figure, suitable values of  $w_{res}$  and  $w_{wg}$  for required  $Q_e$

can be determined.

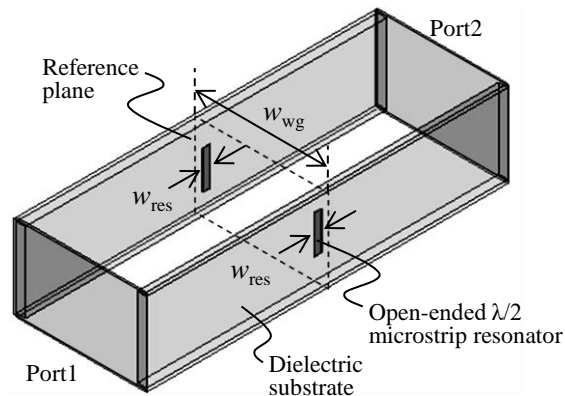


Fig. 2.2.6 The EM-analysis model for estimating  $Q_e$  of the microstrip resonators.

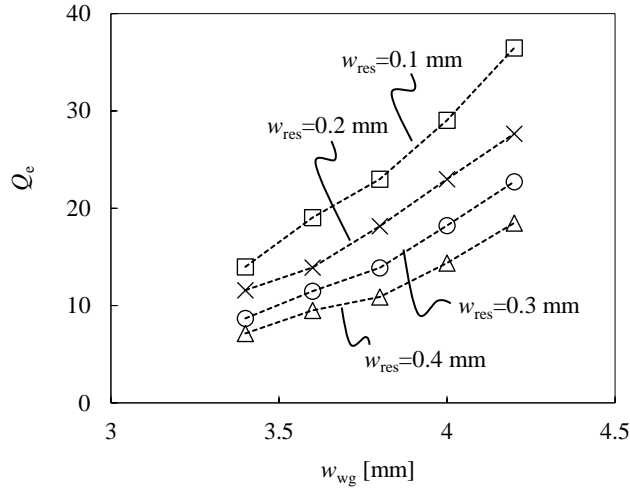


Fig. 2.2.7 The relations between  $(w_{res}, w_{wg})$  and  $Q_e$ .

Table 2.2.2 shows the parameters of the prototype filter used in the design: a loss-less 4th order Chebyshev filter with 0.05-dB of passband ripple. Fig. 2.2.8 shows calculated results of the prototype filter which meets the specification well. By instituting the parameters shown in Table 2.2.2 into (2.2.5), required values for  $Q_{e,j}$  can be obtained. And from the obtained  $Q_{e,j}$  and Fig. 2.2.7,  $w_{res} \times w_{wg}$  of the microstrip resonators can be determined as shown in Table 2.2.3. Though determined  $w_{res} \times w_{wg}$  are not the same, the differences were not so large and  $w_{res} \times w_{wg}$  for the microstrip resonators were supposed to be constant ( $0.2 \times 3.8 \text{ mm}^2$ ) this time to suppress manufacturing errors.

Full EM-analysis model of the waveguide BRF can be configured by cascading the EM-analysis model shown in Fig. 2.2.6. Finally, designed values shown in Table 2.2.4 were obtained after optimization with the full EM-analysis model. The EM-analysis results of the full EM-analysis model of the waveguide BRF is shown in Fig. 2.2.9 which satisfies high attenuation characteristic at the 47 GHz band and meets well with the calculated results of the prototype filter.

Table 2.2.2 The parameters of the prototype filter used in the design.

Chebyshev filter (ripple: 0.05 dB, 4th order)			
$g_0$	1.0	$f_0$	46.85 GHz
$g_1$	0.9333	$w$	8%
$g_2$	1.3923		
$g_3$	1.5795		
$g_4$	0.7636		
$g_5$	1.2222		

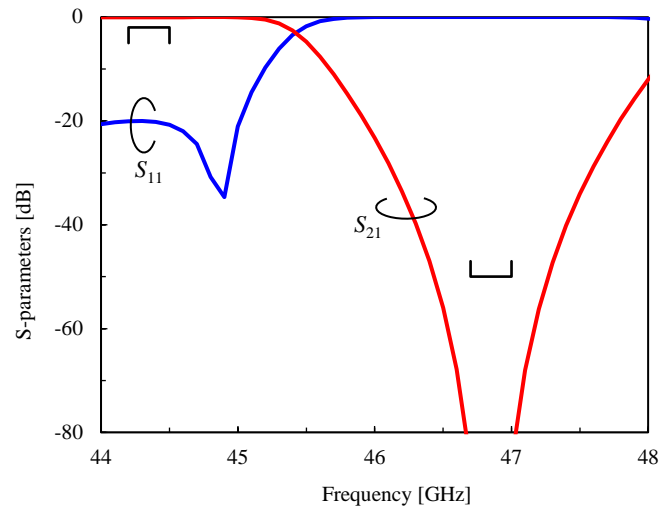


Fig. 2.2.8 Calculated results of the prototype filters.

Table 2.2.3 Required values of  $Q_{e,j}$  and  $w_{\text{res}} \times w_{\text{wg}}$  for the microstrip resonators.

	$Q_{e,1}$	$Q_{e,2}$	$Q_{e,3}$	$Q_{e,4}$
Required value	26.8	19.3	15.8	32.7
$w_{\text{res}} \times w_{\text{wg}} [\text{mm}^2]$	0.1×3.9	0.2×3.8	0.2×3.7	0.1×4.1

Table 2.2.4 Designed values.

Parameter	Designed value [mm]
Length of the microstrip resonators	1.06
Distance between the microstrip resonators	3.5
$w_{res}$	0.2
$w_{wg}$	3.8

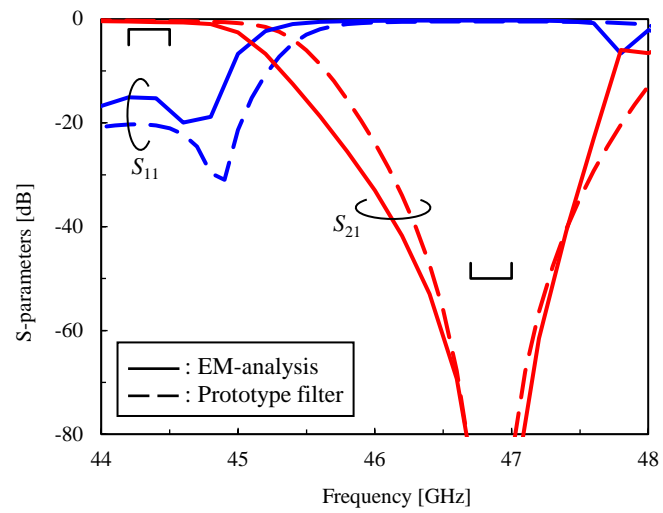


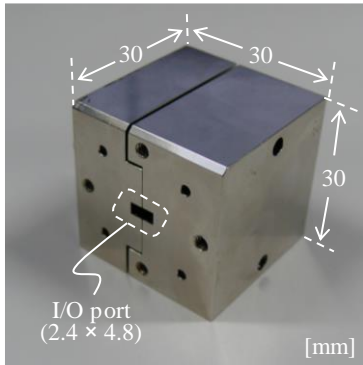
Fig. 2.2.9 The EM-analysis results of the waveguide BRF.

## 2.2.2 Experiment

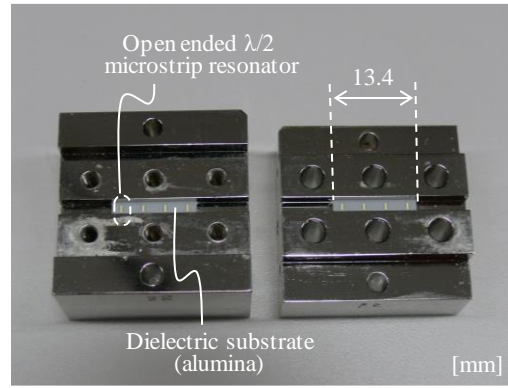
Fig. 2.2.10 shows a fabricated waveguide BRF. The main waveguide is formed by assembled aluminum flanges, and two alumina substrates are placed on both inner side walls by a conductive adhesive, with four open-ended  $\lambda/2$  microstrip resonators mounted on each of them. Though the whole size of the aluminum flanges is  $30 \times 30 \times 30 \text{ mm}^3$ , the actual size of the fabricated BRF itself is  $2.4 \times 4.8 \times 13.4 \text{ mm}^3$ , which is relatively low-profile and compact.

Fig. 2.2.11 shows the experimental results, where EM-analysis results and calculated results of the prototype filter are also represented by dotted and dashed lines, respectively. In the measurement system, waveguide to coaxial adapters are connected to the I/O ports of the waveguide, and each port of the adapters are connected to Port1 and Port2 of a network analyzer. Though a slight frequency shift to higher frequency range was present, relatively high attenuation more than 50 dB at 46.7 - 47.0 GHz and low insertion loss less than 1.3 dB at 44.2 – 44.5 GHz were achieved.

One possible reason for the frequency shift in the measured results is the existence of the conductive adhesive. The thickness of the adhesive was neglected in the EM-analyses, which may have caused slight position fluctuation of the resonators from designed position. Other possible reasons are production errors, such as manufacturing errors in the thickness and the dielectric constant of the substrates.



(a) Perspective view.



(b) Exploded view.

Fig. 2.2.10 The fabricated waveguide BRF.

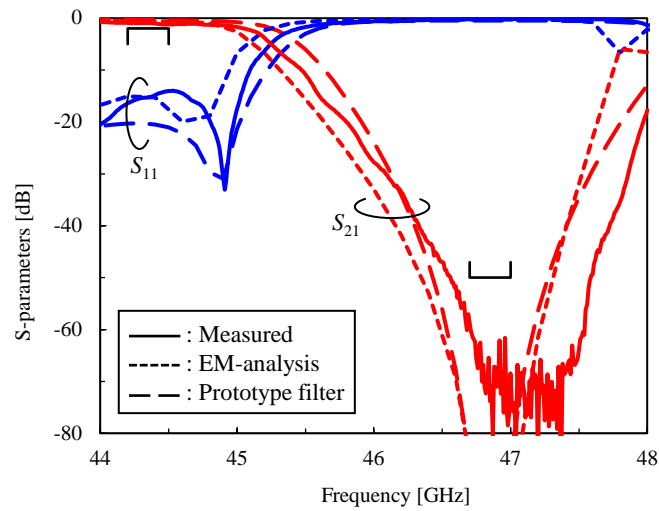


Fig. 2.2.11 The measured results of the fabricated waveguide BRF.



## 2.3 A Q-band Waveguide BRF Using SIW Resonators

### 2.3.1 Design

In this section, waveguide BRF based on the same concept as the previous section is proposed, where SIW resonators are applied as resonators instead of microstrip resonators. Fig. 2.3.1 shows the configuration of the proposed waveguide BRF, which simply consists of two dielectric substrates and a waveguide. The substrates are inserted inside the waveguide, and different from the waveguide BRF in the previous section, they are placed on both upper and lower inner walls by a conductive adhesive. Fig. 2.3.2 shows the dielectric substrates apart. All surfaces of the substrates are metalized except rectangular coupling slots placed  $\lambda_g/4$  at  $f_0$  apart along the waveguide axis, where  $\lambda_g$  is the guide wavelength in the waveguide and  $\lambda_r$  is the wavelength inside the substrate. Parallel via-hole arrays inside the substrates are also placed along the waveguide axis, and the distance between the coupling slot and the via-hole array is  $\lambda_r/4$  at  $f_0$ . SIW resonators are then embedded in the substrates, those resonate at  $f_0$  with the resonant mode where E-fields are the highest around the coupling slots and the lowest near the via-hole array. Fig. 2.3.3 shows the dominant resonant mode of the SIW resonators at the resonant frequency, where E-fields intensity is the highest at the coupling slot and the

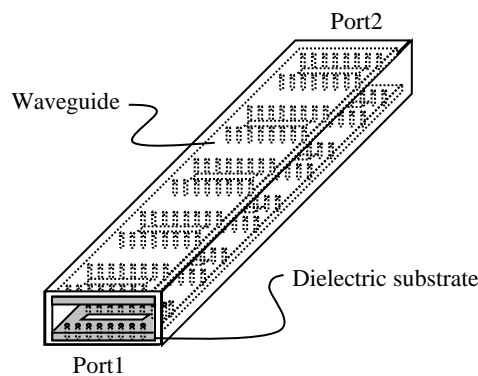


Fig. 2.3.1 A configuration of the waveguide BRF using SIW resonators.

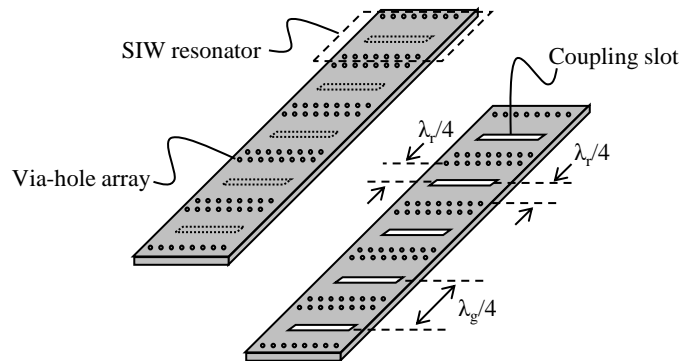


Fig. 2.3.2 The dielectric substrates shown in Fig. 2.3.1.

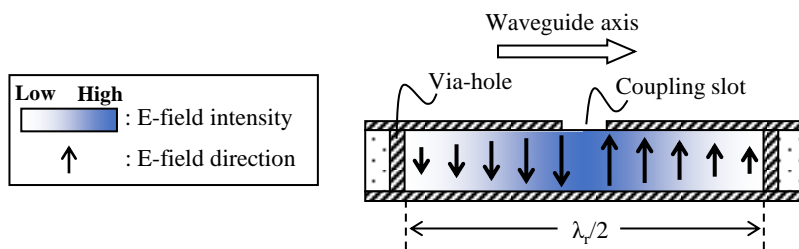


Fig. 2.3.3 The dominant resonant mode of the SIW resonator at the resonant frequency.

lowest near the via-hole. Contrary to the waveguide BRF in the previous section, the comparison of this mode with the main propagation mode in the waveguide suggests that two modes are electrically coupled, since their electric fields are in parallel with each other.

Since the concept of the configuration of this waveguide BRF is same as the previous section, which is to position resonators in a waveguide along the waveguide axis with equal intervals, the equivalent circuit for the waveguide BRF in this section is basically the same with those shown in Fig. 2.2.4 and Fig. 2.2.5 in the previous section. Opposing two SIW resonators can be represented by a series-connected parallel resonator and note that the number of the order is five in this section.

Design specification for the waveguide BRF is shown in Table 2.3.1, which is same as the table 2.2.1 shown in the previous section. An alumina substrate ( $\epsilon_r$ : 10.0,  $\tan\delta$ : 0.0001, thickness: 0.38 mm) is applied for its high-precision metal-patterning process. Same with the previous section, dimension of cross-sectional areas of the I/O ports are  $2.4 \times 4.8 \text{ mm}^2$ , and the cut-off frequency is 31 GHz.

The distance between the coupling slots along the waveguide axis is  $\lambda_g/4$  as shown in Fig. 2.3.2. Though the distance between the coupling slot and the via-hole array in the SIW resonator is denoted as  $\lambda_r/4$  in Fig. 2.3.2, detailed value needs to be obtained through the EM-analysis to consider the diameter and pitch of the via holes. Remained parameters to be determined in the design are lengths of short and long sides of the coupling slot;  $w_{\text{slot}}$  and  $L_{\text{slot}}$ . These parameters can be obtained from following procedures by EM-analysis, performed by commercial Finite-Element-Method (FEM) software.

Fig. 2.3.4 shows an EM-analysis model of the SIW resonator, where two parallel via-hole arrays ( $\phi$ : 0.2 mm, pitch: 0.5 mm) are positioned inside the dielectric substrate and all surfaces of the substrate are metallized. The distance between the two via-hole array along the waveguide axis is defined as  $d_{\text{via}}$ . In the design,  $d_{\text{via}}$  is used as a parameter in the EM-analysis to find suitable  $d_{\text{via}}$  that demonstrates the dominant resonant mode shown in Fig. 2.3.3 at  $f_0$ . The initial value for  $d_{\text{via}}$  is 1.01 mm ( $\lambda_r/2$ ), and from the EM-analysis results, suitable  $d_{\text{via}}$  was found to be 1.13 mm.

Table 2.3.1 The design specification for the waveguide BRF using SIW resonators.

	Passband 44.2 - 44.5 GHz	Stopband 46.7 - 47.0 GHz
$S_{21}$ [dB]	> -2	< -50

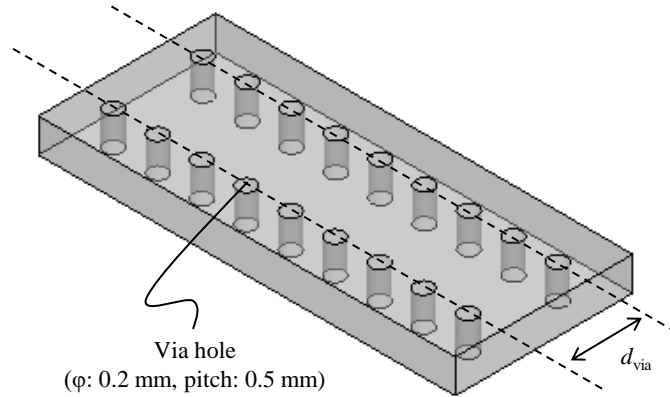
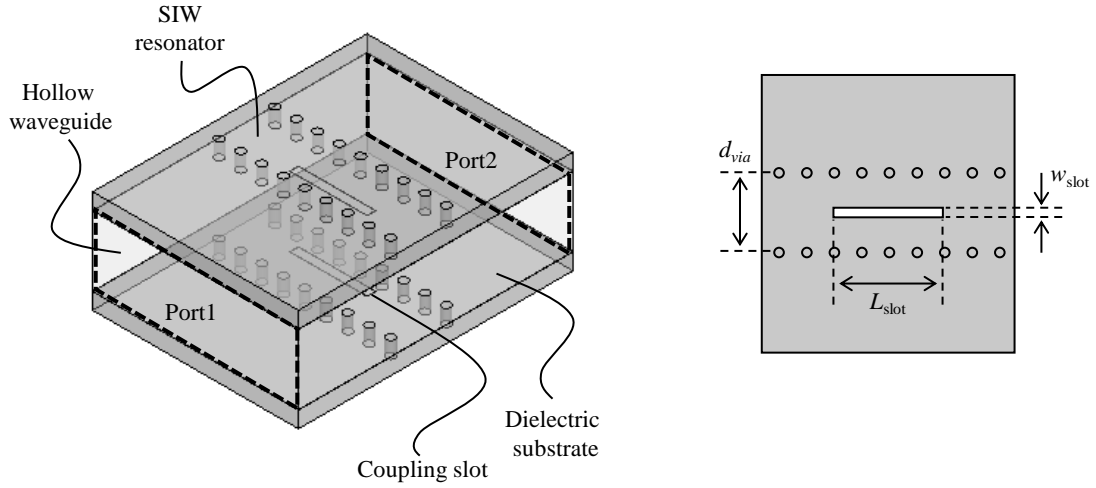


Fig. 2.3.4 The EM-analysis model of the SIW resonator.

Fig. 2.3.5 shows EM-analysis model for estimating  $Q_e$  of the SIW resonators. The model consists of a waveguide and two dielectric substrates placed on both upper and lower inner walls of the waveguide, and one SIW resonator is embedded in each substrate. All surfaces of the substrates are metalized except rectangular coupling slots, whose lengths of short and long sides are  $w_{\text{slot}}$  and  $L_{\text{slot}}$ . At the resonant frequency, the electromagnetic wave would be more likely to resonate in the SIW resonators than to propagate through the waveguide. As a result, the transmission coefficient  $S_{21}$  forms an attenuation pole at the resonant frequency. From the EM-analysis result,  $Q_e$  can be obtained from (2.2.6) and (2.2.7), the equations already shown in the previous section. Fig. 2.3.6 shows obtained relations between  $(w_{\text{slot}}, L_{\text{slot}})$  and  $Q_e$  from the EM-analysis results with several values of  $w_{\text{slot}}$  and  $L_{\text{slot}}$ . Same as the previous section, suitable values of  $w_{\text{slot}}$  and  $L_{\text{slot}}$  for required  $Q_e$  can be determined from the figure.

Table 2.3.2 shows the parameters of the prototype filter used in the design: a loss-less 5th order Chebyshev filter with 0.05-dB of passband ripple. Fig. 2.3.6 shows calculated results of the prototype filters, which meets the specification well. By instituting the parameters shown in



(a) Perspective view of the model.

(b) Top view of the substrate.

Fig. 2.3.5 The EM-analysis model for estimating external  $Q$ -factor of the SIW resonators.

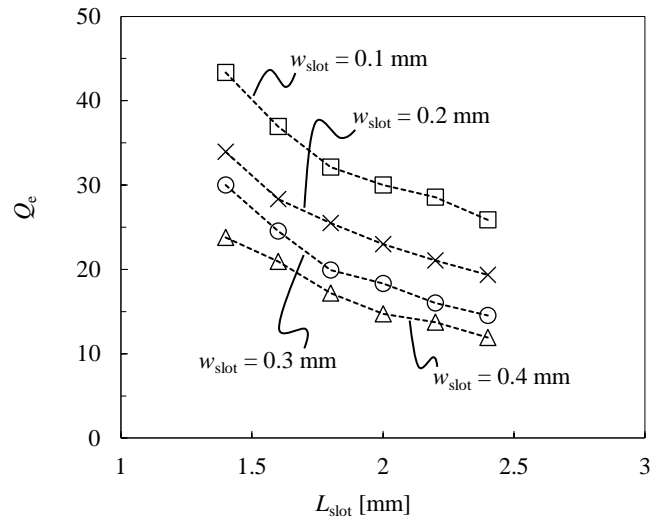


Fig. 2.3.6 The relations between  $(w_{slot}, L_{slot})$  and  $Q_e$ .

Table 2.3.2 into (2.2.5), required values for  $Q_{e,j}$  can be obtained. And from the obtained  $Q_{e,j}$  and Fig. 2.3.7,  $w_{\text{slot}} \times L_{\text{slot}}$  of the SIW resonators can be determined as shown in Table 2.3.3. Although the obtained  $w_{\text{slot}} \times L_{\text{slot}}$  are not the same, however, the differences are not so large and  $w_{\text{slot}} \times L_{\text{slot}}$  for the SIW resonators were supposed to be constant ( $0.2 \times 1.8 \text{ mm}^2$ ) this time to suppress manufacturing errors.

Full EM-analysis model of the waveguide BRF can be configured by cascading the EM-analysis model shown in Fig. 2.3.5. Finally, designed values shown in Table 2.3.4 were obtained after optimization with the full EM-analysis model. Fig. 2.3.8 shows the EM-analysis results of the full EM-analysis model of the waveguide BRF which satisfies high attenuation characteristic at the 47 GHz band and meets well with the calculated result of the prototype filter.

Table 2.3.2 The parameters of the prototype filter used in the design.

Chebyshev filter (ripple: 0.05 dB, 5th order)			
$g_0$	1.0	$f_0$	46.85 GHz
$g_1$	0.9732	$w$	8%
$g_2$	1.3723		
$g_3$	1.8032		
$g_4$	1.3723		
$g_5$	0.9732		
$g_6$	1.0		

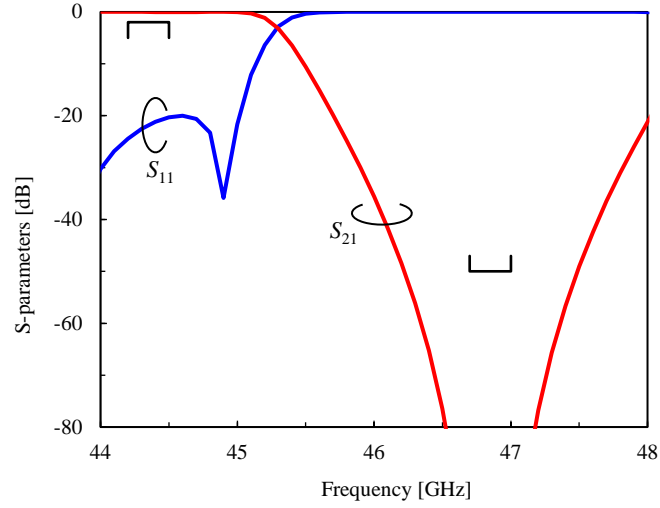


Fig. 2.3.7 Calculated results of the prototype filters.

Table 2.3.3 Required values of  $Q_{e,j}$  and  $w_{\text{slot}} \times L_{\text{slot}}$  for the SIW resonators.

	$Q_{e,1}$	$Q_{e,2}$	$Q_{e,3}$	$Q_{e,4}$	$Q_{e,5}$
Required value	25.7	18.2	13.9	18.2	25.7
$w_{\text{slot}} \times L_{\text{slot}} [\text{mm}^2]$	$0.2 \times 1.7$	$0.3 \times 1.8$	$0.4 \times 2.0$	$0.3 \times 1.8$	$0.2 \times 1.7$

Table 2.3.4 Designed values.

Parameter	Designed value [mm]
$d_{\text{via}}$	1.13
Distance between the coupling slots	2.5
$w_{\text{slot}}$	0.2
$L_{\text{slot}}$	1.8

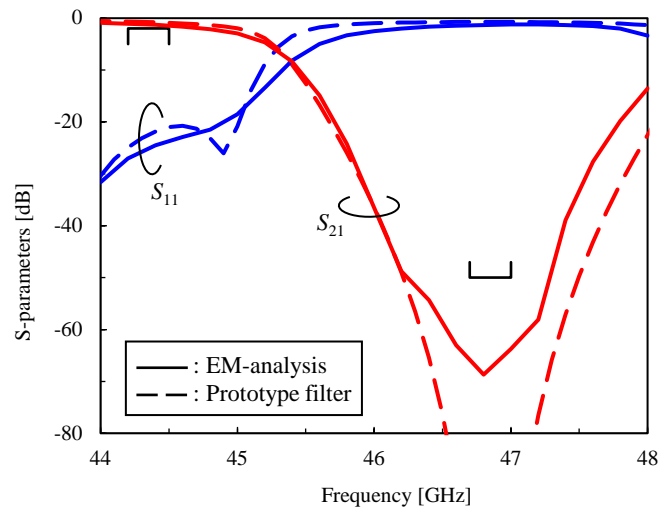


Fig. 2.3.8 The EM-analysis results of the waveguide BRF.



### 2.3.2 Experiment

A fabricated waveguide BRF is shown in Fig. 2.3.9. Five SIW resonators are embedded in each of two alumina substrates placed on both upper and lower inner walls of the main waveguide formed by assembled aluminum flanges. Though the whole size of the aluminum flanges is  $30 \times 30 \times 30$  mm<sup>3</sup>, the actual size of the fabricated BRF itself is  $2.4 \times 4.8 \times 12.0$  mm<sup>3</sup>, which is relatively low-profile and compact.

Fig. 2.3.10 shows the experimental results, where EM-analysis results and calculated results of the prototype filter are also represented by dotted and dashed lines, respectively. The measurement system is same as that used in the previous section. Though a slight frequency shift to higher frequency range was present, the measured results showed relatively high attenuation more than 50 dB at 46.7 - 47.0 GHz and low insertion loss less than 1.6 dB at 44.2 - 44.5 GHz,

The insertion loss was slightly higher than that of the configuration in the previous section. This may come from the difference between the assemblies of the main waveguides. In the first configuration, the main waveguide is separated at the middle of both upper and lower walls, where current is relatively scarce even when electromagnetic wave propagates inside the main waveguide. On the other hand, the main waveguide of the configuration in this section is separated at the middle of side walls, where current is relatively concentrated when electromagnetic wave propagates inside the main waveguide, resulting in deteriorating insertion loss due to the discontinuities.

The frequency shift is possibly caused by the manufacturing error of the via holes depending on the accuracy of the laser process, which is generally worse than that of the patterning process for alumina substrates. It can be expected that the diameter of fabricated via holes were larger than designed, and the resonant frequency of the SIW resonators shifted to higher frequency. Other possible reasons are production errors, such as errors in thickness and dielectric constant of the substrates.

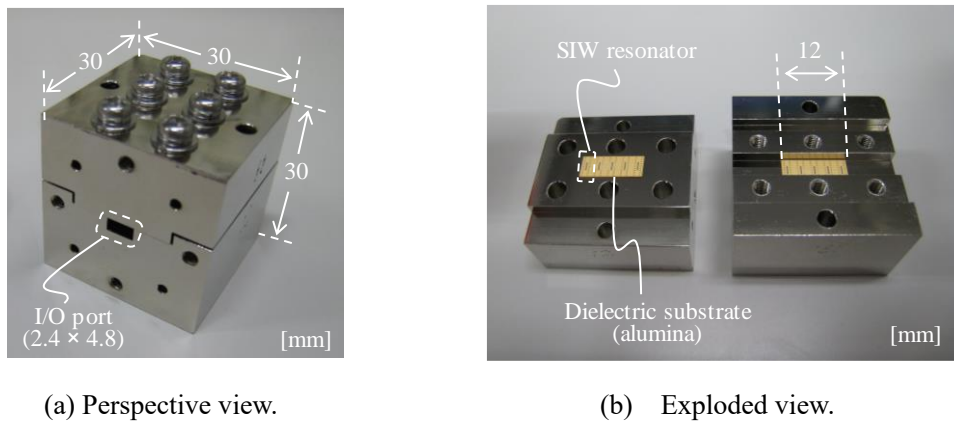


Fig. 2.3.9 The fabricated waveguide BRF.

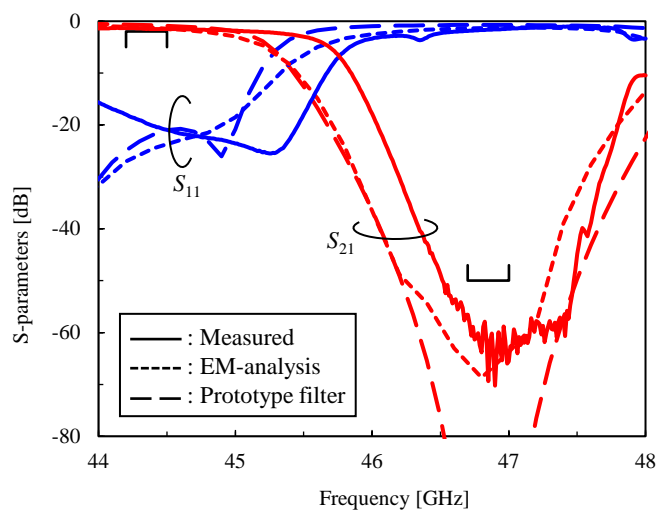


Fig. 2.3.10 The measured results of the fabricated waveguide BRF.

## 2.4 Summary

In this chapter, two configurations of low-profile waveguide BRF were proposed and evaluated. Differ from the conventional waveguide BRF where cavity resonators are located outside the main waveguide, resonators-loaded dielectric substrates are placed on inner walls of the main waveguide in both configurations. At the resonant frequency of the resonator, an electromagnetic wave propagating through the main waveguide would be more likely to resonate at the resonators than to continue propagating through the main waveguide. As a result, propagation of the electromagnetic wave is suppressed and the configurations work as a waveguide BRF.

In the first configuration, open-ended  $\lambda/2$  microstrip resonators are mounted on the dielectric substrates those are inserted inside the waveguide and placed on both inner side walls. A comparison of dominant resonant mode of the open-ended  $\lambda/2$  microstrip resonators with the main propagation mode of the waveguide suggested that the two modes are magnetically coupled. A waveguide BRF of this configuration for Q-band was designed by the design process based on filter theory and EM-analysis. The 4th order waveguide BRF using open-ended  $\lambda/2$  microstrip resonators was fabricated according to the design process, and the measured results showed steep band rejection characteristic with relatively high attenuation more than 50 dB at 46.7 – 47.0 GHz with insertion loss less than 1.3 dB at 44.2 – 44.5 GHz.

In the second configuration, SIW resonators are embedded in the dielectric substrates those are inserted inside the waveguide and placed on both upper and lower inner walls. A comparison of dominant resonant mode of the SIW resonators with the main propagation mode of the waveguide suggested that the two modes are electrically coupled, which is different from the previous configuration. A waveguide BRF of this configuration for Q-band was designed by the design process based on filter theory and EM-analysis. The 5th order waveguide BRF using SIW resonators was

fabricated according to the design process, and the measured results showed steep band rejection characteristic with relatively high attenuation more than 50 dB at 46.7 – 47.0 GHz and insertion loss less than 1.6 dB at 44.2 – 44.5 GHz.

In the two configurations in this chapter, although type of the resonator and the coupling manner from the electromagnetic wave propagating through the main waveguide to the resonators are different, more than 50 dB attenuation at Q-band was obtained by both configurations. However, insertion loss of the first configuration was slightly lower than that of the second configuration. This may be caused by difference between the assemblies of the main waveguides. In the first configuration, the main waveguide is separated at the middle of both upper and lower walls, where current is relatively scarce even when electromagnetic wave propagates inside the main waveguide. On the other hand, the main waveguide of the second configuration is separated at the middle of side walls, where current is relatively concentrated when electromagnetic wave propagates inside the main waveguide, resulting in deteriorating insertion loss due to the discontinuities. From this reason, lower insertion loss can be expected for the first configuration than the second configuration. Nevertheless, the main waveguide is sometimes necessary to be separated at the middle of side walls because of the assembly of the whole system or combination with other components, patch array antennas and coaxial waveguide adapter for example. In these cases, the second configuration is preferable though its disadvantage in insertion loss.

Besides, since power capability of the waveguide BRF is not considered in this dissertation, power consumption and withstand power should be considered additionally for a practical use in high-power applications.

## References

- [2.1] G. Matthaei, L. Young, and E. M. T. Jones, *Microwave Filters, Impedance Matching Networks, and Coupling Structures*, New York: McGraw-Hill, 1964.
- [2.2] M. A. Gerdine, "A Frequency-Stabilized Microwave Band-Rejection Filter Using High Dielectric Constant Resonators," *IEEE Trans. Microwave Theory & Tech.*, vol. 17, no. 7, pp. 354-359, July 1969.
- [2.3] J.A.G. Malherbe and J. C. Coetzee, "Bandstop Filter in Nonradiative Dielectric Waveguide Using Rectangular Resonators," *IEEE Trans. Microwave Theory & Tech.*, vol. 35, no. 12, pp. 1161-1163, December 1987.
- [2.4] K. Kobayashi and C. Inoue, "Bandpass and bandstop filters using dominant TM<sub>01δ</sub> mode dielectric rod resonators," in *1997 IEEE MTT-S Int. Microwave Symp. Dig.*, vol. 2, pp. 793-796, Denver, CO, USA, June 1997.
- [2.5] H. Uchida, J. Nakayama, H. Ikeda, Y. Yoshikawa, Y. Imai, N. Yoneda, and M. Miyazaki, "Dielectric Resonator Elliptic-Function Band Rejection Filter with External Coupling Waveguide," in *Proc. 33rd European Microwave Conference 2003*, pp. 183-185, Munich, Germany, October 2003.
- [2.6] J. Y. Jin, X. Q. Lin and Q. Xue, "A Novel Dual-Band Bandpass E-Plane Filter Using Compact Resonators," *IEEE Trans. Microw. Theory Techn.*, vol. 26, no. 7, pp. 484-486, July 2016.
- [2.7] A. Yamamoto, T. Ohwada, and N. Yoneda, "Waveguide E-plane Band Rejection Filters with Lightning-shape One-wavelength Conductors," in *Proc. 2010 40th European Microwave Conference*, pp. 958-961, Paris, France, September 2010.

- [2.8] S. S. Pajović, M. Potrebić, D. Tošić, Z. Stamenković, “E-plane Waveguide Bandstop Filter with Double-sided Printed-circuit Insert,” *Facta Universitatis, Series: Electronics and Energetics*, vol. 30, no. 2, pp. 223-234, June 2017.
- [2.9] J. Y. Jin and Q. Xue, “A type of E-plane filter using folded split ring resonators (FSRRs),” in *Proc. Asia–Pacific Microw. Conf. (APMC)*, pp. 1-3, Nanjing, China, December 2015.
- [2.10] M. Ito, K. Maruhashi, K. Ikuina, T. Hashiguchi, S. Iwanaga, and K. Ohata, “A 60-GHz-band planar dielectric waveguide filter for flip-chip modules,” *IEEE Trans. Microwave Theory & Tech.*, vol. 49, no. 12, pp. 2431-2436, December 2001.
- [2.11] D. Deslandes and K. Wu, “Design Consideration and Performance Analysis of Substrate Integrated Waveguide Components,” in *Proc. 2002 32nd European Microwave Conference*, pp. 1-4, Milan, Italy, October 2002.
- [2.12] D. Deslandes and K. Wu, “Millimeter-wave substrate integrated waveguide filters,” in *Proc. IEEE CCECE 2003 Canadian Conference on Electrical and Computer Engineering*, vol. 3, pp. 1917-1920, Montreal, QC, Canada, May 2003.
- [2.13] E. N. Torgow and G. E. Collins, “Band-Stop Filters for High-Power Applications,” *IEEE Trans. Microwave Theory & Tech.*, vol. 13, no. 5, pp. 508-513, September 1965.

# Chapter 3

## Configurations for a Gasket-free Electromagnetic Shielding Structure

### 3.1 Introductory Remarks

As wireless devices have been developed and spread widely in recent years, the risks of radio-wave interferences and information leakage may sometimes become a problem. A shielded enclosure is a common and conventional solution, which basically consists of metal walls and shielded doors using contact-type conductive gaskets. However, communication devices are not available inside, since shielding effectiveness (SE) of such a shielded enclosure is continuous in frequency. To realize both SE at specific frequency bands and capability of other device using other frequency bands, a shielded room having frequency selectivity is sometimes required. For such frequency-selective shielded rooms, SE of more than 40 dB is generally required.

For this requirement, various types of shielding structures having SE at specific frequency bands have been developed and reported. For walls and windows of a shielded room, frequency selective surface (FSS) is a standard solution [3.1] - [3.9]. FSS basically consists of planar periodic conductive pattern elements fabricated on a dielectric substrate, and mainly works as a kind of a band stop filter at resonant frequencies of the elements. The FSS is usually designed for decreasing electromagnetic wave whose direction of propagation is almost perpendicular to the surfaces of the walls or the windows. For examples, square-loop periodic elements are used in [3.1] to obtain SE at

2.4 GHz band, two different-sized “four-legged loaded” elements are used in [3.2] to obtain narrower bandwidth, full and split ring elements with varactor diodes and surface mount resistors are used in [3.3] to obtain reconfigurable SE at 2.4 GHz band, two-layered loop and square elements are used in [3.4] to obtain wide-band SE at 7.5 – 16.2 GHz, and convoluted square loop elements with six meander peaks on each arm are used on opaque walls in [3.5] to obtain narrow SE at 1.5 – 2.5 GHz. Moreover, a combination of rings, loops, and slot elements are used in [3.6] to obtain either a reject or passband single-layer filter at 2.4 GHz and 5.2 GHz bands for Wi-Fi applications, five resonant elements are used in [3.7] to obtain SE at 2.4 GHz, 3.5 GHz, 4.5 GHz, and 5.5 GHz bands for the security purpose in mobile communication, two-layered conductive and resistive FSSs are used in [3.8] to obtain low-profile configuration and SE at 5 GHz band, and periodic double ring strip FSSs are used in [3.9] to obtain SE at 2.45 GHz and 5.4 GHz bands.

A shielded room usually has a shielded door, where a gap exists between the door and the door frame. In general, a contact-type conductive gasket is applied to realize SE at the gap, which physically connect the door and the door frame when the door is closed. Though relatively high, sometimes more than 100 dB, SE can be realized, the SE is continuous in frequency and not applicable for realizing frequency selectivity. Furthermore, since high contact pressure is required when the door is closed, aged deterioration mainly due to opening and closing operations of the door is inevitable in principle and regular maintenance is necessary. Aged deterioration caused by corrosive environments is reported in [3.10], and the reliability of a conductive gasket is assessed by using a TEM cell in [3.11] or using a stripline setup in [3.12]. Several types of conductive gaskets in environmentally worst cases are modeled and their SE are estimated and compared with simulated results in [3.13]. Contrary to the contact-type conductive gaskets, some gasket-free shielding structures are reported in [3.14] and this chapter. Since high contact pressure is not needed for such gasket-free shielding structures even when the door is closed, opening and closing operations of the door do not induce the aged deterioration,



and moreover, an ordinary simple door structure is applicable. In [3.14], several kinds of magnetic materials, called magnetic absorbers, are placed on the inner walls of the gap and measured results showed 15-dB improvement of SE in a wide frequency band from 100 MHz to 2.5 GHz.

In this chapter, gasket-free electromagnetic shielding structures using SIW resonators are proposed and evaluated. Fig. 3.1.1 shows a simplified configuration of the structure. In the structures, SIW resonators are embedded in dielectric substrates placed on the inner walls of the gap. The SIW resonators are arranged in a cascaded configuration along the direction of propagation and designed to have slightly different resonant frequencies. At the resonant frequencies of the SIW resonators, electromagnetic wave propagating through the gap would be more likely to resonate at the SIW resonators than to propagate through the gap. As a result, wide-band SE including the resonant frequencies of the SIW resonators can be expected as shown in Fig. 3.1.2. A gasket-free shielding structure for 12 - 15.5 GHz, for 2.4 GHz band, and for both 2.4 GHz and 5 GHz bands are proposed in section 3.2, section 3.3, and section 3.4, respectively. In each section of this chapter, the configuration of the proposed structure is shown first. Design process based on EM analysis is shown next, and finally, measured results of SE of the fabricated structure is shown.

The shielding structures referred above are compared in Table 3.1.1, showing their applicable places, applicable frequencies, and applicability of frequency selectivity. Some other shielding techniques are reported in [3.15] - [3.17]. Magnetic materials are used in [3.15] to mitigate the magnetic field leaked from the joint parts of a shielded enclosure at several kHz up to several hundreds of kHz, showing 20-dB improvement of SE. Alternatives to conductive gaskets are studied in [3.16], and experimental results showed that grounding points or lossy materials can be used instead of conductive gaskets below 1 GHz, when required SE is less than 30 dB. A door-less access passage to a shielded enclosure is studied in [3.17], indicating some design rules and limitations of the passage.

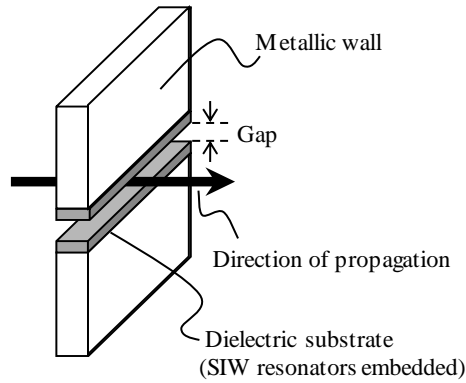


Fig. 3.1.1 A simplified configuration of the gasket-free shielding structure.

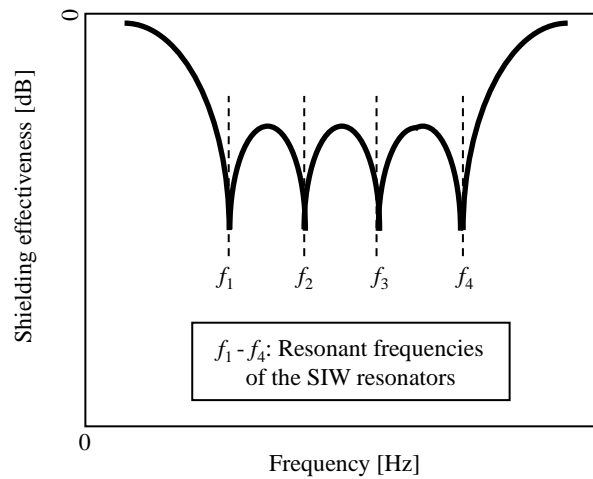


Fig. 3.1.2 A simplified shielding effectiveness of the gasket-free shielding structure.

Table 3.1.1 The comparison of the referred shielding structures.

Shielding structures [ref]	FSS [3.1] - [3.9]	Conductive gasket [3.10] - [3.13]	Magnetic absorber [3.14]	Cascaded SIW resonators (This chapter)
Applicable place	Walls	Gap between door and door frame	Gap between door and door frame	Gap between door and door frame
Applicable frequency	Several GHz to several-tens GHz	All frequency (ideally)	kHz to several GHz	Several GHz to several-tens GHz
Frequency selectivity	Applicable	N/A	N/A	Applicable

## 3.2 A gasket-free Electromagnetic Shielding Structure for 12 – 15.5 GHz Using Cascaded SIW Resonators

### 3.2.1 Configuration

Fig. 3.2.1 shows cascaded SIW resonators embedded in a double-layered dielectric substrate. The surfaces of the substrate are covered with conductive patterns except for coupling slots, and the coupling slots and via-hole arrays are placed alternately along the direction of propagation. In cross section of each SIW resonator, the coupling slot is positioned at the center, and the distance between the via hole and the coupling slot is  $\lambda_r/4$  at its own resonant frequency. Fig. 3.2.2 shows the dominant resonant mode of an SIW resonator, where E-fields intensity is the highest at the coupling slot and the lowest near the via hole.

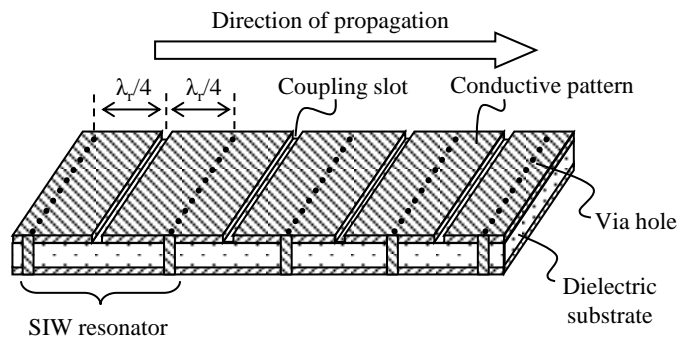


Fig. 3.2.1 Cascaded SIW resonators embedded in a double-layered dielectric substrate.

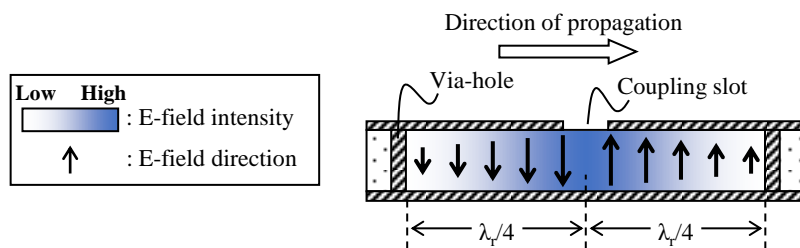


Fig. 3.2.2 The dominant resonant mode of the SIW resonator at the resonant frequency.

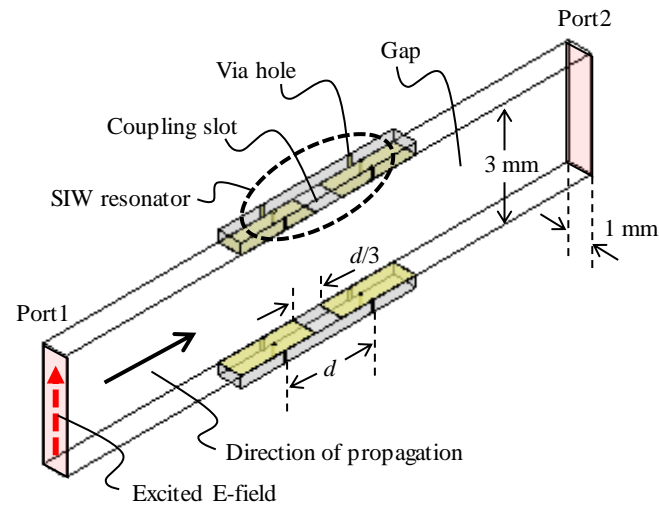
### 3.2.2 Design

The cascaded SIW resonators for the shield band of 12 – 15.5 GHz was design by following design process. Before designing the cascaded configuration, a design process for a single SIW resonator having arbitrary resonant frequency  $f_r$  must be cleared first. The main design parameter of a single SIW resonator is the distance between via-hole arrays,  $d(f_r)$ . As shown in Fig. 3.2.1,  $d(f_r)$  can be roughly estimated by

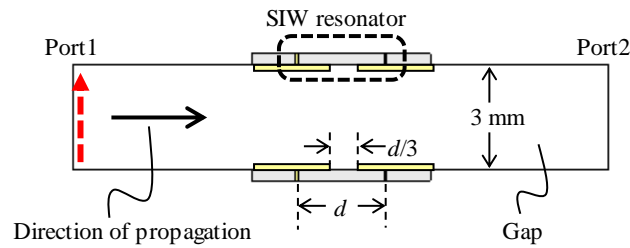
$$d(f_r) = \frac{c}{2f_r\sqrt{\epsilon_r}} , \quad (3.2.1)$$

where  $f_r$  is a resonant frequency of an SIW resonator,  $\epsilon_r$  is a relative dielectric constant of the dielectric substrate, and  $c$  is the speed of light. This equation indicates that  $d(f_r)$  is equivalent to half wavelength at its resonant frequency in the substrate. Though this equation is enough for a rough estimation, a more accurate equation is preferable for the design, because some other parameters are not considered: thickness of the substrate, diameter and pitch of the via holes, width of the coupling slots, for example.

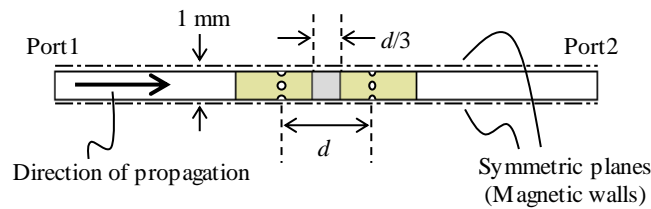
An EM-analysis using the finite element method and a numerical approach can take these parameters into account. Fig. 3.2.3 shows the EM-analysis model to obtain more accurate  $d(f_r)$ , where a gap is modeled by a thin air box of 3-mm height and 1-mm width and note that the sidewalls are defined as magnetic walls to work as symmetric boundaries. Double-sided FR4 substrates ( $\epsilon_r$ : 4.3,  $\tan\delta$ : 0.01, thickness: 0.6 mm) with a copper conductor ( $\sigma$ :  $5.8 \times 10^7$  Sie/m, thickness: 0.02 mm) and via holes ( $\phi$ : 0.15 mm, pitch: 0.5 mm) are placed on both upper and lower inner walls of the gap, and one SIW resonator is embedded in each substrate. The distances between the via holes along the direction of propagation are defined as  $d$ , and width of the coupling slot is fixed to  $d/3$  to simplify the design. Port1 and Port2 are defined at the edges of the gap, and the source of the electromagnetic



(a) Perspective view.



(b) Side view.



(c) Top view.

Fig. 3.2.3 The EM-analysis model to obtain more accurate  $d(f_r)$ .

wave propagating through the gap is modeled by a vertically excited E-field at Port1. In the EM analysis results of this model,  $S_{21}$  forms an attenuation pole at resonant frequency of the SIW resonator, from which one relation between  $d$  and  $f_r$  can be obtained. Fig. 3.2.4 shows an example of the EM-analysis result with  $d$  of 10 mm, where  $S_{21}$  forms an attenuation pole at 8.9 GHz. By applying a

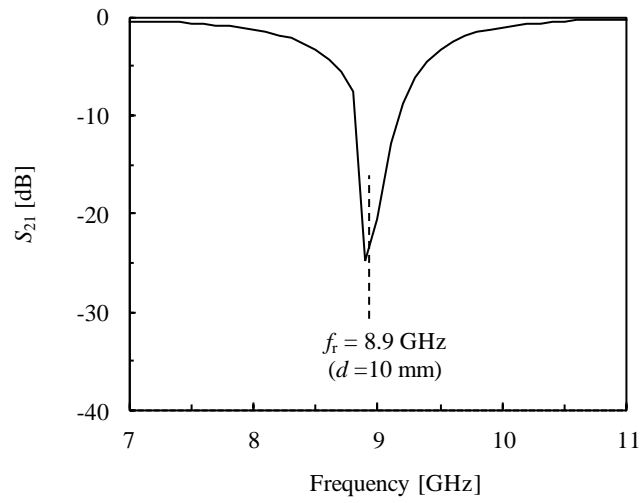


Fig. 3.2.4 An example of the EM-analysis result ( $d=10$  mm).

polynomial approximation to the relations between  $d$  and  $f_r$  obtained from EM-analysis results using various values of  $d$ , a numerical expression of  $d(f_r)$  can be obtained which is expected to be suitable for the design.

By considering the rough estimation of (3.2.1), a 2nd order polynomial of  $1/f_r$  was adopted this time, and the least square method was applied. The obtained approximate equation of  $d(f_r)$  is

$$d(f_r) = -\frac{290}{(f_r[\text{GHz}])^2} + \frac{150}{f_r[\text{GHz}]} - 3.1 \quad [\text{mm}] . \quad (3.2.2)$$

Fig. 3.2.5 shows relations between  $d$  and  $f_r$  obtained from the EM-analysis results, from the rough estimation shown as (3.2.1), and from the approximate equation just shown above as (3.2.2). Since approximate equation (3.2.2) correlates well with the EM-analysis results within wide frequency range including the shield band, the equation can be expected to be suitable for the design.

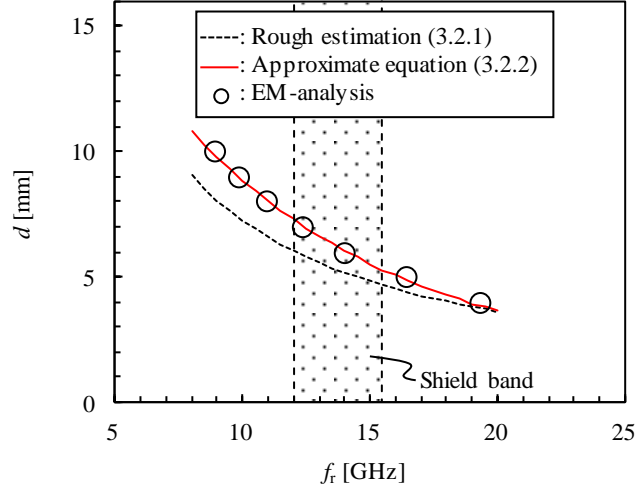


Fig. 3.2.5 Relations between  $d$  and  $f_r$  obtained from the EM-analysis results, the rough estimation of  $d(f_r)$  shown as (3.2.1), and the approximated equation shown as (3.2.2)

A cascaded configuration of SIW resonators can be designed by cascading SIW resonators having resonant frequencies in the shield band. Before designing the individual SIW resonator, the order number of the cascaded configuration should be determined. The initial value of the order number  $N_{\text{init}}$  can be obtained from

$$N_{\text{init}} = \left\lceil \frac{L_{\text{perm}}}{d_{\text{high}}} \right\rceil, \quad (3.2.3)$$

where  $L_{\text{perm}}$  is permitted length for the design along the direction of propagation, and  $d_{\text{high}}$  is  $d$  of the SIW resonator having the resonant frequency at the highest edge of the shield band. Resonant frequencies of the SIW resonators can be then obtained by supposing that resonant frequencies of the SIW resonators are within the shield band at equal frequency interval. The  $d$  of individual SIW resonators can be obtained by substituting corresponding  $f_r$  into  $d(f_r)$ , and total length of the cascaded

configuration along the direction of propagation is sum of them. In the case that the total length exceeds  $L_{\text{perm}}$ , the order number starting with  $N_{\text{init}}$  is required to be reduced by one till the total length becomes less than  $L_{\text{perm}}$ . According to this process, 8th order cascaded configuration was adopted for  $L_{\text{perm}}$  of 55 mm in this case.

Fig. 3.2.6 shows the EM-analysis model of the 8th order cascaded SIW resonators. Eight SIW resonators (SIW<sub>1</sub> - SIW<sub>8</sub>) simply cascaded along the direction of propagation are embedded in the dielectric substrates placed on both upper and lower inner walls of the gap. Note that the side walls are defined as magnetic walls those work as symmetric boundaries, which is same as the EM-analysis model shown in Fig. 3.2.3. Table 3.2.1 shows designed values of  $f_r$  and  $d$  of the cascaded SIW resonators, where  $d$  is obtained by substituting  $f_r$  into (3.2.2), and the total size along the direction of propagation is 52 mm. Fig. 3.2.7 shows the EM-analysis result, demonstrating remarkable decrease of the transmission coefficient  $S_{21}$  at the shield band of 12 - 15.5 GHz. In the case that  $S_{21}$  is not decreased well in the shield band, design conditions should be reconsidered.

The design process described in this section is summarized by a flowchart shown in Fig. 3.2.8. In the process, the resonant frequencies of the SIW resonators are determined to have equal frequency interval and lined up in order from the lowest frequency to the highest frequency, however, establishing other process for determining the resonant frequencies of the SIW resonators to realize better SE will be our future work.



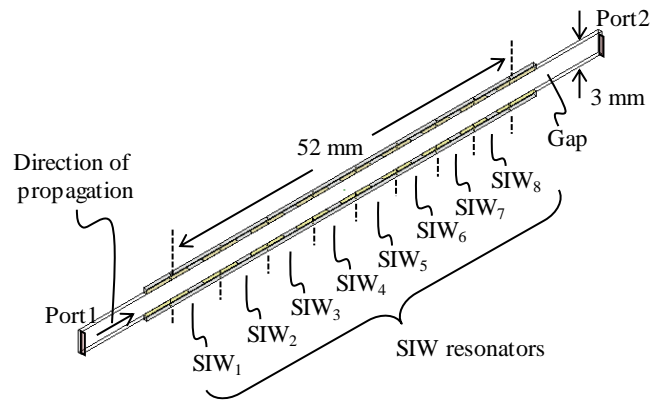


Fig. 3.2.6 The EM-analysis model of the 8th order cascaded SIW resonators.

Table 3.2.1 Designed values of  $f_r$  and  $d$  of the cascaded SIW resonators.

	SIW <sub>1</sub>	SIW <sub>2</sub>	SIW <sub>3</sub>	SIW <sub>4</sub>	SIW <sub>5</sub>	SIW <sub>6</sub>	SIW <sub>7</sub>	SIW <sub>8</sub>
$f_r$ [GHz]	12	12.5	13	13.5	14	14.5	15	15.5
$d$ [mm]	7.6	7.3	6.9	6.6	6.3	6.0	5.8	5.5

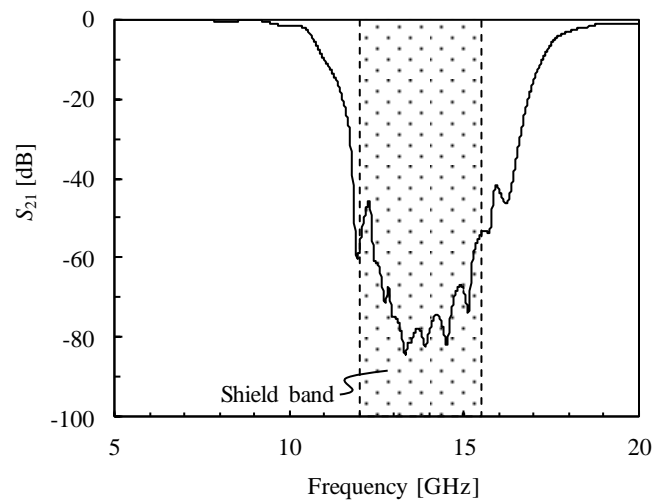


Fig. 3.2.7 The EM-analysis result of the 8th order cascaded SIW resonators.

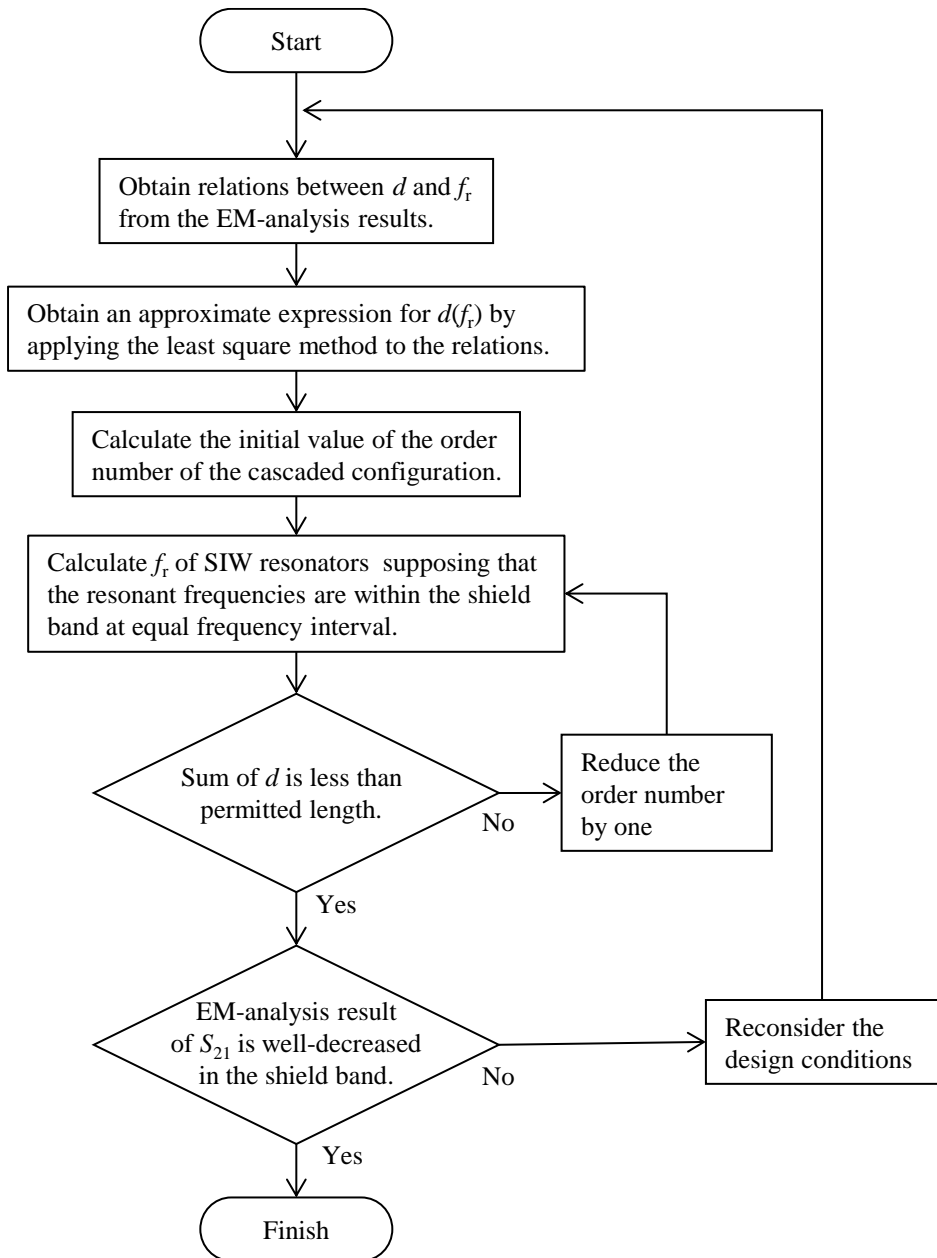


Fig. 3.2.8 A flowchart of the design process for cascaded SIW resonators.

### 3.2.3 Experiment

Fig. 3.2.9 shows a measurement system for evaluating SE. Tx- and Rx-antennas are positioned face to face across the gap of  $200 \times 3 \text{ mm}^2$  aperture size located on the wall of a shielded chamber. The Tx-antenna is connected to Port1 of a network analyzer and placed outside the chamber 1 m apart from the wall, while the Rx-antenna is connected to Port2 of the network analyzer via a pre-amplifier of 40-dB gain and placed inside the chamber at also 1 m apart from the wall. With this measurement system, SE can be evaluated by comparing measured results of  $S_{21}$  with and without the substrates. Fig. 3.2.10 shows a simplified cross-sectional view of the gap and Fig. 3.2.11 shows the gap seen from the Tx- and the Rx-antenna sides. The gap is filled with an elastic styrene foam to fix the substrates on both upper and lower inner walls of the gap. The foam can be almost ignored electromagnetically since the dielectric constant of the foam is almost same with that of the air. Fig. 3.2.12 shows the fabricated substrates whose dielectric constant and other parameters are the same as those used in the EM-analyses in the design process.

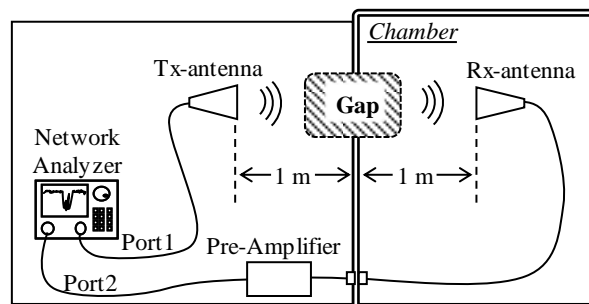


Fig. 3.2.9 The measurement system for evaluating SE.

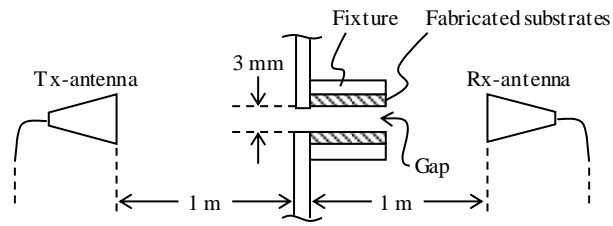
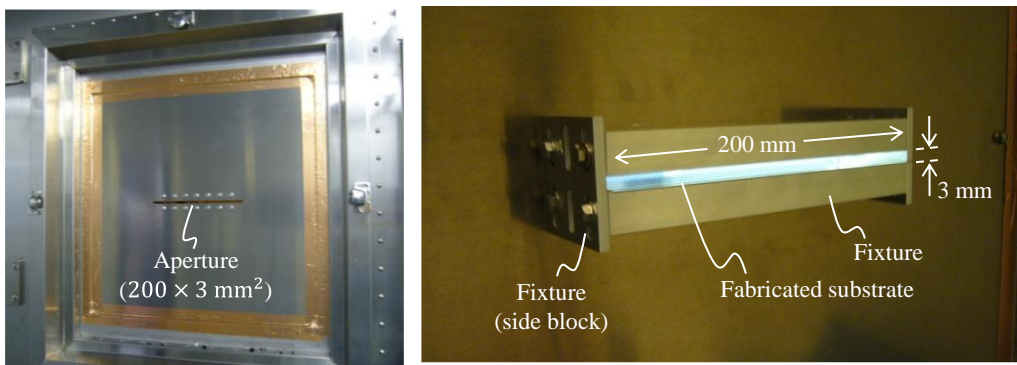


Fig. 3.2.10 A simplified cross-sectional view of the gap.



(a) Tx-antenna side.

(b) Rx-antenna side.

Fig. 3.2.11 The gap seen from both antenna sides.

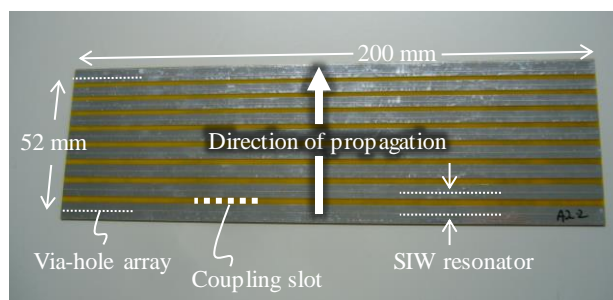


Fig. 3.2.12 The fabricated substrate.

Fig. 3.2.13 shows measured results of  $S_{21}$  of a free space and the gap with/without the substrates where cascaded SIW resonators are embedded. The measured frequency range is 5 - 18 GHz at 12 MHz intervals, and the gain of the pre-amplifier (+40 dB) is included in the measured  $S_{21}$ . SE can be evaluated by defining the measured  $S_{21}$  of a free space as a 0-dB reference. Fig. 3.2.14 shows measured results of SE of the gap with/without the substrates. The measured results showed 40-dB SE at the shield band, which is improved by 25 dB from SE of the gap alone by placing the cascaded SIW resonators on the inner walls of the gap. Note that since these results did not change with the fixture without the side blocks shown in Fig. 3.2.11 (b), the fixtures in the later sections are simplified to a side-block-less configuration.

Besides, tilting the Tx-antenna vertically in this measurement system is not expected to change the electromagnetic wave received at the Rx-antenna since excited E-field at the aperture and the direction of propagation in the gap is basically the same. On the contrary, tilting the Tx-antenna horizontally also tilts the direction of propagation horizontally in the gap. This change practically stretches the wavelength of the electromagnetic wave along the axis of the Rx-antenna, resulting in a shift in the frequency of the electromagnetic wave received at the Rx-antenna to a lower frequency. Therefore, for a practical use, it is desirable for the shielding structure to be designed to have wider-band characteristics on the low frequency side than the specifications.

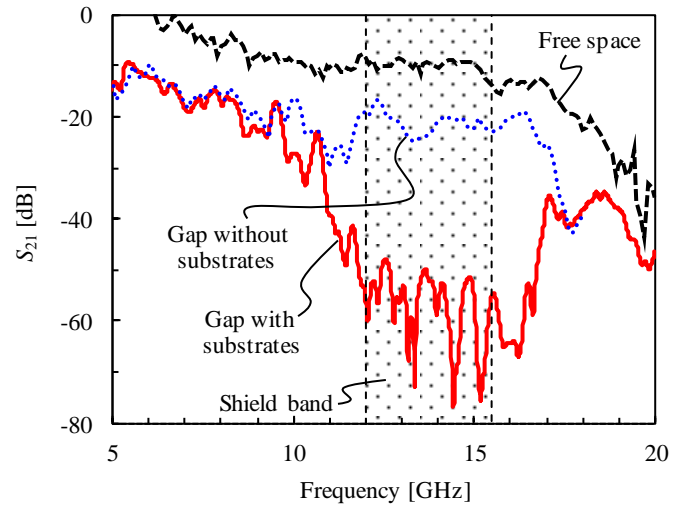


Fig. 3.2.13 The measured results of  $S_{21}$ .

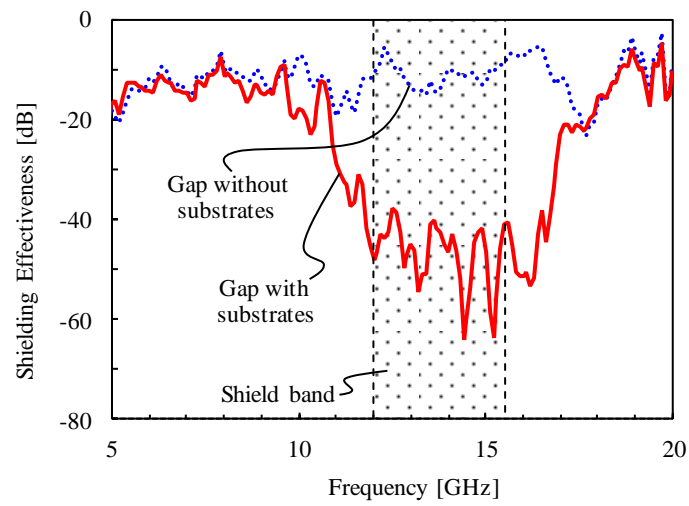


Fig. 3.2.14 The measured results of SE.

## **3.3 A Gasket-free Electromagnetic Shielding Structure for 2.4 GHz band Using Folded $\lambda/4$ SIW Resonators**

### **3.3.1 Configuration**

Since 2.4 GHz band is defined as one of the industrial, science, and medical radio bands (ISM bands), many electrical devices use this band for its convenience of license-free use. Crosstalk and information leakage are therefore more likely to be happened in this band, and a gasket-free shielding structure for this band is sometimes required. Applying conventional SIW resonators evaluated in the previous section at 2.4 GHz band is not practical, because the distance between via-hole arrays is  $\lambda_r/2$  at its own resonant frequency which generally becomes too large for a cascaded configuration in this band. For example, in the case of realizing the conventional SIW resonator at 2.4 GHz using an ordinal FR4 substrate, the distance becomes almost 30 mm, which indicates that miniaturization is necessary to realize the cascaded configuration in practical size. A dielectric substrate of high relative dielectric constant may become another solution for the miniaturization, however, total cost will hardly meet the requirement because such substrates are generally expensive and many substrates are generally required to cover the entire circumference of the shielded door and the door frame.

In this section, a gasket-free shielding structure using folded quarter-wavelength (FQ)-SIW resonators is proposed and evaluated. An FQ-SIW resonator is kind of an SIW resonator miniaturized by applying a multilayered dielectric substrate and modifying the position of the coupling slot. Fig. 3.3.1 shows a cross-sectional view of an FQ-SIW resonator embedded in a five-layered substrate. In contrast to the conventional SIW resonator shown in Fig. 3.2.1, whose coupling slot is placed at the

center, the coupling slot of the FQ-SIW resonator is placed adjacent to a via-hole array. Inside the FQ-SIW resonator, the inner path of the electromagnetic wave is folded three times by multilayered structure, and the total length of the inner path is  $\lambda_r/4$ . Fig. 3.3.2 shows the dominant resonant mode of the FQ-SIW resonator at the resonant frequency, where E-fields intensity is the highest at the coupling slot and the lowest at the end of the inner path. Compared with the conventional SIW resonator, the distance between the via-hole arrays of the FQ-SIW resonator is miniaturized from  $\lambda_r/2$  to  $\lambda_r/16$ , which is 1/8 of that of the conventional SIW resonator.

In general, the distance  $d$  between via-hole arrays of an FQ-SIW resonator can be roughly estimated by

$$d = \frac{1}{(N - 1)} \cdot \frac{c}{4f_r\sqrt{\epsilon_r}}, \quad (3.3.1)$$

where  $N$  is the number of conductive layers of the multilayered dielectric substrate ( $N=5$  in this case),  $f_r$  is the resonant frequency,  $\epsilon_r$  is the relative dielectric constant of the multilayered dielectric substrate, and  $c$  is the speed of light.



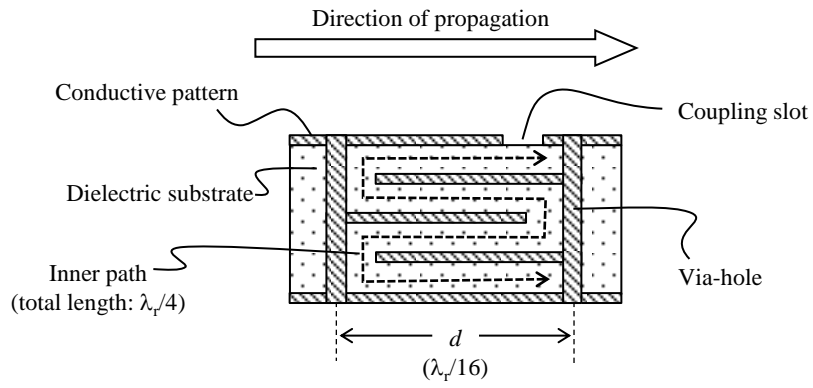


Fig. 3.3.1 A cross-sectional view of an FQ-SIW resonator.

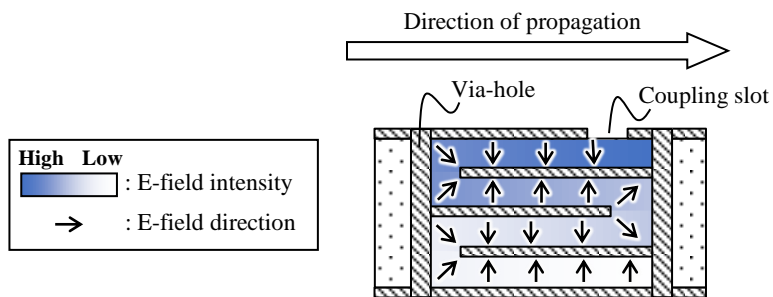
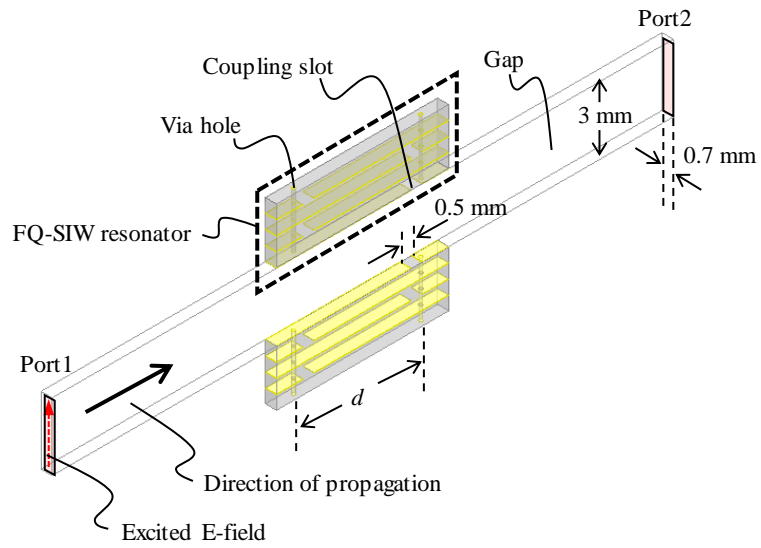


Fig. 3.3.2 The dominant resonant mode of the FQ-SIW resonator at the resonant frequency.

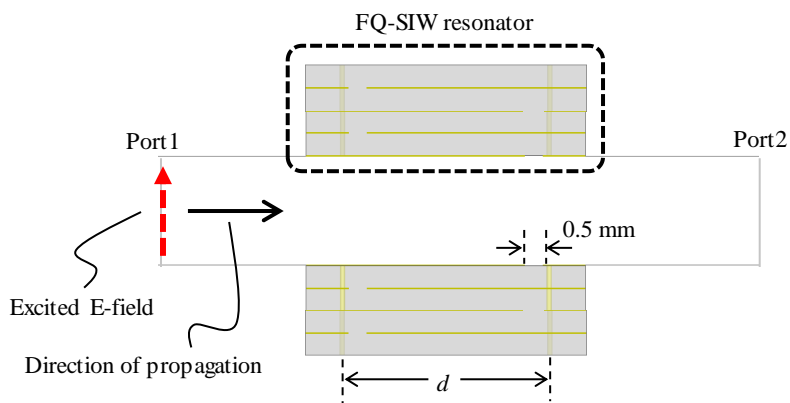
### 3.3.2 Design

The cascaded FQ-SIW resonators for the shield band of 2.4 GHz band (2.4 – 2.5 GHz) was design by following design process which is almost the same as that shown in Fig. 3.2.8 in the previous section. As with the case of the cascaded SIW resonators in the previous section, a design process for a single FQ-SIW resonator having arbitrary resonant frequency,  $f_r$ , must be cleared first before designing the cascaded configuration. The main design parameter of a single FQ-SIW resonator is the distance between via-hole arrays,  $d(f_r)$ . As shown in the previous subsection,  $d(f_r)$  can be roughly estimated by (3.3.1). Though this equation is enough for rough estimation, a more accurate equation is preferable for the design, because some other parameters are not considered: thickness of the layers of the substrate, diameter and pitch of the via holes, width of the coupling slots, for example.

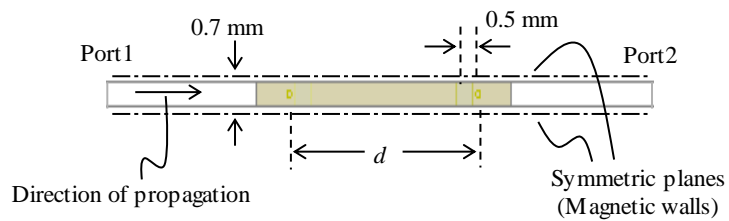
To take these parameters into account, an EM-analysis using the finite element method and a numerical approach are applied. Fig. 3.3.3 shows the EM-analysis model to obtain more accurate  $d(f_r)$ , where a gap is modeled by a thin air box of 3-mm height and 0.7-mm width and note that the sidewalls are defined as magnetic walls to work as symmetric boundaries. A five-layered FR4 substrate (thickness: 0.6×4 mm,  $\epsilon_r$ : 4.3,  $\tan\delta$ : 0.01) with a copper conductor ( $\sigma$ :  $5.8 \times 10^7$  Sie/m, thickness: 20  $\mu\text{m}$ ) and via holes ( $\phi$ : 0.3 mm, pitch: 0.7 mm) are placed on both upper and lower inner walls of the gap, and one FQ-SIW resonator is embedded in each substrate. The distances between the via holes along the direction of propagation are defined as  $d$ , and width of the both coupling slots and the slots of the inner-conductive layers are 0.5 mm. Port1 and Port2 are defined at the edges of the gap, and the source of the electromagnetic wave propagating through the gap is modeled by a vertically excited E-field at Port1. In the EM-analysis results of this model,  $S_{21}$  forms an attenuation pole at resonant frequency of the FQ-SIW resonator, from which one relation between  $d$  and  $f_r$  can be obtained. Fig. 3.3.4 shows an example of the EM-analysis result with  $d$  of 4.75 mm, where  $S_{21}$  forms an attenuation



(a) Perspective view.



(b) Side view.



(c) Top view.

Fig. 3.3.3 The EM-analysis model to obtain more accurate  $d(f_r)$ .

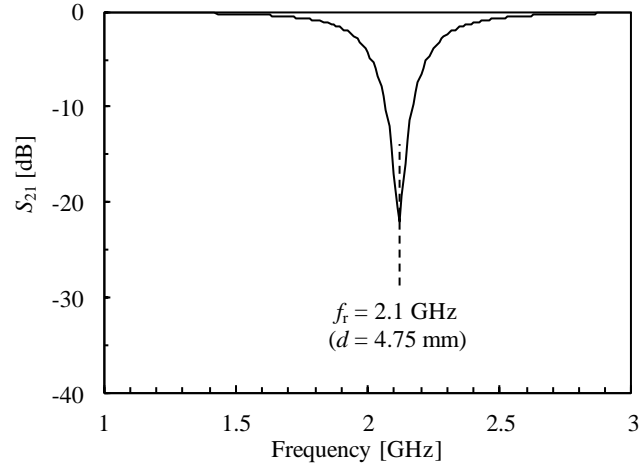


Fig. 3.3.4 An example of the EM-analysis result ( $d=4.75$  mm).

pole at 2.1 GHz. By applying a polynomial approximation to the relations between  $d$  and  $f_r$  obtained from EM-analysis results using various values of  $d$ , a numerical expression of  $d(f_r)$  can be obtained which is expected to be suitable for the design.

By considering the rough estimation of (3.3.1), a 1st order polynomial of  $1/f_r$  was adopted this time, and the least square method was applied. The obtained approximate equation of  $d(f_r)$  was

$$d(f_r) = \frac{72.32}{f_r[\text{GHz}]} - 0.54 \quad [\text{mm}]. \quad (3.3.2)$$

Fig. 3.3.5 shows relations between  $d$  and  $f_r$  obtained from the EM-analysis results, from the rough estimation shown as (3.3.1), and from the approximate equation shown above as (3.3.2). Since approximate equation (3.3.2) correlates well with the EM-analysis results widely including the shield band, the equation would be suitable for the design in this case.

A cascaded configuration of FQ-SIW resonators can be designed by cascading FQ-SIW resonators having resonant frequencies in the shield band. Before designing the individual FQ-SIW resonator, the order number of the cascaded configuration should be estimated according to the process

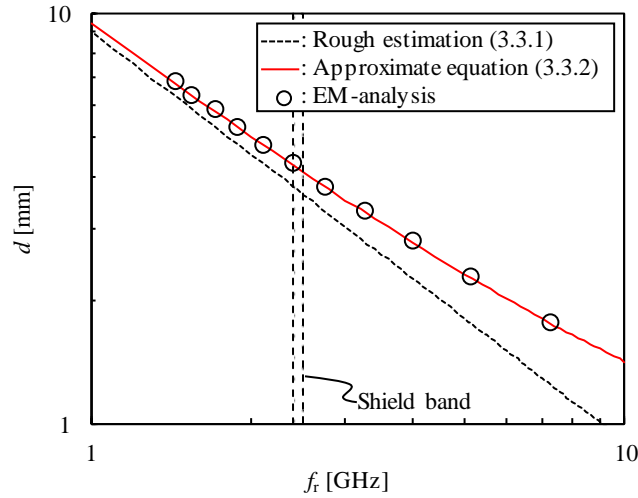


Fig. 3.3.5 Relations between  $d$  and  $f_r$  obtained from the EM-analysis results, the rough estimation of  $d(f_r)$  shown as (3.3.1), and the approximated equation shown as (3.3.2)

almost the same as that shown in Fig. 3.2.8 in the previous section. In this case, 6th order cascaded configuration was adopted to meet the conditions that resonant frequencies of the FQ-SIW resonators are within the shield band at equal frequency interval and sum of  $d(f_r)$  is less than permitted size of 30 mm along the direction of propagation.

Fig. 3.3.6 shows the EM-analysis model of the 6th order cascaded FQ-SIW resonators. Six FQ-SIW resonators (FQ-SIW<sub>1</sub> - FQ-SIW<sub>6</sub>) cascaded along the direction of propagation are embedded in the multilayered dielectric substrates placed on both upper and lower inner walls of the gap. Note that the side walls are defined as magnetic walls those work as symmetric boundaries, as same as the EM-analysis models in the previous subsection. Table 3.3.1 shows designed values of  $f_r$  and  $d$  of the cascaded FQ-SIW resonators, where  $f_r$  is selected to have equal frequency interval to simplify the design and  $d$  is obtained by substituting  $f_r$  into (3.3.2). With these designed values, total size along the direction of propagation is 27.1 mm. Fig. 3.3.7 shows the EM-analysis result, demonstrating decrease of the transmission coefficient  $S_{21}$  at the shield band and 7.5 GHz band: the former is the designed response originates from the dominant resonant mode of the FQ-SIW resonators, while the latter is the

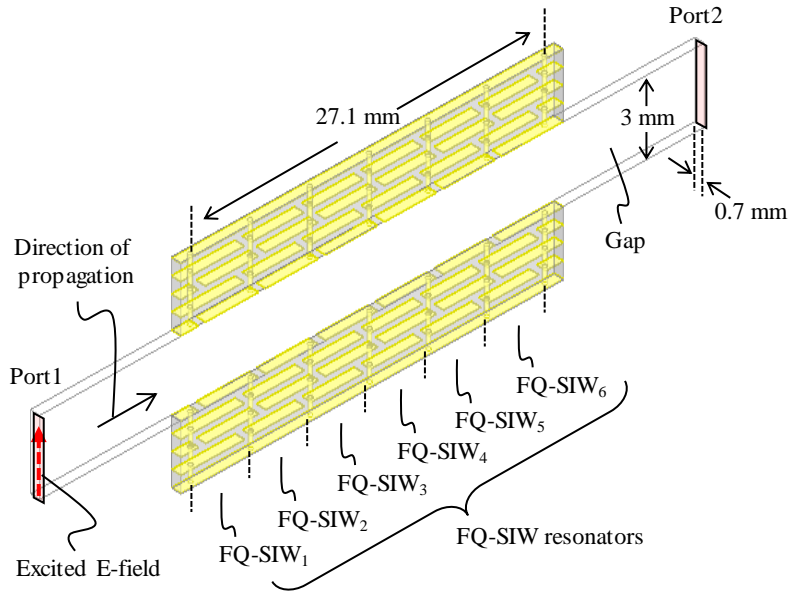


Fig. 3.3.6 The EM-analysis model of the 6th order cascaded FQ-SIW resonators.

Table 3.3.1 Designed values of  $f_r$  and  $d$  of the cascaded FQ-SIW resonators.

	FQ-SIW <sub>1</sub>	FQ-SIW <sub>2</sub>	FQ-SIW <sub>3</sub>	FQ-SIW <sub>4</sub>	FQ-SIW <sub>5</sub>	FQ-SIW <sub>6</sub>
$f_r$ [GHz]	2.40	2.42	2.44	2.46	2.48	2.50
$d$ [mm]	4.26	4.23	4.20	4.17	4.14	4.11

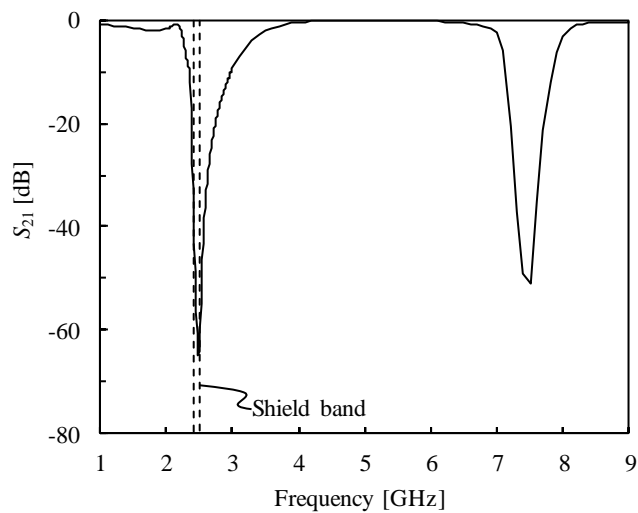


Fig. 3.3.7 The EM-analysis result of the 6th order cascaded FQ-SIW resonators.

spurious response caused by the higher-order resonant mode of the resonators. In the case that  $S_{21}$  is not decreased well in the shield band, design conditions should be reconsidered. The design process described in this section is summarized in a flowchart shown in Fig. 3.3.8, which is almost the same with that shown in the previous section.

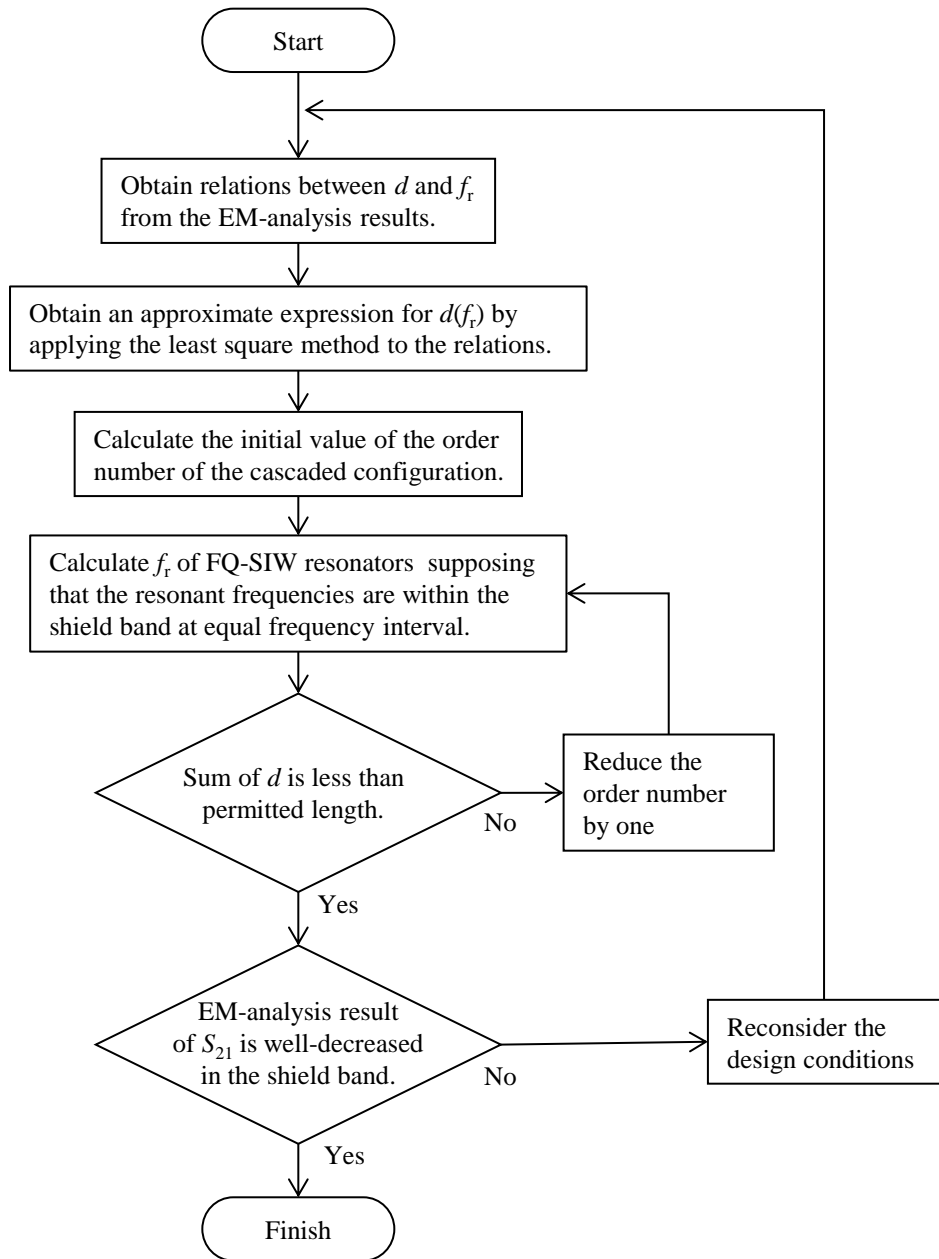


Fig. 3.3.8 A flowchart of the design process for cascaded FQ-SIW resonators.

### 3.3.3 Experiment

Fig. 3.3.9 shows a measurement system for evaluating SE, which is almost the same with what was shown in the previous section. Tx- and Rx-antennas are positioned face to face across the gap of  $200 \times 3 \text{ mm}^2$  aperture size located on the wall of a shielded chamber. The Tx-antenna is connected to Port1 of a network analyzer and placed outside the chamber 1 m apart from the wall, while the Rx-antenna is connected to Port2 of the network analyzer via a pre-amplifier of 40-dB gain and placed inside the chamber at also 1 m apart from the wall. With this measurement system, SE can be evaluated by comparing measured results of  $S_{21}$  with and without the substrates. Fig. 3.3.10 shows a simplified cross-sectional view of the gap and Fig. 3.3.11 shows the gap seen from the Tx- and the Rx-antenna sides. Two fabricated substrates are placed on both upper and lower inner walls of the gap by L-shaped fixtures of copper plate, attached to the ground planes of the substrates by conductive double-sided tapes. Fig. 3.3.12 shows the fabricated substrates whose dielectric constant and other parameters are the same as those used in the EM-analyses in the design process.

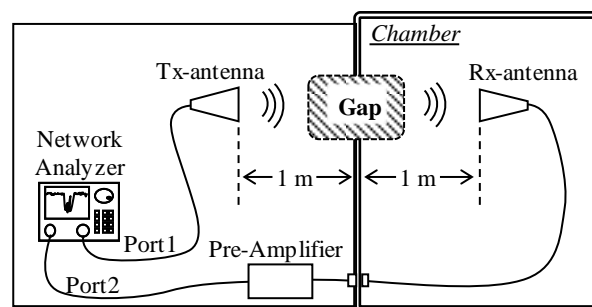


Fig. 3.3.9 The measurement system for evaluating SE.



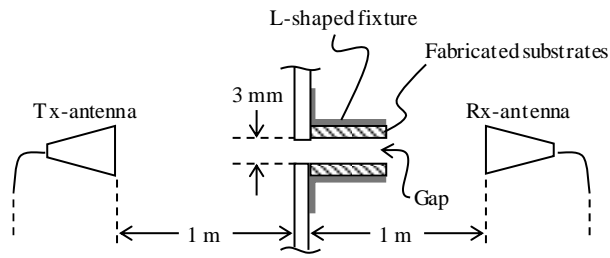
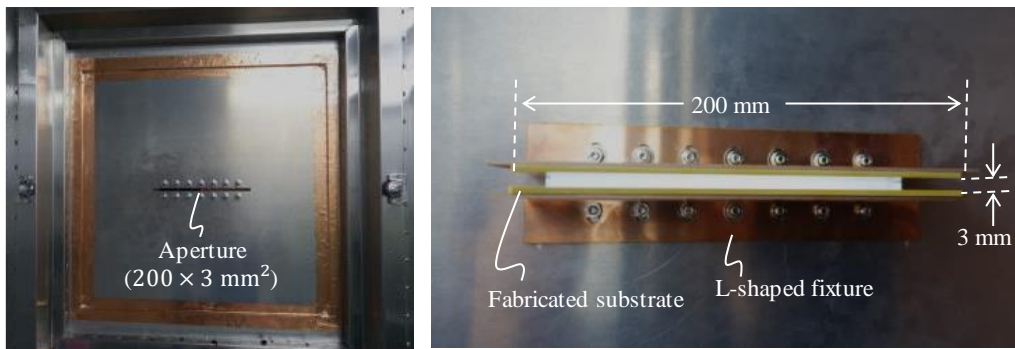


Fig. 3.3.10 A simplified cross-sectional view of the gap.



(a) Tx-antenna side.

(b) Rx-antenna side.

Fig. 3.3.11 The gap seen from both antenna sides.

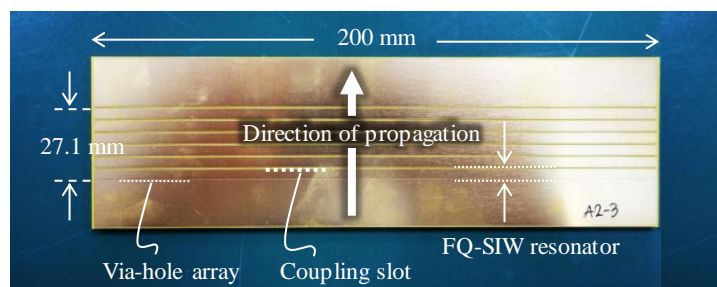
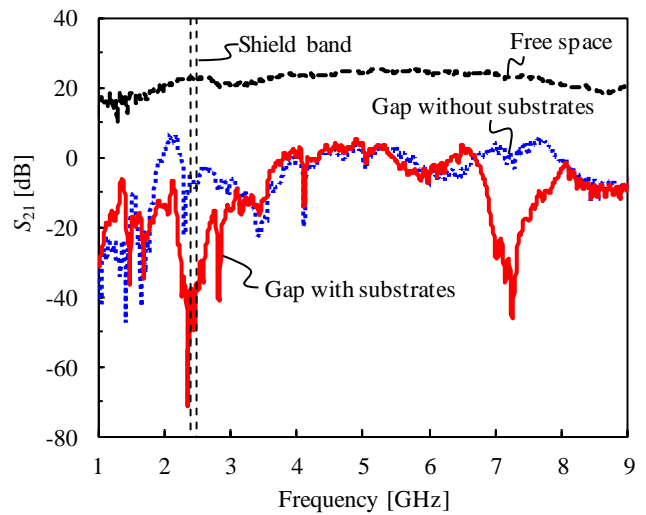
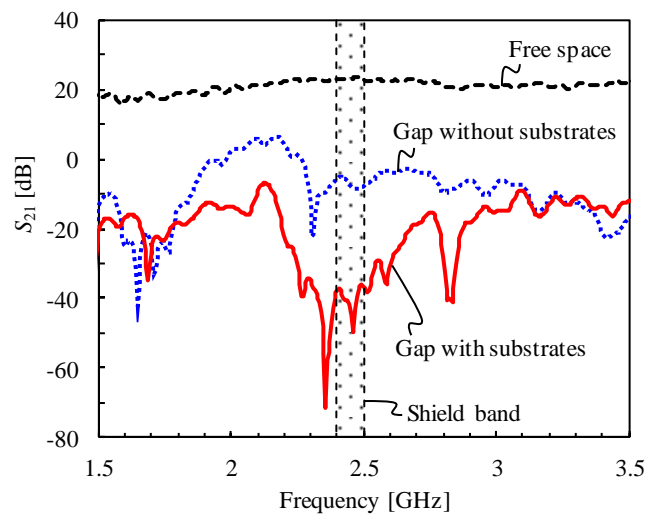


Fig. 3.3.12 The fabricated substrate.

Fig. 3.3.13 shows measured results of  $S_{21}$  of a free space and the gap with/without the substrates where cascaded FQ-SIW resonators are embedded. The measured frequency range is 1 - 9 GHz at 5.6 MHz intervals, and the gain of the pre-amplifier (+40 dB) is included in the measured  $S_{21}$ . SE can be evaluated by defining the measured  $S_{21}$  of a free space as a 0-dB reference. Fig. 3.3.14 shows measured results of SE of the gap with/without the substrates. The measured results showed 60-dB SE at 2.4 GHz band, which is improved by 30 dB from SE of the gap alone by placing the cascaded FQ-SIW resonators on the inner walls of the gap.

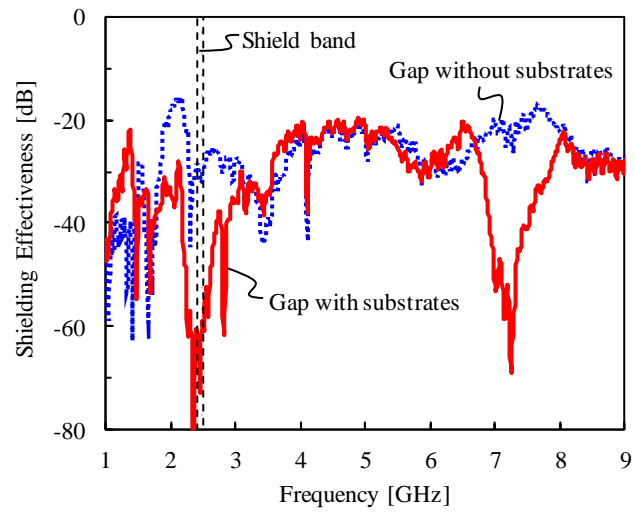


(a) 1 - 9 GHz

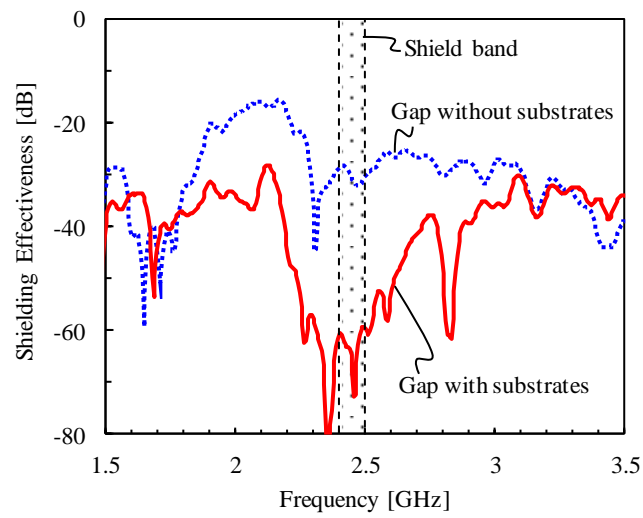


(b) 1.5 - 3.5 GHz

Fig. 3.3.13 The measured results of  $S_{21}$ .



(a) 1 – 9 GHz



(b) 1.5 – 3.5 GHz

Fig. 3.3.14 The measured results of shielding effectiveness.

## 3.4 A Gasket-free Electromagnetic Shielding Structure for 2.4 GHz and 5 GHz Bands Using Dual-Behavior SIW Resonators

### 3.4.1 Configuration

Although the previous section showed the validity of the gasket-free electromagnetic shielding structure for 2.4 GHz band using FQ-SIW resonators, current wireless local area network system uses not only 2.4 GHz band but also 5 GHz band, which is not covered by the structure. A gasket-free electromagnetic shielding structure covering both 2.4 GHz and 5 GHz bands is therefore worth to be studied.

In this section, a gasket-free shielding structure using dual-behavior (DB)-SIW resonators is proposed and evaluated. A DB-SIW resonator mainly consists of two FQ-SIW resonators sharing one coupling slot and has two almost-independent two resonant frequencies. Fig. 3.4.1 shows a cross-sectional view of a DB-SIW resonator embedded in a five-layered substrate. Note that an interstitial via hole (IVH) is positioned underneath the coupling slot. As shown in the figure, a DB-SIW resonator has two independent inner paths, and hence, can realize almost-independent two resonant frequencies. Fig. 3.4.2 shows the dominant resonant modes of the DB-SIW resonator at two resonant frequencies:  $f_1$  and  $f_2$ . At  $f_1$ , total length of the inner path1 becomes  $\lambda_r/4$  and the intensity of the E-field is the highest at the coupling slot and the lowest at the end of the inner path1. At  $f_2$ , on the other hand, total length of the inner path2 becomes  $\lambda_r/4$  and the intensity of the E-field is the highest at the coupling slot and the lowest at the end of the inner path2. Compared with an FQ-SIW resonator, which has one independent resonant frequency, a DB-SIW resonator can be expected to have two independent

resonant frequencies. Compared with a configuration of simply cascaded two FQ-SIW resonators, both have two independent resonant frequencies, however, some miniaturization can be expected for a DB-SIW resonator since number of coupling slot is decreased from two to one.

In general, the distances  $d_i$  ( $i=1,2$ ) between via-hole arrays and the IVH of an DB-SIW resonator can be roughly estimated by

$$d_i = \frac{1}{(N-1)} \cdot \frac{c}{4f_i\sqrt{\epsilon_r}} \quad (i = 1,2), \quad (3.4.1)$$

where  $N$  is the number of conductive layers of the multilayered dielectric substrate ( $N=5$  in this case),  $f_i$  is the resonant frequencies,  $\epsilon_r$  is the relative dielectric constant of the multilayered dielectric substrate, and  $c$  is the speed of light.

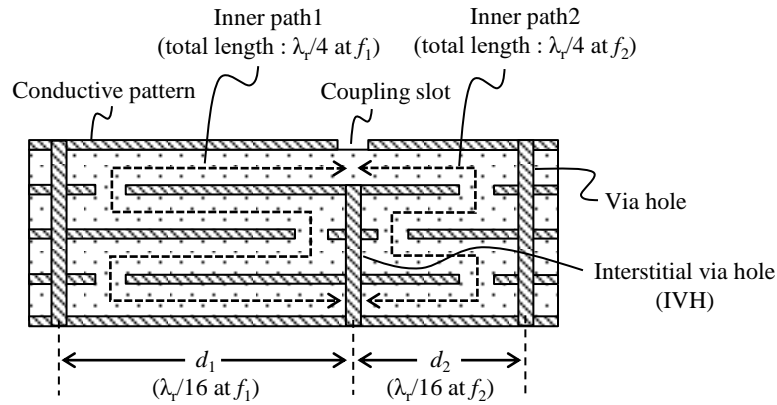
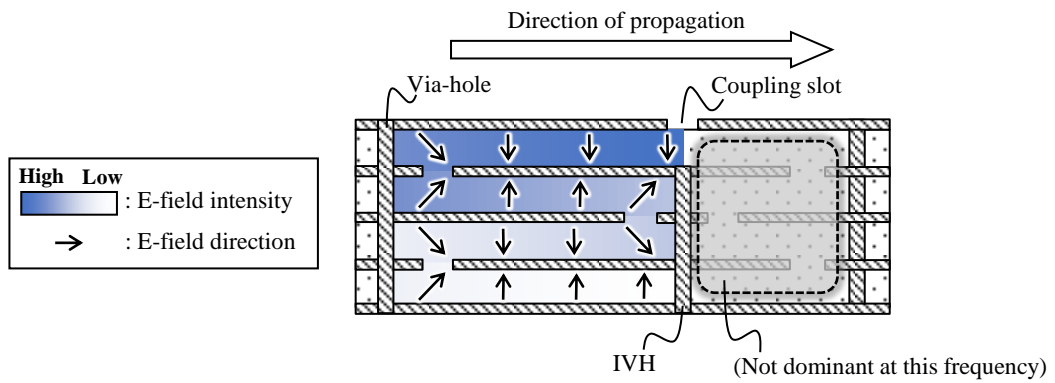
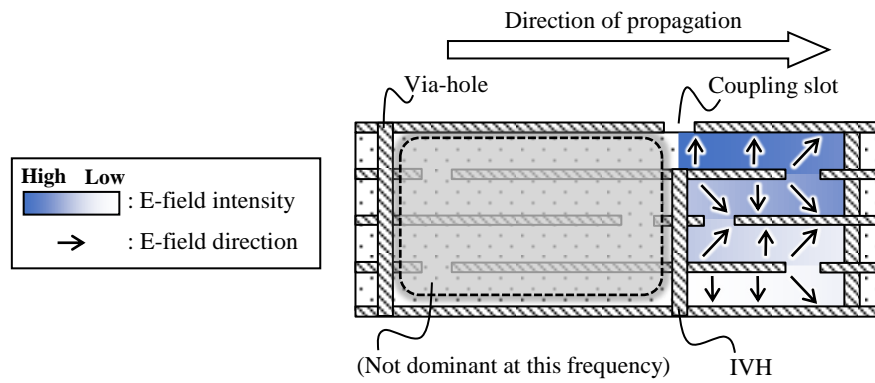


Fig. 3.4.1 A cross-sectional view of a DB-SIW resonator.



(a) At the resonant frequency  $f_1$ .



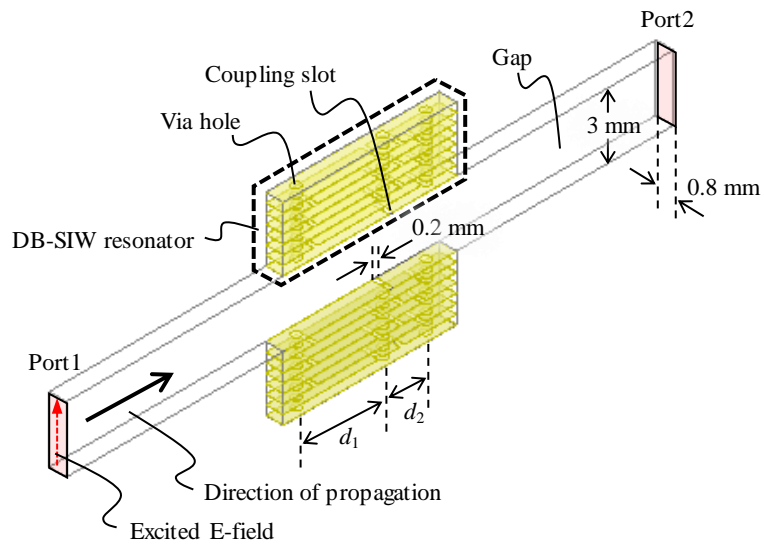
(b) At the resonant frequency  $f_2$ .

Fig. 3.4.2 The dominant resonant mode of the DB-SIW resonator at the resonant frequencies.

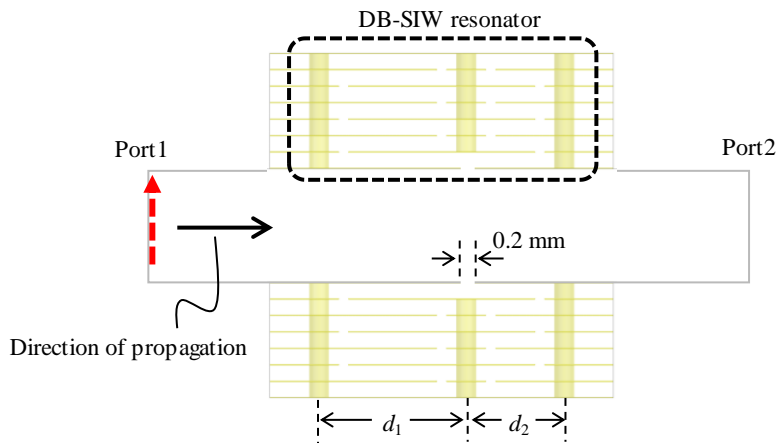
### 3.4.2 Design

The cascaded DB-SIW resonators for the shield band of 2.4 GHz band (2.35 – 2.55 GHz) and 5 GHz band (5.10 – 5.80 GHz) was design by following design process which is almost the same as those shown in the previous sections. As with the case of the design processes for the cascaded SIW resonators and cascaded FQ-SIW resonators shown in the previous sections, a design process for a single DB-SIW resonator having arbitrary resonant frequencies,  $f_1$  and  $f_2$ , must be cleared first before designing the cascaded configuration. The main design parameters of a single DB-SIW resonator is the distances between the via-hole arrays and the IVH,  $d_1(f_1)$  and  $d_2(f_2)$ . As shown in the previous subsection,  $d_1(f_1)$  and  $d_2(f_2)$  can be roughly estimated by (3.4.1). Though this equation is enough for rough estimation, a more accurate equation is preferable for the design, because some other parameters are not considered: thickness of the layers of the substrate, diameter and pitch of the via holes and the IVH, width of the coupling slots, for example.

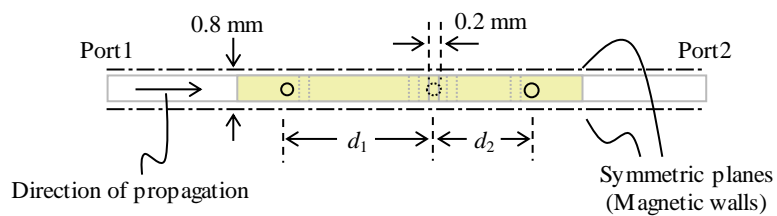
To take these parameters into account, an EM-analysis using the finite element method and a numerical approach are applied. Fig. 3.4.3 shows the EM-analysis model to obtain more accurate  $d_1(f_1)$  and  $d_2(f_2)$ , where a gap is modeled by a thin air box of 3-mm height and 0.8-mm width and note that the sidewalls are defined as magnetic walls to work as symmetric boundaries. Eight-layered FR4 substrates [ $\epsilon_r$ : 4.3,  $\tan\delta$ : 0.016, thickness: 0.4 mm (dielectric layers), 18  $\mu\text{m}$  (conductive layers)] are placed on both upper and lower inner walls of the gap, and one DB-SIW resonator is embedded in each substrate. The diameters of via hole and IVH are 0.4 mm and their pitches are 0.8 mm. The distances between the via-holes and the IVH along the direction of propagation are defined as  $d_1$  and  $d_2$ , and width of both the coupling slots and slots of the inner-conductive layers are 0.2 mm. Port1 and Port2 are defined at the edges of the gap, and the source of the electromagnetic wave propagating through the gap is modeled by a vertically excited E-field at Port1. In the EM-analysis results of this



(a) Perspective view.



(b) Side view.



(c) Top view.

Fig. 3.4.3 The EM-analysis model to obtain more accurate  $d_1(f_1)$  and  $d_2(f_2)$ .



model,  $S_{21}$  forms attenuation poles at resonant frequencies of the DB-SIW resonators.

The initial values of  $d_1$  and  $d_2$  can be roughly estimated from (3.4.1). For examples, by substituting  $f_1=2.35$  GHz and  $f_2=5.10$  GHz into (3.4.1),  $d_1=2.2$  mm and  $d_2=1.0$  mm can be obtained. From these results,  $d_1=2.2$  mm and  $d_2=1.0$  mm were chosen as initial values. Fig. 3.4.4 shows the EM-analysis result of  $S_{21}$  with these initial values, where  $f_1$  and  $f_2$  are higher than expected and not in the shield bands. To move  $f_1$  into the 2.4 GHz band first,  $d_1$  was increased from 2.2 mm and it was cleared that  $f_1$  becomes 2.35 GHz when  $d_1=2.6$  mm. Fig. 3.4.5 shows the EM-analysis result of  $S_{21}$  with  $d_1=2.6$  mm and  $d_2=1.0$  mm, where  $f_1=2.35$  GHz and  $f_2$  is almost stable. Note that the attenuation pole at 7 GHz can be comprehensible as a spurious response caused by the higher-order resonant mode at the inner path1. In the same way,  $d_2$  was increased from 1.0 mm to move  $f_2$  into the 5 GHz band, and it was cleared that  $f_2$  becomes 5.10 GHz when  $d_2=1.4$  mm. Fig. 3.4.6 shows the EM-analysis result of  $S_{21}$  with  $d_1=2.6$  mm and  $d_2=1.4$  mm, accomplished both  $f_1=2.35$  GHz and  $f_2=5.10$  GHz within each shield bands.

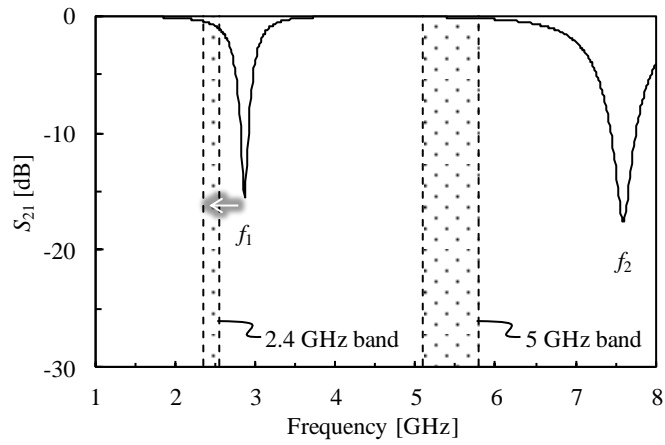


Fig. 3.4.4 The EM-analysis result of  $S_{21}$  with  $d_1=2.2$  mm and  $d_2=1.0$  mm.

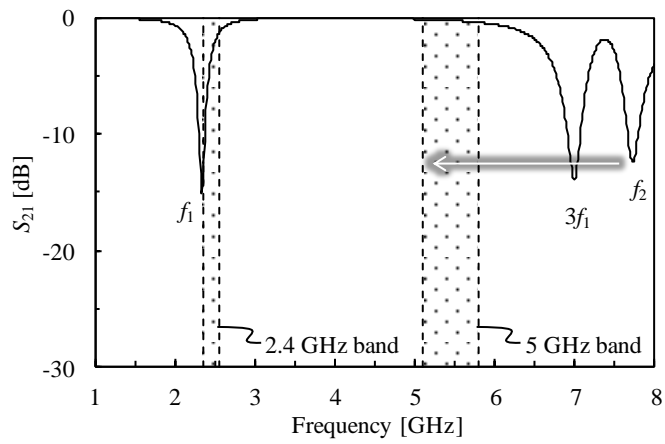


Fig. 3.4.5 The EM-analysis result of  $S_{21}$  with  $d_1=2.6$  mm and  $d_2=1.0$  mm.

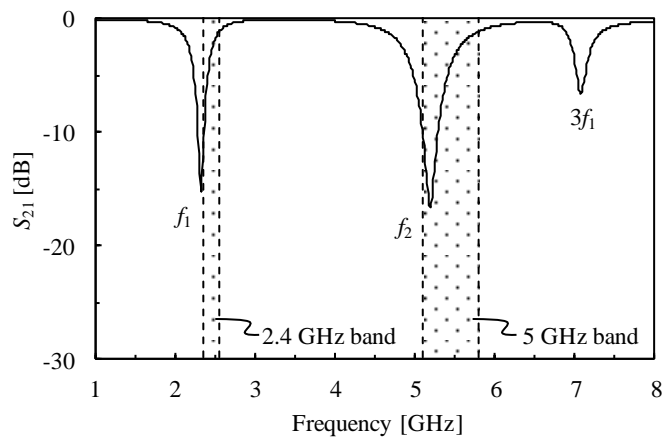


Fig. 3.4.6 The EM-analysis result of  $S_{21}$  with  $d_1=2.6$  mm and  $d_2=1.4$  mm.

Before deriving the design equations, the independency of  $f_1$  from  $d_2$  and  $f_2$  from  $d_1$  should be confirmed. Fig. 3.4.7 shows an extracted  $f_1$  from the EM-analysis results with  $d_1$  varied from 2.2 mm to 2.8 mm and  $d_2$  varied from 1.0 mm to 2.0 mm both in 0.2 mm increments. In the figure,  $f_1$  is almost stable against varied  $d_2$ , which indicates the independency of  $f_1$  from  $d_2$  within the range. Similarly, Fig. 3.4.8 shows an extracted  $f_2$  from the EM-analysis results with  $d_1$  varied from 2.0 mm to 3.0 mm and  $d_2$  varied from 1.2 mm to 1.6 mm both in 0.2 mm increments, indicating stability and independency of  $f_2$  from  $d_1$  within the range.

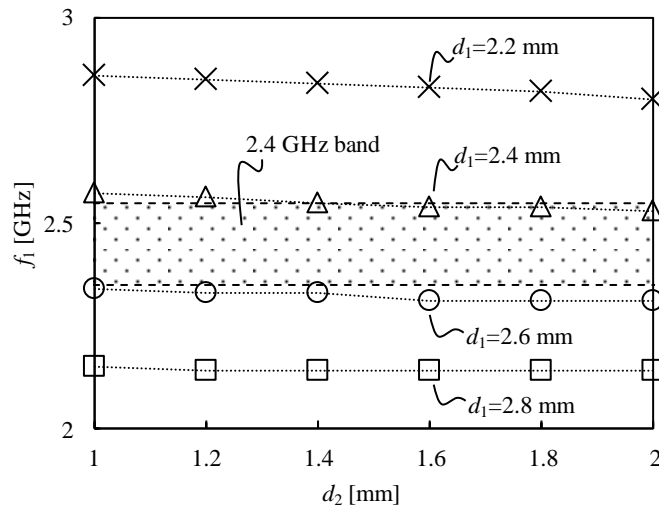


Fig. 3.4.7 Extracted  $f_1$  from the EM-analysis results.

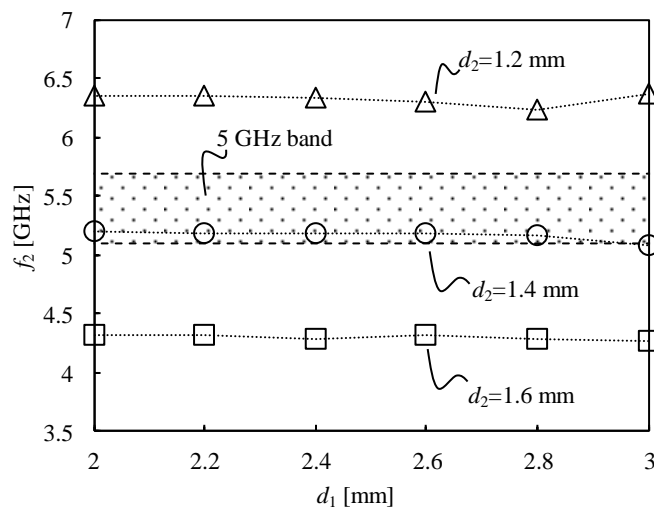


Fig. 3.4.8 Extracted  $f_2$  from the EM-analysis results.

Considering these results,  $d_1(f_1)$  can be derived as an approximate equation from the EM-analysis results when  $d_1$  varies from 2.2 mm to 2.8 mm with  $d_2$  fixed to 1.4 mm. In the same way,  $d_2(f_2)$  can be also derived as an approximate equation from the EM-analysis results when  $d_2$  varies from 1.2 mm to 1.6 mm with  $d_1$  fixed to 2.6 mm. In the approximating process, a 1st order linear equation of  $1/f_i$  ( $i=1, 2$ ) was applied considering the rough estimation of (3.4.1) this time, and the least square method was applied. The derived approximate equations were

$$d_1(f_1) = \frac{5.20}{f_1[\text{GHz}]} + 0.37 \quad [\text{mm}] \quad (d_2 = 1.4 \text{ mm}) \quad (3.4.2)$$

and

$$d_2(f_2) = \frac{5.35}{f_2[\text{GHz}]} + 0.34 \quad [\text{mm}] \quad (d_1 = 2.6 \text{ mm}) \quad (3.4.3)$$

Fig. 3.4.9 and Fig. 3.4.10 show the relations between  $d_i$  and  $f_i$  ( $i=1, 2$ ) obtained from the EM-analysis results and from the approximate equations just shown above as (3.4.2) and (3.4.3). Since these approximate equations correlates well with the EM-analysis results within the shield band, the equations would be suitable for the design in this case.

A cascaded configuration of DB-SIW resonators can be designed by cascading DB-SIW resonators having resonant frequencies in each shield band. Before designing the individual DB-SIW resonator, the order number of the cascaded configuration must be estimated according to the process almost same as those shown in the previous sections. The permitted size of the configuration along the direction of propagation was 46 mm in this case. Resonant frequencies of the smallest DB-SIW resonator in the configuration are the highest frequencies in the shield bands:  $f_1=2.55$  GHz and  $f_2=5.80$  GHz. Since  $d_1$  and  $d_2$  for these frequencies can be obtained from (3.4.2) and (3.4.3) as  $d_1=2.41$  mm and  $d_2=1.26$  mm, the smallest size of the DB-SIW resonator along the direction of propagation is 3.67 mm, which is sum of  $d_1$  and  $d_2$ . By comparing this size with the permitted size of 46 mm, the initial

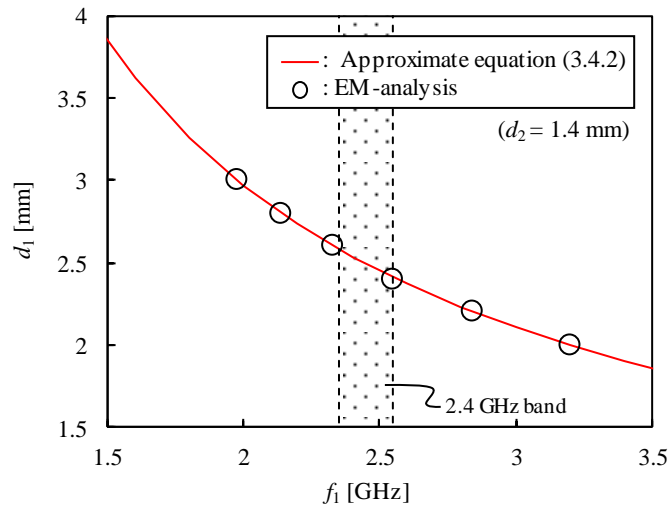


Fig. 3.4.9 Relations between  $d_1$  and  $f_1$  obtained from the EM-analysis results and the approximate equation shown as (3.4.2).

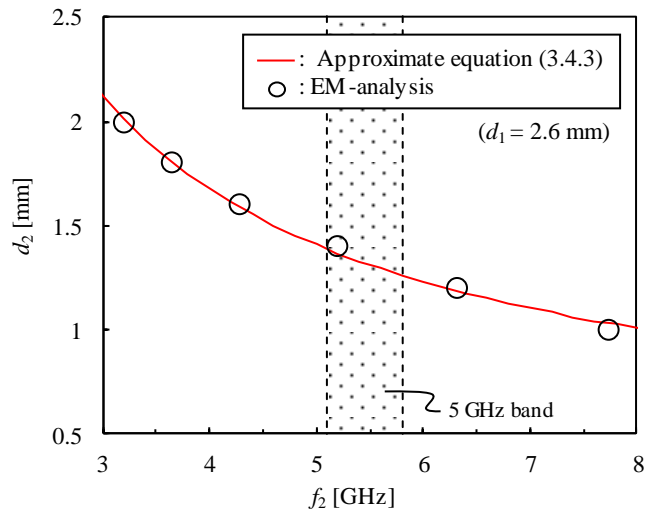


Fig. 3.4.10 Relations between  $d_2$  and  $f_2$  obtained from the EM-analysis results and the approximate equation shown as (3.4.2).

value for the order number of the cascaded configuration was estimated to be 12. Supposing that the numbers of resonant frequencies in each shield band are the same and that frequency interval is same in each shield band to simplify the design,  $d_1$  and  $d_2$  can be estimated by substituting  $f_i$  into (3.4.2) or (3.4.3). Table 3.4.1 shows the obtained values of  $f_i$  and  $d_i$  ( $i=1, 2$ ) of the cascaded DB-SIW resonators, where total size along the direction of propagation, sum of  $d_1$  and  $d_2$ , is 45.79 mm which satisfies the condition for the size along the direction of propagation.

Fig. 3.4.11 shows the EM-analysis model of the 12th order cascaded DB-SIW resonators. Twelve DB-SIW resonators (DB-SIW<sub>1</sub> – DB-SIW<sub>12</sub>) are cascaded along the direction of propagation and placed on both upper and lower inner walls of the gap. Note that the side walls are defined as magnetic walls those work as symmetric boundaries, as same as the EM-analysis models shown in previous sections. For a comparison, 24th order cascaded FQ-SIW resonators having the same 24 resonant frequencies on Table 3.4.1 were also designed by the design process in previous section using the same substrate. Fig. 3.4.12 shows the EM-analysis results of  $S_{21}$  of designed configurations of 12th order cascaded DB-SIW resonators and 24th order cascaded FQ-SIW resonators having the same resonant frequencies. The results demonstrate that attenuation characteristics at 2.4 GHz and 5 GHz bands are achieved by both configurations and that the two results are almost the same. In the case that  $S_{21}$  is not decreased well in the shield bands, design conditions should be reconsidered. The design process described in this section is summarized in a flowchart shown in Fig. 3.4.13, which is almost the same with those shown in the previous sections.

The total size along the direction of propagation are 45.79 mm for the designed 12th order cascaded DB-SIW resonators, and 47.82 mm for the designed 24th order cascaded FQ-SIW resonators. The difference between them indicates that the cascaded DB-SIW resonators can realize attenuation characteristics comparable to the cascaded FQ-SIW resonators in a configuration miniaturized along the direction of propagation, 4%-miniaturization in this case.

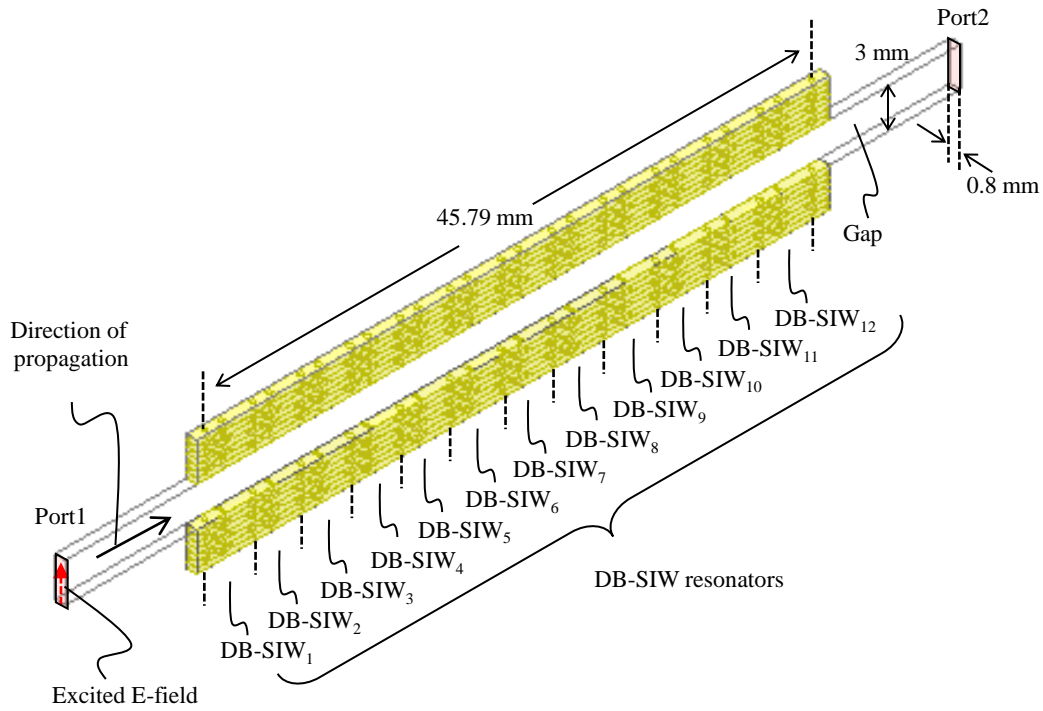


Fig. 3.4.11 The EM-analysis model of the 12th order cascaded DB-SIW resonators.

Table 3.4.1 Designed values of  $f_i$  and  $d_i$  ( $i=1, 2$ ) of the cascaded DB-SIW resonators.

	DB-SIW <sub>1</sub>	DB-SIW <sub>2</sub>	DB-SIW <sub>3</sub>	DB-SIW <sub>4</sub>	DB-SIW <sub>5</sub>	DB-SIW <sub>6</sub>
$f_1$ [GHz]	2.35	2.37	2.39	2.40	2.42	2.44
$f_2$ [GHz]	5.10	5.16	5.23	5.29	5.35	5.42
$d_1$ [mm]	2.58	2.57	2.55	2.53	2.52	2.50
$d_2$ [mm]	1.39	1.38	1.36	1.35	1.34	1.33

	DB-SIW <sub>7</sub>	DB-SIW <sub>8</sub>	DB-SIW <sub>9</sub>	DB-SIW <sub>10</sub>	DB-SIW <sub>11</sub>	DB-SIW <sub>12</sub>
$f_1$ [GHz]	2.46	2.48	2.50	2.51	2.53	2.55
$f_2$ [GHz]	5.48	5.55	5.61	5.67	5.74	5.80
$d_1$ [mm]	2.48	2.47	2.45	2.44	2.42	2.41
$d_2$ [mm]	1.32	1.30	1.29	1.28	1.27	1.26

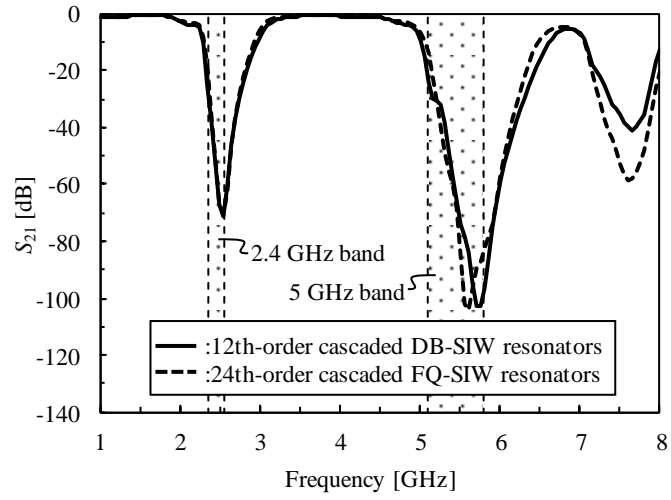


Fig. 3.4.12 The EM-analysis results of  $S_{21}$  of designed configurations of 12th order cascaded DB-SIW resonators and 24th order cascaded FQ-SIW resonators having the same resonant frequencies.



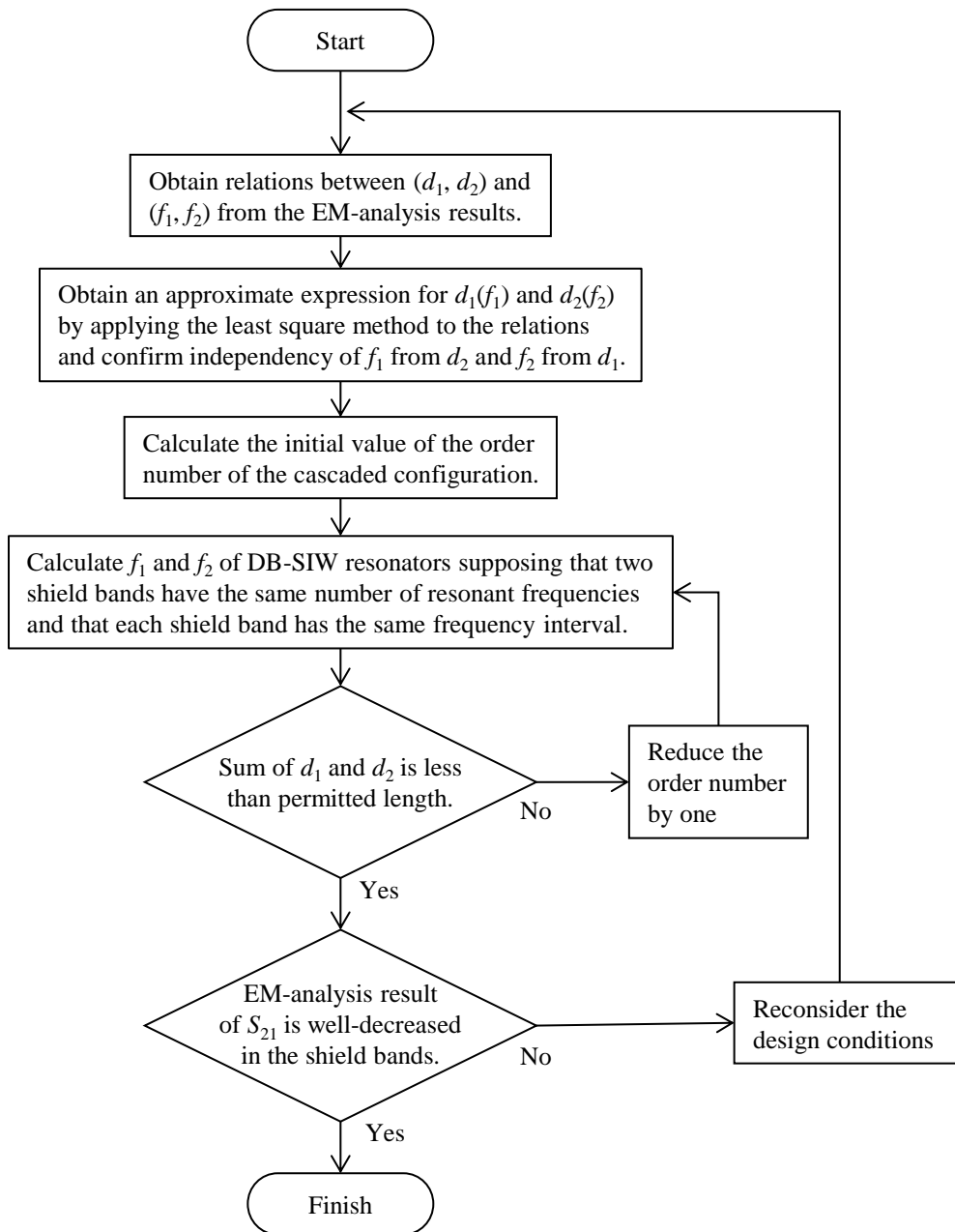


Fig. 3.4.13 A flowchart of the design process for cascaded DB-SIW resonators.

### 3.4.3 Experiment

Fig. 3.4.14 shows a measurement system for evaluating SE, which is almost the same with what was shown in the previous sections. Tx- and Rx-antennas are positioned face to face across the gap of  $200 \times 3 \text{ mm}^2$  aperture size located on the wall of a shielded chamber. The Tx-antenna is connected to Port1 of a network analyzer and placed outside the chamber 1 m apart from the wall, while the Rx-antenna is connected to Port2 of the network analyzer and placed inside the chamber at also 1 m apart from the wall. With this measurement system, SE can be evaluated by comparing measured results of  $S_{21}$  with and without the substrates. Fig. 3.4.15 shows a simplified cross-sectional view of the gap and Fig. 3.4.16 shows the gap seen from the Tx- and the Rx-antenna sides. Two fabricated substrates are placed on both upper and lower inner walls of the gap by L-shaped fixtures of copper plate, attached to the ground planes of the substrates by conductive double-sided tapes. Fig. 3.4.17 shows the fabricated substrates whose relative dielectric constant and other parameters are the same as those used in the EM-analyses in the design process.

Fig. 3.4.18 shows measured results of  $S_{21}$  of a free space and the gap with/without the substrates where cascaded DB-SIW resonators are embedded. The measured frequency range is 1 – 8 GHz at 5.6 MHz intervals. SE can be evaluated by defining the measured  $S_{21}$  of a free space as a 0-dB

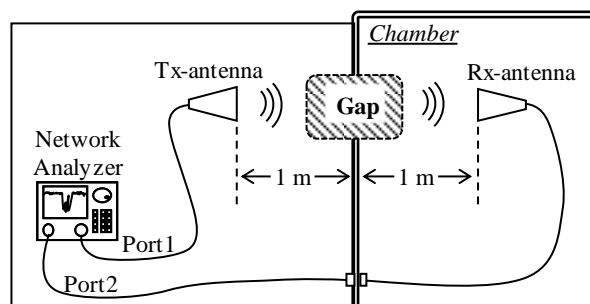


Fig. 3.4.14 The measurement system for evaluating SE.

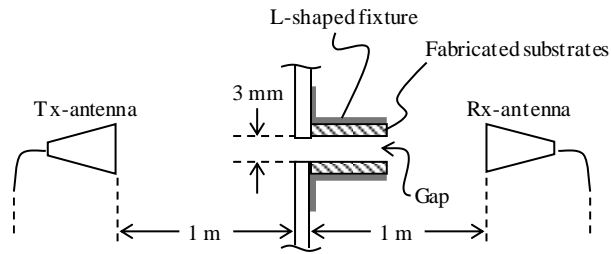
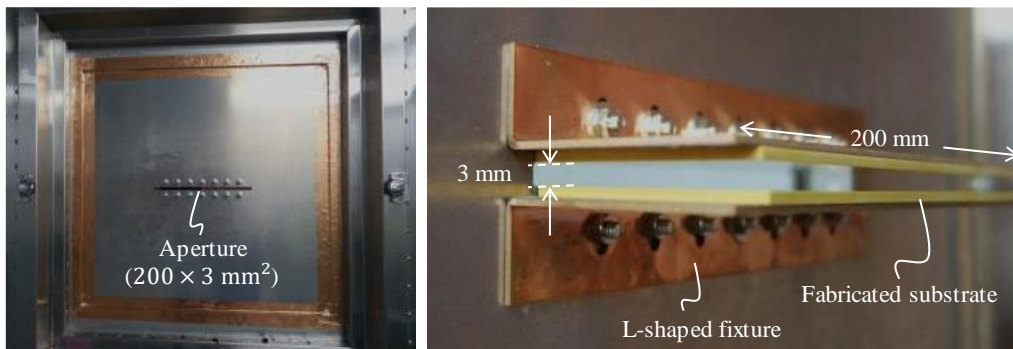


Fig. 3.4.15 A simplified cross-sectional view of the gap.



(a) Tx-antenna side.

(b) Rx-antenna side.

Fig. 3.4.16 The gap seen from both antenna sides.

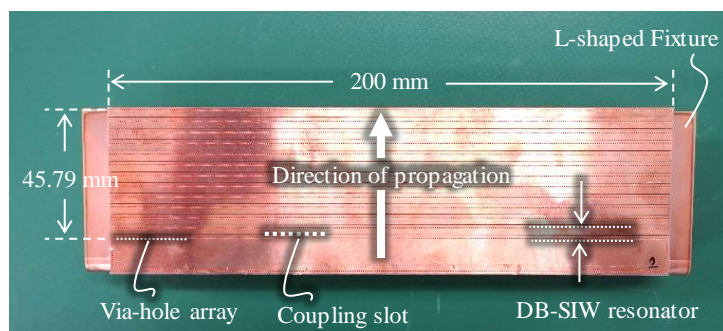


Fig. 3.4.17 The fabricated substrate.

reference. Fig. 3.4.19 shows measured results of SE of the gap with/without the substrates. Though some frequency shift was presented, the measured results showed 50-dB SE near the higher frequency sides of the shield bands, those are improved by 20 dB from SE of the gap alone by placing the cascaded DB-SIW resonators on the inner walls of the gap.

A main cause of the frequency shift must be cleared for the practical use of this configuration, which can be estimated by comparing the EM-analysis and the measured results. As previously shown

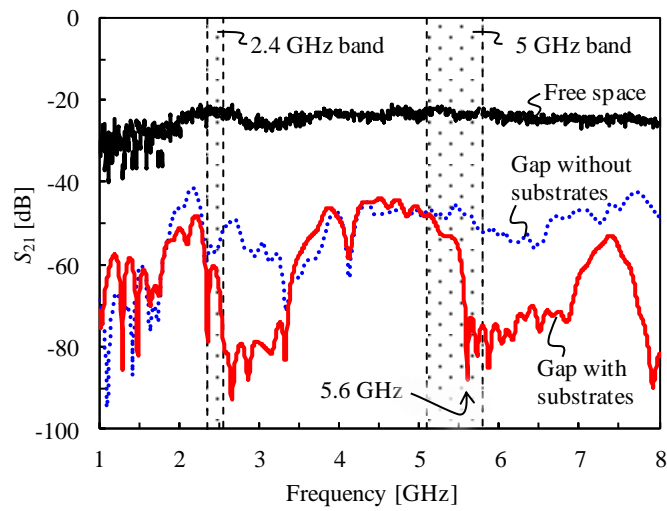


Fig. 3.4.18 The measured results of  $S_{21}$ .

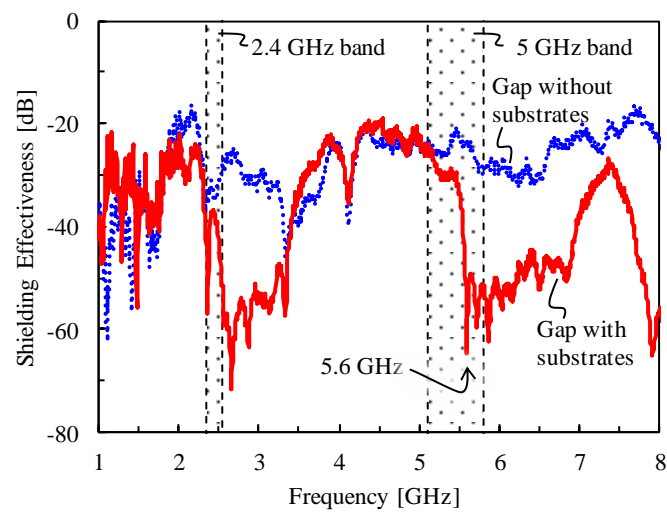


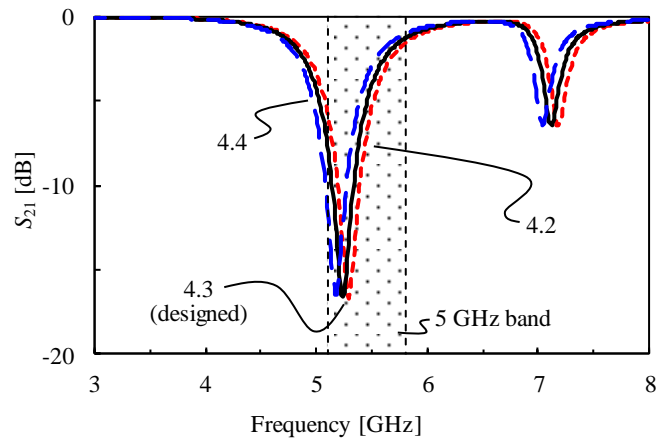
Fig. 3.4.19 The measured results of shielding effectiveness.

in Table 3.4.1, the lowest resonant frequency of the cascaded DB-SIW resonators in 5 GHz band was designed to be 5.1 GHz. In the measured results, however, the lowest resonant frequency in 5 GHz band which appears as the lowest attenuation pole in 5 GHz band was 5.6 GHz. From this discrepancy between these two resonant frequencies, the frequency shift occurred in the measured results can be estimated to be +9.8%.

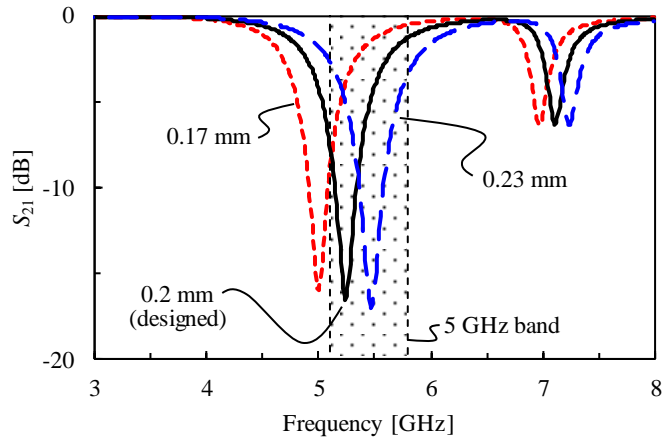
This frequency shift could have been caused by manufacturing errors: (a) dielectric constant ( $4.3 \pm 0.1$ ), (b) width of the coupling slots ( $0.2 \pm 0.03$  mm), and (c) diameter of via holes ( $0.4 \pm 0.1$  mm), for example. Potential frequency shifts due to these manufacturing errors can be estimated by EM-analysis. Fig. 3.4.20 shows the EM-analysis results of the 1st order DB-SIW resonators considering each of these manufacturing errors. This analysis can be performed using the EM-analysis model previously shown in Fig. 3.4.3 with the DB-SIW resonator indicated as DB-SIW<sub>1</sub> in Table 3.4.1 designed to have the resonant frequency  $f_2$  at 5.1 GHz. Table 3.4.2 summarizes the amounts of frequency shifts obtained from the EM-analysis results. Compared with the frequency shift presented in the measured results, it can be inferred that the main reason for the frequency shift is the manufacturing error in the diameter of via holes.

Table 3.4.2 The frequency shift obtained from the EM-analysis results.

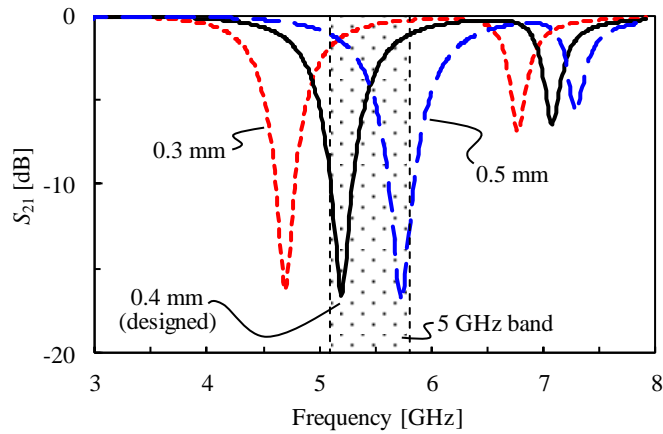
Items	Design value	Manufacturing error	Frequency shift
(a) Dielectric constant	4.3	- 0.1	+ 1.0%
		+ 0.1	- 1.1%
(b) Width of the coupling slots	0.2 mm	- 0.03 mm	- 4.6%
		+ 0.03 mm	+ 4.4%
(c) Diameter of the via holes	0.4 mm	- 0.1 mm	- 9.5%
		+ 0.1 mm	+ 10.1%
Measured Result	-	-	+ 9.8 %



(a) Dielectric constant ( $4.3 \pm 0.1$ ).



(b) Width of the coupling slots ( $0.2 \pm 0.03$  mm).



(c) Diameter of via holes ( $0.4 \pm 0.1$  mm).

Fig. 3.4.20 The EM-analysis results of the 1st-order DB-SIW resonators considering manufacturing errors.

## 3.5 Summary

In this chapter, three configurations of a gasket-free electromagnetic shielding structure were proposed and evaluated. In the structures, three types of SIW resonators are embedded in dielectric substrates, and the substrates are placed on the inner walls of a gap between a shielded door and a door frame. The SIW resonators are arranged in a cascaded configuration along the direction of propagation and designed to have slightly different resonant frequencies to realize wide band SE including the resonant frequencies. Contrary to the ordinary contact-type conductive gaskets, the structures are gasket-free and then high contact pressure is not required even when the door is closed, and therefore, opening and closing operations of the door do not induce the aged deterioration.

In the first configuration, a gasket-free shielding structure using cascaded SIW resonators for 12 – 15.5 GHz was designed with a design process based on EM-analysis. In the design result, eight SIW resonators having resonant frequency within the shield band were cascaded along the direction of propagation and the total size along the direction of propagation was 52 mm. The measured result showed 40-dB SE at the shield band, which is improved by 25 dB from SE of the gap alone by placing the cascaded SIW resonators on the inner walls of the gap.

The second configuration was designed for 2.4 GHz band (2.4 – 2.5 GHz) using folded quarter-wavelength (FQ)-SIW resonators, which is kind of an SIW resonator miniaturized by applying a multilayered dielectric substrate. In the configuration, FQ-SIW resonators were embedded in five-layered dielectric substrates and the size of the FQ-SIW resonator along the direction of propagation was  $\lambda/16$  in the substrate at its resonant frequency, which is one-eighth of that of the SIW resonator used in the first configuration. A gasket-free shielding structure using cascaded FQ-SIW resonators for 2.4 GHz band was designed with a design process based on EM-analysis. In the design result, six FQ-SIW resonators having resonant frequency within the shield band were cascaded along the

direction of propagation and the total size along the direction of propagation was 27.1 mm. The measured results showed 60-dB SE at 2.4 GHz band, which is improved by 30 dB from SE of the gap alone by placing the cascaded FQ-SIW resonators on the inner walls of the gap.

The third configuration was designed for 2.4 GHz band (2.35 – 2.55 GHz) and 5 GHz band (5.10 – 5.80 GHz) using dual behavior (DB)-SIW resonators. The DB-SIW resonator mainly consists of two FQ-SIW resonators sharing one coupling slot and has almost-independent two resonant frequencies. In the configuration, DB-SIW resonators were embedded in eight-layered dielectric substrates and designed to have one resonant frequency within each shield band. A gasket-free shielding structure using cascaded DB-SIW resonators for 2.4 GHz and 5 GHz bands was designed with a design process based on EM-analysis. In the design result, twelve DB-SIW resonators were cascaded along the direction of propagation and the total size along the direction of propagation was 45.79 mm. Though some frequency shift of +9.8% was presented, the measured results showed 50-dB SE near the shield bands, those are improved by 20 dB from SE of the gap alone by placing the cascaded DB-SIW resonators on the inner walls of the gap. Afterward, EM-analysis results inferred that the frequency shift was mainly caused by the manufacturing error in the diameter of the via holes.

Note that direction of the incident waves in this chapter was fixed vertical to the aperture of the gap. Although a wideband design to the low frequency side is qualitatively expected to be effective for the incident waves from the tilted direction, however, quantitatively analyses and measurements against the incident waves from tilted directions should be considered for a practical use. In addition, the resonant frequencies of resonators were almost uniquely determined according to the design process shown in each section, however, to establish more optimized method for determining resonant frequencies is another future issue.



## References

- [3.1] M. Raspopoulos and S. Stavrou, "Frequency selective buildings through frequency selective surfaces," *IEEE Trans. Antennas Propag.*, vol. 59, no. 8, pp. 2998–3005, August 2011.
- [3.2] M. Kartal, B. Doken, and I. Gungor, "Design for the structural surface material enabling shielding for interference mitigation within the buildings in the unlicensed 2.4 GHz ISM band," in *Proc. Gen. Assem. Sci. Symp.*, pp. 1-4, Istanbul, Turkey, August 2011.
- [3.3] B. Sanz-Izquierdo and E. A. Parker, "Dual polarized reconfigurable frequency selective surfaces," *IEEE Trans. Antennas Propag.*, vol. 62, no. 2, pp. 764–771, February 2014.
- [3.4] S. Habib, G. I. Kiani, and M. F. U. Butt, "An efficient UWB FSS for electromagnetic shielding," in *Proc. Int. Conf. Electromagn. Adv. Appl.*, pp. 1543–1546, Verona, Italy, September 2017.
- [3.5] A. A. Dewani, S. G. O'Keefe, D. V. Thiel, and A. Galehdar, "Window RF shielding film using printed FSS," *IEEE Trans. Antennas Propag.*, vol. 66, no. 2, pp. 790–796, February 2018.
- [3.6] D. Ferreira, T. Fernandes, I. Cuiñas, and R. Caldeirinha, "A dual-band single-layer frequency selective surface for Wi-Fi applications," in *Proc. 9th Eur. Conf. Antennas Propag.*, pp. 1-4, Lisbon, Portugal, April 2015.
- [3.7] N. Choudhary, A. Sharma, and S. Yadav, "A novel band stop frequency selective surface for the security of quad band mobile applications," in *Proc. IEEE Appl. Electromagn. Conf.*, pp. 1-2, Maharashtra, India, December 2017.
- [3.8] S. Habib, G. I. Kiani, and M. F. U. Butt, "An efficient FSS absorber for WLAN security," in *Proc. IEEE Int. Symp. Antennas Propag. USNC-URSI Radio Sci. Meet.*, pp. 689–690, San Diego, CA, USA, July 2017.

- [3.9] X. Xiong, W. Hong, Z. Zhao, L. Deng, and S. Li, "WiFi band-stop FSS for increased privacy protection in smart building," in *Proc. IEEE 6<sup>th</sup> Int. Symp. Microw., Antenna, Propag., EMC Technol.*, pp. 826–828, Shanghai, China, October 2015.
- [3.10] H. W. Denny and K. R. Shouse, "EMI shielding of conductive gaskets in corrosive environments," in *Proc. IEEE Int. Symp. Electromagn. Compat.*, pp. 20–24, Washington, D.C., USA, August 1990.
- [3.11] P. Faraji, J. L. Drewniak, D. S. McBain, and D. Pommerenke, "SE measurements with a TEM cell to study gasket reliability," in *Proc. IEEE Int. Symp. Electromagn. Compat.*, pp. 462–465, Denver, CO, USA, August 2013.
- [3.12] T. Claeys, J. Catrysse, D. Pissoort, and Y. Arien, "Stripline set-up for characterizing the effect of corrosion and ageing on the shielding effectiveness of emi gaskets with improved repeatability," in *Proc. EMC Europe*, pp. 725–729, Amsterdam, The Netherlands, August 2018.
- [3.13] D. Tsyantenka, Y. Arlou, and E. Sinkevich, "Worst-case model for considering gaskets in calculation of shielding effectiveness of metallic enclosures," in *Proc. EMC Europe*, pp. 178–183, Amsterdam, The Netherlands, August 2018.
- [3.14] Y. Murata, T. Kanamoto, and F. Murase, "Wideband shield door with a magnetic absorber," *IEEE Trans. Electromagn. Compat.*, vol. 55, no. 3, pp. 526–531, June 2013.
- [3.15] T. Tsuruta, S. Hirosato, and K. Fujiwara, "High performance shield room for intermediate frequency magnetic fields," in *Proc. EMC Europe*, pp. 1069–1073, Gothenburg, Sweden, September 2014.
- [3.16] F. Centola, D. J. Pommerenke, X. Kai, and J. L. Drewniak, "Alternatives to gaskets in shielding an enclosure," in *Proc. IEEE Int. Symp. Electromagn. Compat.*, pp. 205–209, Minneapolis, MN, USA, August 2002.

- [3.17] V. Rodriguez, “On the design of door-less access passages to shielded enclosures,” in *Proc. Antenna Meas. Techn. Assoc. Symp.*, pp. 1–6, Atlanta, GA, USA, October 2017.

# Chapter 4

## Conclusions

This dissertation relates to studies on suppressing propagation of electromagnetic waves by using resonators-loaded dielectric substrates. A waveguide BRF and a gasket-free electromagnetic shielding structure were proposed as applications, and their design procedures and evaluated results were summarized in two chapters.

In Chapter 2, two configurations of a waveguide BRF using resonators-loaded dielectric substrates were described. Though different resonators are applied, both configurations have lower profile than the conventional waveguide BRF has because nothing is located outside the waveguide. Furthermore, high precision at relatively high frequency bands can be expected because machining process is not required for manufacturing the resonators. The configurations described in this chapter can be expected to contribute to the miniaturization and high-density fabrication of the entire waveguide system, and are suitable for use in systems where miniaturization and high attenuation at high frequency band are required, for example, the millimeter-wave frequency band wireless communication system (shown in Fig. 1.1.1), automotive millimeter-wave radar systems, and measuring systems for radio astronomy. However, it is necessary to clarify the factors that caused the difference between the measured results and the design results to put the configurations into a practical use.

In section 1 of Chapter 2, the configuration of the waveguide BRF using open-ended  $\lambda/2$  microstrip resonators was proposed and evaluated. In the configuration, open-ended  $\lambda/2$  microstrip resonators are mounted at regular intervals on two dielectric substrates placed on the inner side walls

of the waveguide. The waveguide BRF using open-ended  $\lambda/2$  microstrip resonators for Q-band (47 GHz) was designed according to the design process based on filter theory and EM-analysis, and the evaluated results of the fabricated waveguide BRF showed a steep and relatively high attenuation characteristic more than 50 dB at 46.7 – 47.0 GHz.

In section 2 of Chapter 2, the configuration of the waveguide BRF using SIW resonators was proposed and evaluated. In the configuration, SIW resonators are embedded at regular intervals in two dielectric substrates placed on both upper and lower inner walls of the waveguide. The waveguide BRF using SIW resonators for Q-band (47 GHz) was designed according to the design process based on filter theory and EM-analysis, and the evaluated results of the fabricated waveguide BRF also showed a steep and relatively high attenuation characteristic more than 50 dB at 46.7 – 47.0 GHz.

Comparing the two configurations, lower insertion loss can be expected for the first configuration than the second configuration. This may be caused by difference between the assemblies; while the first configuration is separated at the middle of upper and lower walls, the second configuration is separated at the middle of side walls where current is relatively concentrated when electromagnetic wave propagates through the main waveguide. However, although the second configuration is disadvantageous in terms of insertion loss, it may become preferable in case when the main waveguide is required to be separated at the middle of side walls considering assembly of the whole system or combination with other components.

In Chapter 3, three configurations of a gasket-free electromagnetic shielding structure were described as another application for using resonators-loaded dielectric substrates. The substrates are placed on inner walls of a gap between a shielded door and a door frame. Contrary to the contact-type conductive gasket, frequency selectivity can be realized in the structure, and moreover, the structure is almost free from deterioration, because high contact pressure is not needed even when the door is

closed. The configurations described in this chapter are suitable for use in shielded environments having frequency selectivity, for example, offices and laboratories in an urban area where interference with outside should be suppressed in bands of the wireless LAN while communication with outside is possible in bands of other communication devices such as cell phones. The configurations are also suitable for broadcast studios and theaters where interferences of wireless microphones should be prevented. Note that for practical use, however, frequency-selective shielding structures for walls, ceilings, floors, doors, and sometimes windows must be applied at the same time.

In section 1 of Chapter 3, the gasket-free electromagnetic shielding structure for 12 - 15.5 GHz using conventional SIW resonators was proposed and evaluated. SIW resonators having slightly different resonant frequencies are arranged in a cascaded configuration along the direction of propagation of electromagnetic waves and are embedded in dielectric substrates placed on inner walls of the gap. The design process based on EM-analysis and polynomial approximation was described, and the evaluated result showed more than 25-dB improvement of SE at 12 - 16 GHz by placing the cascaded SIW resonators.

In section 2 of Chapter 3, the gasket-free electromagnetic shielding structure for 2.4 GHz band using folded quarter-wavelength (FQ)-SIW resonators was proposed and evaluated. An FQ-SIW resonator is kind of a miniaturized SIW resonator by applying a multilayered dielectric substrate, and the miniaturization enables realizing cascaded configuration in a practical size for frequency bands of several GHz. The design process based on EM-analysis and polynomial approximation was described, and the evaluated result showed more than 30-dB improvement of SE at 2.4 GHz band by placing the cascaded FQ-SIW resonators.

In section 3 of Chapter 3, the gasket-free electromagnetic shielding structure for 2.4 GHz and 5 GHz bands using dual behavior (DB)-SIW resonators was proposed and evaluated. A DB-SIW resonator mainly consists of two FQ-SIW resonators sharing one coupling slot and has almost-

independent two resonant frequencies. The design process based on EM-analysis and polynomial approximation was described, and the evaluated result showed more than 20-dB improvement of SE at 2.4 GHz and 5 GHz bands by placing the cascaded DB-SIW resonators. The measured result included +9.8%-frequency shift, however, EM-analysis results considering manufacturing errors inferred that the main reason for the shift was the manufacturing error in the diameter of the via holes.

The author would like to expect that the configurations and the structures described in this dissertation contribute in some way to the radio communication technology field where higher frequency and more complex environment are anticipated.

# Publication list

## Referred journals

### Chapter 2

1. S. Yoneda, H. Uchida, M. Tanaka, T. Sasaki, N. Yoneda, and Y. Konishi, “A Millimeter-wave Band Low-profile Waveguide BRF with Built-in Open-ended  $\lambda/2$  Microstrip Resonators,” *IEICE Trans.*, vol. J96-C, no. 5, pp. 65-72, April 2013 (in Japanese).
2. S. Yoneda, H. Uchida, M. Tanaka, T. Sasaki, N. Yoneda, and Y. Konishi, “A Q-band Low-profile Waveguide BRF with Built-in Cavity-Embedded Dielectric Substrates,” *IEICE Trans.*, vol. J93-C, no. 4, pp. 113-118, April 2010 (in Japanese).

### Chapter 3

3. S. Yoneda, Y. Shiraki, Y. Sasaki, N. Oka, and H. Oh-hashii, “A GHz-Band Gasket-Free Electromagnetic Shielding Structure with Built-In Cascaded SIW Resonators,” *IEICE Trans.*, vol. J99-B, no. 3, pp. 115-123, March 2016 (in Japanese).
4. S. Yoneda, Y. Shiraki, Y. Sasaki, N. Oka, and H. Oh-hashii, “A Gasket-Free Electromagnetic Shielding Structure for 2.4 GHz Band Using Folded Quarter-Wavelength SIW Resonators,” *IEICE Trans.*, vol. J101-B, no. 7, pp. 507-514, July 2018 (in Japanese).
5. S. Yoneda, Y. Shiraki, Y. Sasaki, and C. Miyazaki, “A Gasket-Free Electromagnetic Shielding Structure for 2.4-GHz and 5-GHz Bands Using Cascaded Dual-Behavior SIW Resonators,” *IEEE Trans. Electromagn. Compat.*, vol. 62, no. 2, pp. 377–385, April 2019.



## International conferences

### Chapter 2

1. S. Yoneda, H. Uchida, M. Tanaka, T. Sasaki, H. Yukawa, and Y. Hirano, “A Q-band Low-profile Waveguide BRF with Built-in Cavity-Embedded Dielectric Substrates,” in *2008 38<sup>th</sup> European Microwave Conference Dig.*, pp.741-744, Amsterdam, Netherlands, October 2008.
2. S. Yoneda, H. Uchida, M. Tanaka, T. Sasaki, H. Yukawa, and Y. Hirano, “A Q-band low-profile waveguide BRF with built-in open-ended  $\lambda/2$  microstrip resonators,” in *2011 IEEE MTT-S Int. Microw. Symp. Dig.*, pp. 1-4, Baltimore, MD, USA, June 2011.

### Chapter 3

3. S. Yoneda, Y. Shiraki, Y. Sasaki, N. Oka, and H. Oh-Hashi, “A GHz-band gasket-free electromagnetic shielding structure with built-in cascaded SIW resonators,” in *Proc. EMC Europe 2014*, pp. 432–437, Gothenburg, Sweden, September 2014.

Note that the paper was selected for the best paper award of EMC Europe 2014.

4. S. Yoneda, Y. Shiraki, Y. Sasaki, N. Oka, and H. Oh-Hashi, “A gasketfree electromagnetic shielding structure for 2.4 GHz band using folded quarter-wavelength SIW resonators,” in *Proc. IEEE Int. Symp. Electromagn. Compat.*, pp. 271–276, Ottawa, ON, Canada, July 2016.

# Domestic conferences and technical reports in Japan

## Chapter 2

1. S. Yoneda, H. Uchida, M. Tanaka, T. Sasaki, and N. Yoneda, “A Q-band Low-profile Waveguide BRF with Built-in Cavity-Embedded Dielectric Substrates,” in *Proc. of the 2008 Society Conf. of IEICE*, C-2-66, September 2008.
2. S. Yoneda, H. Uchida, M. Tanaka, T. Sasaki, and N. Yoneda, “A Q-band Low-profile Waveguide BRF with Built-in Cavity-Embedded Dielectric Substrates,” in *Technical Report of IEICE*, MW2008-118, November 2008.
3. S. Yoneda, H. Uchida, M. Tanaka, T. Sasaki, and N. Yoneda, “Measurements of A Q-band Low-profile Waveguide BRF with Built-in Cavity-Embedded Dielectric Substrates,” in *Proc. of the 2009 IEICE General Conf.*, C-2-57, March 2009.
4. S. Yoneda, H. Uchida, M. Tanaka, T. Sasaki, H. Yukawa, and Y. Hirano, “Measurements of a Q-band Low-profile Waveguide BRF with Built-in Open-ended  $\lambda/2$  Microstrip Resonators,” in *Proc. of the 2010 Society Conf. of IEICE*, C-2-59, September 2010.
5. S. Yoneda, H. Uchida, M. Tanaka, T. Sasaki, H. Yukawa, and Y. Hirano, “A Q-band Low-profile Waveguide BRF with Built-in Open-ended  $\lambda/2$  Microstrip Resonators,” in *Technical Report of IEICE*, MW2010-115, November 2010.

## Chapter 3

6. S. Yoneda, Y. Shiraki, Y. Sasaki, N. Oka, and H. Oh-Hashi, “A GHz-band Electromagnetic Shielding Structure with built-in Arrayed SIW Resonators,” in *Proc. of the 2013 Society Conf. of IEICE*, B-4-9, September 2013.

7. S. Yoneda, Y. Shiraki, Y. Sasaki, N. Oka, and H. Oh-Hashi, "A GHz-band Electromagnetic Shielding Structure with built-in Arrayed SIW Resonators," in *Technical Report of IEICE*, EMCJ2013-122, January 2014.
8. S. Yoneda, Y. Shiraki, Y. Sasaki, N. Oka, and H. Oh-Hashi, "A Gasket-Free Electromagnetic Shielding Structure with Built-in Cascaded SIW Resonators for Shielding Effectiveness at Discrete Frequencies," in *Proc. of the 2015 Society Conf. of IEICE*, B-4-28, September 2015.
9. S. Yoneda, Y. Shiraki, Y. Sasaki, N. Oka, and H. Oh-Hashi, "A Gasket-Free Electromagnetic Shielding Structure for 2.4 GHz band Using Folded Quarter-wavelength SIW Resonators," in *Technical Report of IEICE*, EMCJ2015-81, November 2015.
10. S. Yoneda, Y. Shiraki, Y. Sasaki, N. Oka, and H. Oh-Hashi, "A Gasket-Free Electromagnetic Shielding Structure for 2.4 GHz band Using Folded Quarter-wavelength SIW Resonators," in *Proc. of the 2016 IEICE General Conf.*, B-4-21, March 2016.
11. S. Yoneda, Y. Shiraki, Y. Sasaki, and C. Miyazaki, "A Gasket-Free Electromagnetic Shielding Structure for 2.4-GHz and 5-GHz Bands Using Cascaded Dual-Behavior SIW Resonators," in *Technical Report of IEICE*, EMCJ2018-18, July 2018.

# Appendix A: Representations of Equivalent circuits for a BRF

In Fig. 2.2.5 in chapter 2, an equivalent circuit of the waveguide BRF was shown which consists of ideal  $J$ -inverters and series-connected parallel resonators those alternately connected between I/O ports. However, a BRF can be represented by other equivalent circuits, since a BRF can be generally represented by alternately connected ideal  $K$ - or  $J$ - inverters and two types of resonators: series-connected parallel resonators or shunt-connected series resonators. As which inverters and resonators to use depends on a designer, four types of equivalent circuits are available as a result in principle. In this appendix, the four representations of equivalent circuits for a BRF are shown and summarized. Note that  $\omega_1'$ , the cut-off angular frequency of the prototype filter, is set to one through this appendix to simplify the representations.

As the first one, Fig. A.1 shows an equivalent circuit for a 4th order BRF using ideal  $K$ -inverters and shunt-connected series resonators, those alternately connected between I/O ports. In the figure,  $Z_A$  and  $Z_B$  are terminating impedance,  $X_j(\omega)$  is reactance of the resonators,  $\chi_j$  is reactance slope parameter of the resonators, and  $K_{j,j+1}$  are impedance of ideal  $K$ -inverters (note that  $K_{01}$  and  $K_{45}$  are included in the I/O ports). These parameters can be obtained as

$$K_{01} = \sqrt{wZ_A\chi_1g_0g_1} \quad , \quad (\text{A.1})$$

$$K_{45} = \sqrt{w\chi_4Z_Bg_4g_5} \quad , \quad (\text{A.2})$$

$$K_{j,j+1} \Big|_{j=1 \text{ to } 3} = w\sqrt{\chi_j\chi_{j+1}g_jg_{j+1}} \quad , \quad (\text{A.3})$$

and

$$\chi_j = \frac{\omega_0}{2} \frac{dX_j(\omega)}{d\omega} \Big|_{\omega=\omega_0} \quad , \quad (\text{A.4})$$

where  $w$  is the fractional bandwidth,  $\omega_0$  is the center angular frequency of the stop band, and  $g_j$  is  $g$ -values for the prototype filter [2.1].

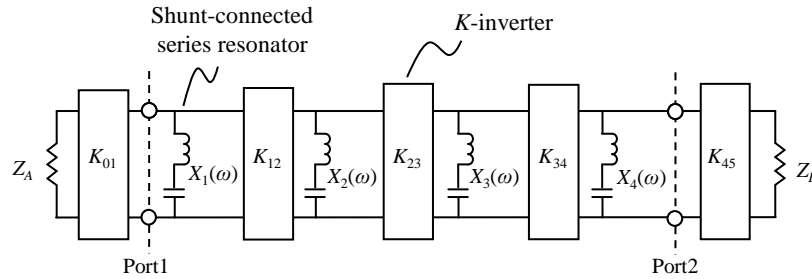


Fig. A.1 The equivalent circuit for a 4th order BRF using alternately connected ideal  $K$ -inverters and shunt-connected series resonators.

As the second one, Fig. A.2 shows an equivalent circuit for a 4th order BRF using ideal  $K$ -inverters and series-connected parallel resonators, those connected alternately between I/O ports.

The parameters  $K_{j,j+1}$  can be obtained as

$$K_{01} = \sqrt{\frac{Z_A}{\omega b_1 g_0 g_1}} \quad , \quad (\text{A.5})$$

$$K_{45} = \sqrt{\frac{Z_B}{\omega b_4 g_4 g_5}} \quad , \quad (\text{A.6})$$

and

$$K_{j,j+1} \Big|_{j=1 \text{ to } 3} = \frac{1}{\omega} \sqrt{\frac{1}{b_j b_{j+1} g_j g_{j+1}}} \quad , \quad (\text{A.7})$$

using the same variables previously denoted in this appendix and chapter 2.

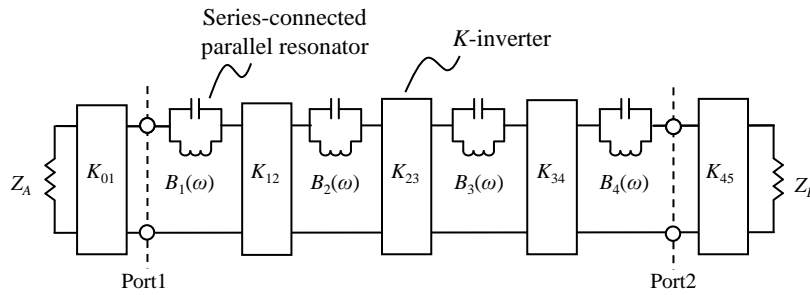


Fig. A.2 The equivalent circuit for a 4th order BRF using alternately connected ideal  $K$ -inverters and series-connected parallel resonators.

As the third one, Fig. A.3 shows an equivalent circuit for a 4th order BRF using ideal  $J$ -inverters and shunt-connected series resonators, those connected alternately between I/O ports. The parameters  $J_{j,j+1}$  can be obtained as

$$J_{01} = \sqrt{\frac{G_A}{w\chi_1g_0g_1}}, \quad (\text{A.8})$$

$$J_{45} = \sqrt{\frac{G_B}{w\chi_4g_4g_5}}, \quad (\text{A.9})$$

and

$$J_{jj+1}|_{j=1 \text{ to } 3} = \frac{1}{w} \sqrt{\frac{1}{\chi_j\chi_{j+1}g_jg_{j+1}}}, \quad (\text{A.10})$$

using the same variables previously denoted in this appendix and chapter 2.

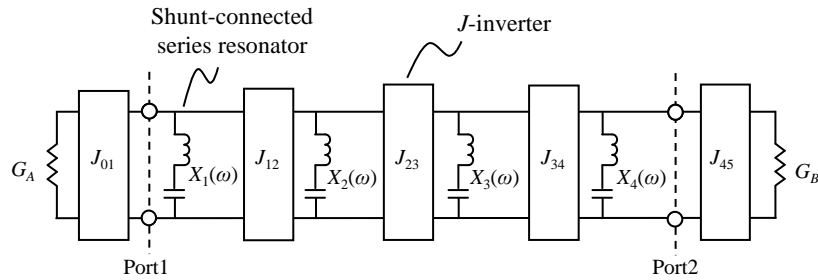


Fig. A.3 The equivalent circuit for a 4th order BRF using alternately connected ideal  $J$ -inverters and shunt-connected series resonators.

As the last one, although which is already shown in chapter 2, Fig. A.4 shows the equivalent circuit for a 4th order BRF using ideal  $J$ -inverters and series-connected parallel resonators, those connected alternately between I/O ports. The parameters  $J_{j,j+1}$  can be obtained as

$$J_{01} = \sqrt{wG_A b_1 g_0 g_1} \quad , \quad (\text{A.11})$$

$$J_{45} = \sqrt{wb_4 G_B g_4 g_5} \quad , \quad (\text{A.12})$$

and

$$J_{j,j+1} \Big|_{j=1 \text{ to } 3} = w \sqrt{b_j b_{j+1} g_j g_{j+1}} \quad , \quad (\text{A.13})$$

those are already shown in chapter 2.

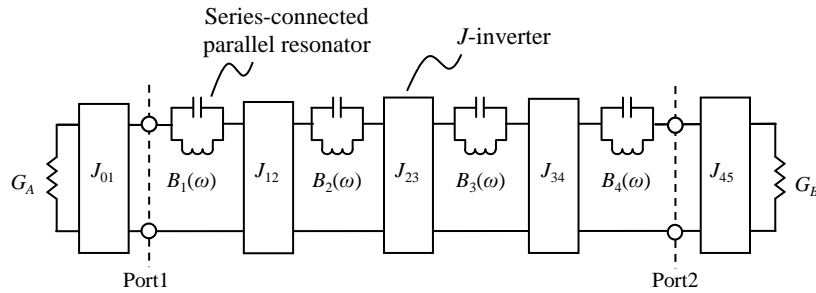
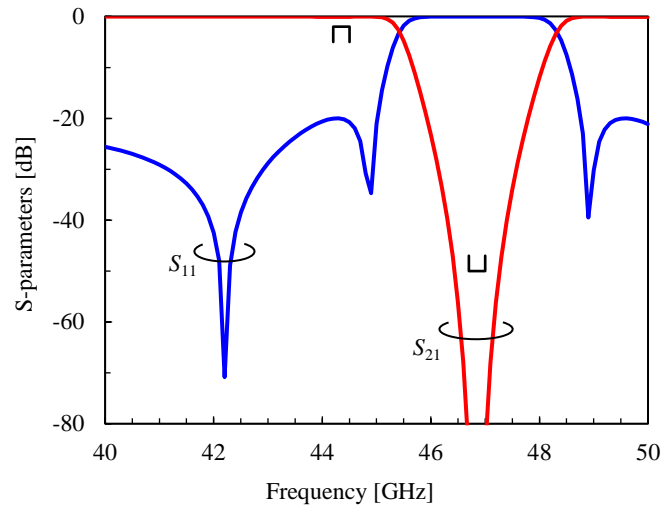


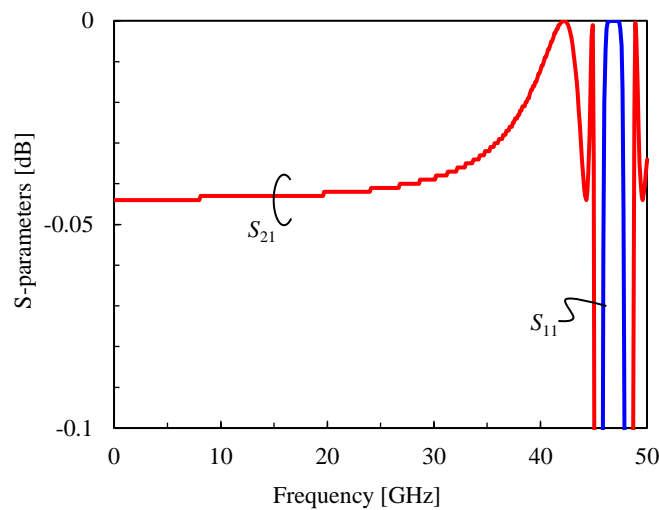
Fig. A.4 The equivalent circuit for a 4th order BRF using alternately connected ideal  $J$ -inverters and series-connected parallel resonators.



Fig. A.5 shows calculated results of the prototype filter applying the four equivalent circuits described in this appendix. The parameters for a loss-less 4th order Chebyshev filter with 0.05-dB of passband ripple were used, those are already shown in Table 2.2.2 in chapter 2. The calculated results were the same for the four equivalent circuits, showing Chebyshev characteristics as intended. This result confirms the validity of the four equivalent circuits. The equations for  $K_{j,j+1}$  and  $J_{j,j+1}$  of the four equivalent circuits of an  $n$ -th order BRN are summarized in Table A.1.



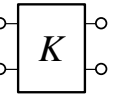
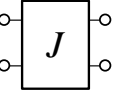
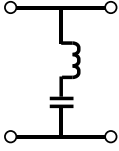
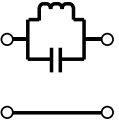
(a) 40 – 50 GHz.



(b) 0 – 50 GHz.

Fig. A.5 Calculated results of the prototype filter applying the four equivalent circuits.

Table A.1 The summary of  $K_{j,j+1}$  and  $J_{j,j+1}$  of the four equivalent circuits for an  $n$ -th order BRF.

Ideal inverters Resonators	$K$ -inverter  $\begin{pmatrix} 0 & j * K \\ j / K & 0 \end{pmatrix}$	$J$ -inverter  $\begin{pmatrix} 0 & j / J \\ j * J & 0 \end{pmatrix}$
Shunt-connected series resonator 	$K_{01} = \sqrt{wZ_A\chi_1g_0g_1}$ $K_{n,n+1} = \sqrt{w\chi_nZ_Bg_n g_{n+1}}$ $K_{j,j+1} \Big _{j=1 \text{ to } n-1} = w\sqrt{\chi_j\chi_{j+1}g_jg_{j+1}}$	$J_{01} = \sqrt{\frac{G_A}{w\chi_1g_0g_1}}$ $J_{n,n+1} = \sqrt{\frac{G_B}{w\chi_n g_n g_{n+1}}}$ $J_{j,j+1} \Big _{j=1 \text{ to } n-1} = \frac{1}{w} \sqrt{\frac{1}{\chi_j\chi_{j+1}g_jg_{j+1}}}$
Series-connected paralle resonator 	$K_{01} = \sqrt{\frac{Z_A}{wb_1g_0g_1}}$ $K_{n,n+1} = \sqrt{\frac{Z_B}{wb_n g_n g_{n+1}}}$ $K_{j,j+1} \Big _{j=1 \text{ to } n-1} = \frac{1}{w} \sqrt{\frac{1}{b_j b_{j+1} g_j g_{j+1}}}$	$J_{01} = \sqrt{wG_A b_1 g_0 g_1}$ $J_{n,n+1} = \sqrt{wb_n G_B g_n g_{n+1}}$ $J_{j,j+1} \Big _{j=1 \text{ to } n-1} = w \sqrt{b_j b_{j+1} g_j g_{j+1}}$

(Note:  $\omega'_1 = 1$ )